



UNIVERSITY
OF
JOHANNESBURG

COPYRIGHT AND CITATION CONSIDERATIONS FOR THIS THESIS/ DISSERTATION

 creative
commons



- Attribution — You must give appropriate credit, provide a link to the license, and indicate if changes were made. You may do so in any reasonable manner, but not in any way that suggests the licensor endorses you or your use.
- NonCommercial — You may not use the material for commercial purposes.
- ShareAlike — If you remix, transform, or build upon the material, you must distribute your contributions under the same license as the original.

How to cite this thesis

Surname, Initial(s). (2012) Title of the thesis or dissertation. PhD. (Chemistry)/ M.Sc. (Physics)/ M.A. (Philosophy)/M.Com. (Finance) etc. [Unpublished]: [University of Johannesburg](https://ujcontent.uj.ac.za/vital/access/manager/Index?site_name=Research%20Output). Retrieved from: https://ujcontent.uj.ac.za/vital/access/manager/Index?site_name=Research%20Output (Accessed: Date).

Development, characterisation and analysis of an active Q-switched fiber laser based on the modulation of a fiber Fabry-Perot tunable filter

By

KABOKO JEAN-JACQUES MONGA

DISSERTATION

Submitted for partial fulfillment of the requirements

for the degree

DOCTOR OF PHILOSOPHY

in

ELECTRICAL AND ELECTRONIC ENGINEERING SCIENCES

in the

FACULTY OF ENGINEERING

at the

UNIVERSITY OF JOHANNESBURG

STUDY LEADERS: Dr. Rodolfo Martinez Manuel

Pr. Johan Meyer

April 2018

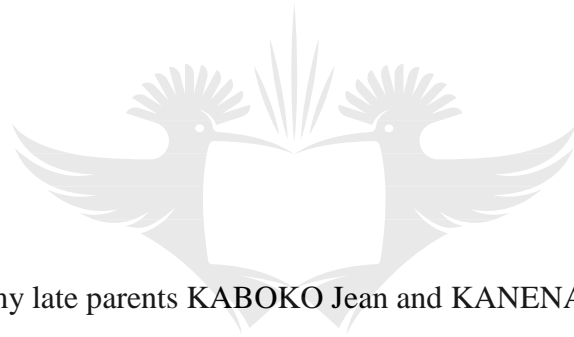
Abstract

The field of fiber lasers and fiber optic devices has experienced a sustained rapid growth. In particular, all-fiber Q-switched lasers offer inherent advantages of relatively low cost, compact design, light weight, low maintenance, and increased robustness and simplicity over other fiber laser systems. In this thesis, a design of a new Q-switching approach in all-fiber based laser is proposed. The Q-switching principle is based on dynamic spectral overlapping of two filters, namely fiber Bragg grating based filter and fiber Fabry-Perot tunable filter. When the spectra overlap, the filter system has the maximum transparency, the laser cavity has minimal losses and it can release the stored power in the form of the giant pulse. Using this Q-switching technique, experimental construction of an all-fiber active Q-switched Erbium-doped fiber lasers is successfully demonstrated in both ring cavity and linear cavity fiber laser configurations. The output peak power of 9.7 W and time duration of 500 ns are obtained at 1 kHz of repetition rate for ring cavity Q-switched Erbium-doped fiber laser; and 5.6 W output peak power with a 450 ns pulse time duration are achieved for linear cavity Q-switched Erbium-doped fiber laser at the same repetition rate. The repetition rate of the pulses can be continuously varied from a single shot to a few kHz.

Furthermore, the characteristics of designed all-fiber lasers like output power stability, extinction ratio and linewidth fiber laser are evaluated. The effects of fiber laser cavities parameters such as Erbium-doped fiber length, Erbium ion concentration, pump power and coupling ratio on the fiber laser output are reported. Techniques to produce stable and narrow linewidth fiber laser are investigated. Using a saturable absorber based un-pumped Erbium-doped fiber, under optimized fiber laser cavity; extinction ratio up 40 dB is obtained. Linewidth of 10 kHz and 16 kHz are demonstrated for ring and linear cavity fiber laser, respectively.

A novel theoretical model is derived to validate the Q-switching approach introduced in this project. Numerical simulation is performed to demonstrate the Q-switching behavior in Erbium-doped fiber ring laser. The output peak power and pulse duration are characterized with respect to the pump power, cavity length and scanning speed of the spectral overlap between fiber Bragg grating and Fabry-Perot filter. Simulation results agree well with the experimental investigation. The proposed fiber laser systems provide a simple and cost-effective approach to realize a stable, high extinction ratio and narrow linewidth fiber laser systems suitable for application in the field of optical fiber sensor and optical communication.

Dedication



To my late parents KABOKO Jean and KANENA Jacqueline

UNIVERSITY
OF
JOHANNESBURG

Jean-Jacques MONGA KABOKO

Acknowledgements

It is a great privilege to have had the opportunity to directly experience the depth of theoretical and experimental knowledge from many gifted people during the path of my doctorate studies. This experience will always be with me for the rest of my journey. The magnificent time could not have been possible without the support of all the people I worked with at the University of Johannesburg.

First, praise to the almighty GOD who gave me the opportunity to do a doctorate project. The God of my heart has always been there to support, guide, and strengthen me in each step of this project.

I gratefully acknowledge my supervisors, Dr. Rodolfo Martinez Manuel. He has been my invaluable mentor and guide. His valuable advices, assistance in my experimental work, and availability in orientating me when things could not breakthrough are highly appreciated. I will never fail to remember his sincerity and encouragement.

I own the deepest appreciation to my co-supervisor, Professor Johan Meyer who provided to me the opportunity to join the photonics research group of the University of Johannesburg and work on such an active research area. Throughout the years, Professor Johan Meyer has offered invaluable guidance, support, and let me mature as

a researcher. He is my personal role model for efficient communication and hard-working.

I present my gratitude to all the individuals that have unconditionally assisted and helped me in any way during my research. Justice Sompo and Dr Diethelm Schmieder are acknowledged for their helpful suggestions, for being there helping me during this project. I have enjoyed the time working with them and have highly developed my knowledge.

I thank Shantelle Sass, Dudu Kanyi, University of Johannesburg officers who have written many letters for me, for visas and scholarships applications, during the past years. My sincere wish is to see them continuing to cooperate well with other people like they did with me.

I am particularly grateful to the past and present members of the Photonics research group of the University of the Johannesburg; Michael Gobbler, Della Tamin, Stephanie Mukarugina, Mulundumina Shimaponda.

I am deeply indebted to my family; especially to my wife KINUA Ghislaine MONGA, my children SCHONS-ARCHE MONGA, SCOTT-BLISS MONGA and SKY-TRINITY MONGA, who have accepted to pay the price of great sacrifice as this research took me a lot of time away from them.

KABOKO Jean-Jacques MONGA.

Table of content

Abstract	i
Dedication	iii
Acknowledgements	iv
Table of content	vi
List of figures	x
List of tables	xvii
List of acronyms	xviii
Chapter 1 Introduction	1
1.1 Background	2
1.2 Project motivation	7
1.3 Research objectives	10
1.4 Research methodology	11
1.5 Layout of the dissertation	13
Chapter 2 Fiber lasers and Q-switched fiber lasers	16
2.1 Introduction	17
2.2 Rare-earth doped fibers	17
2.3 Erbium-doped fiber	20
2.3.1 Emission and absorption cross-section	21
2.3.2 Lifetimes of the Erbium-doped fiber levels	23
2.4 Basics of fiber lasers.....	25
2.4.1 Erbium-doped fiber laser configurations	31
2.4.2 Pumping process in Erbium-doped fiber lasers	34

2.5 Theoretical model of Erbium-doped fiber lasers.....	35
2.6 Q-Switched Erbium-doped fiber laser.....	39
2.6.1 Q-Value of a fiber laser cavity	40
2.6.2 Principle of Q-switching in fiber laser	40
2.7 Q-switched fiber laser pulse characteristics	42
2.7.1 Output pulse energy	46
2.7.2 Pulse time duration	47
2.7.3 Peak power characteristic for a train of Q-switched fiber laser pulses	48
2.8 State of the art of all-fiber actively Q-Switched lasers.....	51
2.9 Summary	61
Chapter 3 Implementation all-fiber Q-witched Erbium-doped ring laser	62
3.1 Introduction	63
3.2 Construction of an all-fiber Erbium-doped fiber ring laser.....	63
3.2.1 Fiber Fabr-Perot tunable filter	64
3.2.2 Experimental characterisation of the fiber Fabry-Perot tunable filter	67
3.2.3 Fiber Bragg grating	70
3.2.4 Characterisation of a fiber Bragg grating	72
3.2.5 All-Fiber Q-switching device	74
3.3 All-fiber active Q-switched fiber laser.....	76
3.4 Experimental Q-switched fiber ring laser.....	78
3.4.1. Optimal output coupling ratio	81
3.4.2 Optimum Erbium-doped fiber Length	83
3.4.3 Pulsed regime of fiber laser	86
3.4.4 Effect of Erbium ion concentration and Erbium-doped fiber length	89
3.4.5 Effect of scanning frequency of the fiber Fabry-Perot tunable filter	91

3.4.6 Extinction ratio	94
3.5 Summary	95
Chapter 4 Implementation all-fiber Q-witched Erbium-doped laser in a linear cavity	97
4.1 Introduction	98
4.2 Design of the linear cavity Q-switched fiber laser	99
4.3 Experimental set-up of linear cavity Q-switched fiber laser	104
4.4 Experimental results of Q-switched fiber laser	108
4.5 Summary	112
Chapter 5 Output stability and linewidth of fiber lasers	113
5.1 Introduction	114
5.2 Background of single longitudinal mode fiber laser	115
5.3 Methods of achieving narrow linewidth fiber laser operation.....	120
5.4 Linewidth measurement techniques.	122
5.5 Delay self-heterodyne measurement technique.....	126
5.6 Experimental procedures and results.....	129
5.7 Summary	140
Chapter 6 Modelling of a Q-Switched Erbium-doped fiber ring laser	141
6.1 Introduction	142
6.2 Background	143
6.3 Travelling wave model.....	147
6.4 Active Q-switched fiber laser modeling.....	148
6.5 Solution algorithm	152

6.6 Simulation results	154
6.7 Model validation with experimental results	162
6.8 Summary	163
Chapter 7 Conclusions	167
7.1 Chapter overview	168
7.2 Discussions and future work.	168
Bibliography	176



List of figures

Figure 1.1: Schematic illustration of an all-fiber active Q-switched fiber laser (Pérez-Millán et al., 2005). -----	5
Figure 1.2: a) Reflection spectrum of two fiber Bragg gratings when the cavity is open; b) Reflection spectrum of two fiber Bragg gratings when the cavity is closed (Pérez-Millán et al., 2005). -----	6
Figure 2. 1: Optical fiber structure. -----	18
Figure 2.2: Lifetimes and absorption wavelength for Erbium energy levels (Bellemare, 2003).-----	20
Figure 2.3: Intensity distribution for emission and absorption spectra of an Erbium-doped fiber as a function of the wavelength. -----	22
Figure 2.4: Illustration of the quenching effect in Erbium-doped fibers (Snitzer, 1964). -----	25
Figure 2.5: Two energy levels representations illustrating: (a) Stimulated absorption, (b) Spontaneous emission and (c) Stimulated emission.-----	26
Figure 2.6: Basic laser configuration: The feedback is accomplished with the help of two mirrors. -----	30
Figure 2.7: Example of a linear cavity fiber laser.-----	32
Figure 2.8: Example of a ring fiber laser cavity.-----	33

Figure 2.9: Schematic illustration of a Q-switched Erbium-doped fiber linear cavity.	39
Figure 2.10: Formation of a Q-switched fiber laser pulse. N_i is the population inversion at the beginning of the Q-switched pulse; N_t is the population inversion at the threshold and N_f is the population inversion at the end of the Q-switched pulse.	41
Figure 2.11: Illustration of an all-fiber Q-switched fiber ring laser (X.P Chang et al. (2008)).	55
Figure 2.12: Illustration of an all-fiber Q-switched fiber ring laser (X.P Chang et al. (2008)).	56
Figure 2.13: All-optical Q-switched laser using a Fabry-Perot etalon and a scanning Fabry-Perot filter.	57
Figure 2.14: All-fiber Q-switched laser using an acousto-optic modulator of a fiber Bragg grating linear cavity (Delgado-Pinar M.et al., 2006).	57
Figure 2.15: All-fiber Q-switched laser using an acousto-optic modulator of a fiber Bragg grating ring cavity (Miguel V. Andrés et al., 2006).	58
Figure 2.16: Illustration of all-optical Q-switched fiber lasers using an optically-tunable fiber Bragg grating in a fiber laser (Robert et al. (2010)).	59
Figure 2.17: Experimental set-up of a pulse time duration tunable Erbium fiber laser (Zhi-Zheng et al., 2010).	60
Figure 3.1: Schematic configuration of a fiber Fabry-Perot tunable filter.	65

Figure 3.2: Experimental setup used to characterize the fiber Fabry-Perot tunable filter -----	67
Figure 3.3: Dependence of the transmission wavelength of the fiber Fabry-Perot tunable filter versus the applied voltage. -----	68
Figure 3.4: Transmittance spectrum of the Fabry-Perot filter, optical power versus the wavelength.-----	69
Figure 3.5: Schematic diagram of a fiber Bragg grating. Λ : grating period, n_{eff} : effective core index.-----	71
Figure 3.6: Experimental set-up used to characterize the fiber Bragg grating. -----	72
Figure 3.7: Reflection spectrum of a fiber Bragg grating.-----	73
Figure 3.8: Illustration of all-fiber Q-switching device. -----	74
Figure 3. 9: Illustrations of the spectral overlap between the transmission spectrum of Fabry-Perot filter and reflection spectrum of fiber Bragg grating. -----	75
Figure 3.10: Experimental set-up of an all-fiber active Q-switched ring laser. -----	77
Figure 3.11: Power spectrum when the spectra of the fiber Bragg grating and Fabry- Perot filter do not overlap. -----	79
Figure 3.12: Illustration of the emission spectrum of the fiber laser when the reflected spectrum of the fiber Bragg grating and the transmission spectrum of Fabry-Perot filter overlap. -----	80
Figure 3.13: Normalized output power versus output coupling ratio. -----	82
Figure 3.14: The output power of the fiber ring laser as a function of Erbium-doped fiber length and different Erbium concentration. -----	84

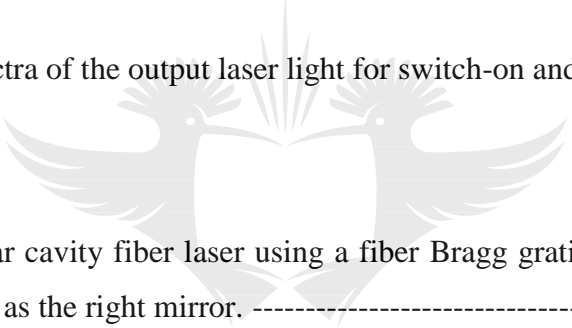
Figure 3.15: Output power versus pump power in continuous wave fiber ring laser.	85
Figure 3.16: Train of the generated light pulses.	86
Figure 3.17: Dependence of the laser output peak power on the length of the Erbium-doped fibers with different ion concentration.	89
Figure 3.18: Output peak power and time duration of the light pulses as a function of the scanning frequency of the Fabry-Perot filter.	91
Figure 3.19: Dependence of the output peak power on the frequency and amplitude of the sinusoidal signal.	93
Figure 3.20: Spectra of the output laser light for switch-on and switch-off.	94
	
Figure 4.1: Linear cavity fiber laser using a fiber Bragg grating as left mirror and a looped circulator as the right mirror.	100
Figure 4.2: Multi-wavelength laser emissions in 1600 nm window.	101
Figure 4.3: Linear cavity fiber laser using a fiber Bragg grating as right mirror and a looped circulator as left mirror. The tunable filter is inserted between the FBG and the EDF.	102
Figure 4.4: Broad spectrum emissions of the fiber laser in 1560 nm region.	103
Figure 4.5: Experimental set-up of the linear cavity Q-switched fiber laser.	104
Figure 4.6: Illustration of the transmission spectrum of fiber Fabry-Perot tunable filter and reflection spectrum of the fiber Bragg grating.	106
Figure 4.7: Output power versus absorbed pump power.	107

Figure 4. 8: Output peak power and time duration of the Q-switched fiber laser pulses as a function of repetition rate. -----	109
Figure 4.9: Output peak power and time duration of Q-switched pulses as a function pump power. -----	110
Figure 4. 10: Spectra of the output laser light for Q-switch-on and Q-switch-off. -	111
Figure 5.1: Field distribution of two adjacent modes and population inversion of the initial oscillation. -----	119
Figure 5.2: Coherent detection technique for linewidth measurements. -----	123
Figure 5. 3: Delayed self-heterodyne interferometer (DHSI) technique using a Mach-Zehnder interferometer (MZI). -----	126
Figure 5.4: Erbium-doped fiber ring laser with linewidth measurement system. ---	130
Figure 5.5: Beat spectrum of Erbium-doped fiber ring laser measurements averaged 100 times without un-pumped fiber (blue) experimental collected data (red) Lorentzian fitting for the beat spectrum. -----	132
Figure 5.6: Output power stability for Erbium-doped fiber ring cavity fiber laser: (a) Normalized power stability versus time with output coupling ratios as parameters and without an un-pumped fiber for different coupling ratio (b) Normalized power stability versus time for 10 % and 90 % output coupling ratios with an un-pumped fiber. --	133
Figure 5.7: Beat spectrum of Erbium-doped fiber ring laser measurements averaged 100 times with un-pumped EDF fiber; (blue) experimental collected data (red) Lorentzian fitting for the beat spectrum. -----	135

Figure 5.8: Erbium-doped fiber ring laser with linewidth measurement system. ---	136
Figure 5.9: Normalized power stability versus time for fiber linear cavity (blue) without additional un-pumped doped fiber (green) with 1.5 m additional un-pumped Erbium-doped fiber.-----	137
Figure 5.10: Beat spectrum of Erbium-doped fiber linear cavity laser measurements averaged 100 times without un-pumped fiber (blue) experimental collected data (red) Lorentzian fitting for the beat spectrum. -----	138
Figure 5.11: Beat spectrum of Erbium-doped fiber linear cavity fiber laser measurements averaged 100 times with un-pumped EDF fiber; (blue) experimental collected data (red) Lorentzian fitting for the beat spectrum. -----	139
Figure 6.1: Q-switched Erbium-doped fiber laser set-up. -----	147
Figure 6.2: Flowchart of the simulation algorithm. -----	152
Figure 6.3: Output peak power and gain evolution at 60 mW pump power. -----	156
Figure 6.4: Output peak power versus pump power. -----	157
Figure 6.5: a) Output peak power versus pump power at different repetition rates and b) pulse time duration versus pump power at different repetition rates. -----	158
Figure 6.6: a) Output peak power versus repetition rate at different pump powers and b) pulse time duration versus repetition rate at different pump powers. -----	160
Figure 6.7: Output peak power versus Erbium-doped fiber length.-----	161
Figure 6.8: Time duration of pulses as a function of the scanning frequency, simulation (green) and experimental results (blue).-----	162

Figure 6.9: Multi-peak generation of Q-switched fiber laser pulses at low scanning frequency of the fiber Fabry-Perot tunable filter.-----163

Figure 6.10: Output peak powers as a function of Fabry-Perot filter scanning frequency: simulation results compared to experimental results.**Error! Bookmark not defined.**



List of tables

Table 5.1: Delayed self-heterodyne linewidth relations (Dennis Derickson , 1998).
-----128

Table 6.1: Parameters used in the simulation of the actively Q-switched fiber laser.
-----155



List of acronyms

AOM	Acousto-Optic Modulator
ASE	Amplified Spontaneous Emission
CW	Continuous Wave
EDF	Erbium-Doped Fiber
EOM	Electro-Optic Modulator
Er	Erbium
FBG	Fiber Bragg Grating
F-PF	Fabry-Perot Filter
F-PTF	Fabry-Perot Tunable Filter
FF-PTF	Fiber Fabry-Perot Tunable Filter
fs	Femtosecond
FWHM	Full Width Half Maximum
HR	High Reflectance
HT	High Transmittance
IR	Infrared
LD	Laser Diode
LASER	Light Amplification by Stimulated Emission of Radiation
MM	Magnetostrictive Modulators

MASER	Microwave amplification by stimulated emission of radiation
mW	milliwatt
ns	Nanosecond
OC	Output Coupler
OSA	Optical spectrum analyzer
PD	Photo-Diode
ps	Picoseconds
PZT	Piezoelectric
QSMZFL	Q-switched Mach-Zehnder Fiber Laser
TFPF	Tunable Fabry-Perot Filter
WDM	Wavelength Division Multiplexing
XPM	Cross Phase Modulation
Yb	Ytterbium
μm	Micrometer
CFBG FP	Chirped Fiber Bragg grating Fabry-Perot

Chapter 1

Introduction



UNIVERSITY
OF
JOHANNESBURG

1.1 Background

Rare-earth-doped fiber lasers have attracted growing interest in various fields, such as telecommunications, optical time domain reflectometry (OTDR), laser machining, and medicine. The optical confinement admitted by the optical fiber, associated with the exceptional intrinsic laser properties of rare-earth ions, make this kind of lasers significantly coherent in time and space, with good compactness and diverse wavelength selection range. Rare-earth ions such as Thulium (Tm^{3+}), Praseodymium (Pr^{3+}), Erbium (Er^{3+}), Ytterbium (Yb^{3+}), Neodymium (Nd^{3+}) and Holmium (Ho^{3+}) have been used in optical fiber lasers for different wavelength emission (Digonnet, 2001).

Rare-earth doped fiber lasers have been pioneered by experiment reported in (Snitzer, 1961) and (Koester and Snitzer, 1964), respectively. Since then, tremendous work followed, and fiber lasers have become valuable research direction. Fiber lasers are generated in two main temporal regimes namely continuous-wave and pulsed laser operation. Continuous-wave and pulsed fiber lasers were demonstrated and employed in a variety of applications. Particularly, the repetition rate, time duration and peak power and system smallness required for these applications make the generation of laser pulses a very active research area (Sharma, Kim and Kang, 2004).

Different techniques like pulse carving, gain switching, mode-locking and Q-switching are utilized in short pulse generation. Mode-locking and Q-switching are the most popular

and effective techniques to obtain laser pulses. Nonetheless, in this project, the focus is oriented toward fiber laser based on Q-switching technique. The topic is broadly covered by (Siegman, 1986; Digonnet, 2001; Silfvast, 2011; Shi *et al.*, 2014).

The Q-switching technique consists on the modulation of the quality factor Q of a fiber laser. The quality factor of a fiber laser cavity is defined as the ratio between the stored energy in the gain medium and that lost per oscillation cycle (Sveto, 1998). Thus, the higher the quality factor, the lower the fiber laser cavity loss, and vice-versa. The active gain medium of the Q-switching fiber laser is pumped while the lasing process is initially prevented by a low Q factor. As soon as the quality factor is modulated from low to high, the stored energy is then released in a large pulse of duration ranging from microsecond to nanosecond. The lifetime of the rare-earth ions in the active gain medium, participating in the amplification process, determines the time needed to stock up the extracted energy between two consecutive pulses.

The Q-switching of the fiber laser can be performed in a passive or active way. Passive Q-switched fiber lasers use a passive element like a saturable absorber (Filippov, Starodumov and Kir'yanov, 2001; Paschotta, 2009; Tsai and Fang, 2009). Active Q-switched fiber lasers need active control elements such as acousto-optic modulator (AOM) and electro-optic modulator (EOM) (Myslinski *et al.*, 1992; Morkel, Jedrzejewski and Taylor, 1993; Alvarez-Chavez *et al.*, 2000; Wang and Xu, 2007a).

Recently, there has been a certain technological interest in active Q-switched fiber lasers development because of their possibility of controlling the repetition rate, peak power and time duration of laser pulses. This is not possible with passive Q-switched fiber lasers. Above all, the trend of research in the Q-switched fiber laser is oriented toward developing all-fiber-based laser cavity which allows robust construction, high efficiency, all-fiber splicing cavities, and narrow spectral linewidth.

Newly methods for actively all-fiber Q-switched lasers have been developed for telecommunication wavelengths around 1550 nm (Chandonnet and Larose, 1993; Huang, Liu and Yang, 2000; Russo *et al.*, 2002; Kaneda *et al.*, 2004; Pérez-Millán *et al.*, 2005). All-fiber Q-switched lasers based on a variety of switching mechanisms, including all-fiber acoustically modulated attenuators (Huang D. W., 2000), microsphere resonator (Kieu K and Mansuripur M., 2006), and all-fiber phase modulators (Sheu F. W. and Kang J. J., 2007) have been reported.

Another reported method to switch the quality factor Q of a fiber laser cavity is based on tuning the reflection bands of fiber Bragg gratings (FBGs) used as laser mirrors; stretching and relaxing the FBG using magnetostrictive transducers (Pérez-Millán P. *et al.*, 2005), acousto-optic modulators (Cuadrado-Laborde C *et al.*, 2007), and piezoelectric actuators (Cheng X. P., 2008).

An example of an all-fiber actively Q-switched laser is illustrated in Figure 1.1.

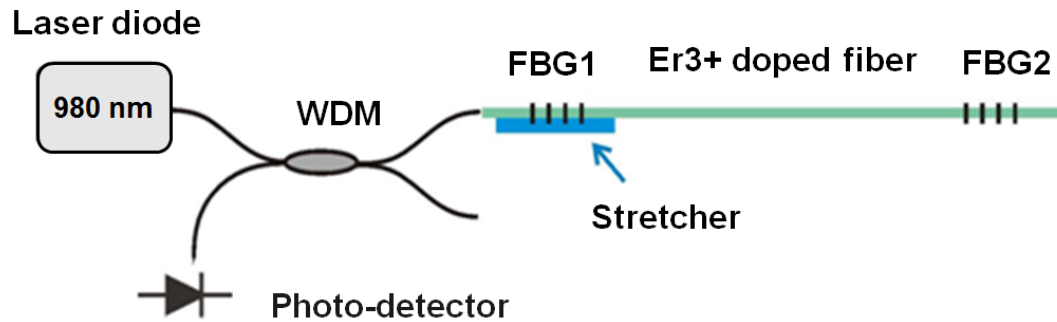


Figure 1.1: Schematic illustration of an all-fiber active Q-switched fiber laser (Pérez-Millán *et al.*, 2005).

The fiber laser includes an Erbium-doped fiber used as gain medium and a laser diode emitting at 980 nm wavelength used as a pump source. The Erbium-doped fiber is spliced between two fibers Bragg gratings (FBG1 and FBG2) used as mirrors. In this configuration, the reflection spectrum of FBG1 can be changed by applying an external stress on it, while the reflection spectrum of FBG2 remains unchanged.

Initially, the reflection spectra of the two fiber Bragg gratings are different (Figure 1.2 a) and the fiber laser cavity is open (low Q). The fiber laser experience high cavity loss which inhibits the output power from the fiber laser. Then, after the reflection spectra of both fibers Bragg gratings are the same (Figure 1.2 b), the fiber laser cavity is closed (high Q). The Q-switching is achieved by periodically stretching and releasing the active fiber Bragg grating FBG1, which is attached to a stretcher.

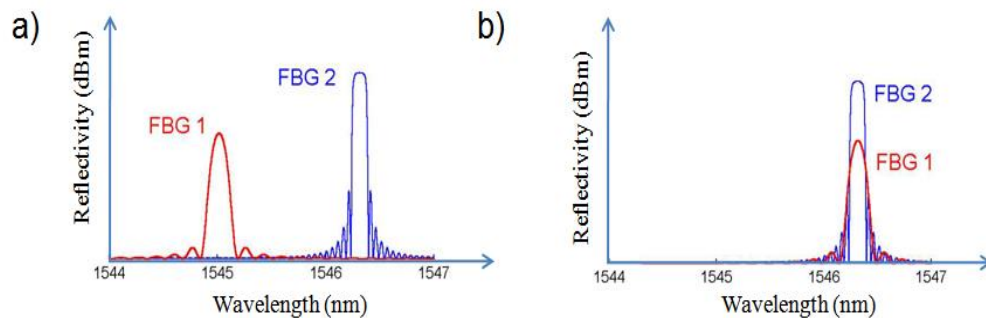


Figure 1.2: a) Reflection spectrum of two fiber Bragg gratings when the cavity is open; b) Reflection spectrum of two fiber Bragg gratings when the cavity is closed (Pérez-Millán *et al.*, 2005).

Regardless of their simplicity, these methods have some limitations such as unwanted strain in the FBG as it is usually attached to the modulator, as well as the speed of the deformation applied to the fiber Bragg grating for tuning purposes: it is very easy to damage the fiber Bragg grating if it is stretched and relaxed at high frequency. Depending of the fiber exposure to ultraviolet light during manufacturing, fiber Bragg grating make support scanning speed up to some kilohertz. To avoid these unwanted effects, another reported configuration includes a Fabry–Perot filter and an in-line abrupt-tapered Mach–Zehnder filter (Chen N. K. *et al.*, 2010). The FBG does not require tuning; the cavity is switched as the spectral transmittance of the filters overlap on/off. However, the tapered fiber makes the configuration fragile. The Mach–Zehnder fiber filter is manufactured using highly Erbium-Ytterbium co-doped fiber. In this configuration, the extinction ratio (switched-on/switched-off power ratio) of

the laser is only 17.1 dB, which is relatively low compared to similar reported fiber laser configuration. In order to increase it, a special attention while manufacturing the Mach-Zehnder filter is crucial (Chen N. K. *et al.*, 2010).

In this thesis, a new Q-switching approach is proposed. The active Q-switching mechanism is based on a spectral overlap between the reflection spectrum of a fiber Bragg grating and transmission spectrum a tunable fiber Fabry-Perot filter. In this technique, the active fiber Bragg grating is substituted with a tunable fiber Fabry-Perot filter to take advantage of its robustness as compared fiber Bragg grating during modulation at high frequency.

1.2 Project motivation

Q-switched fiber lasers are important for a variety of applications including telecommunication; remote sensing and distributed fiber-optic sensors based on linear reflection from multiplexed FBG based interferometers and/or Rayleigh backscattering (Wang Y. and Xu C. Q., 2007). For application in fiber optic sensors and telecommunication, some of the most important required parameters of the laser are system robustness, the high contrast of output light pulses (extinction ratio), narrow linewidth of the output light and possibility to rapidly switch the output wavelength or dual-wavelength operation (Durán-Sánchez M. *et al.*, 2015; González-García A. *et al.*,

2015). Sharma *et al.* (2004) developed a Q-switched Erbium-doped fiber laser for a differential absorption Lidar. This laser was pumped with 100 mW and delivered pulse energy of 10 μJ /pulse; with pulse width of 1.5 μs at 20 kHz repetition rate. Kaneda *et al.* (2004) reported a Lidar using a fiber laser characterized by 20 W output peak power, 12 ns pulse duration at 80 kHz of repetition rate. The fiber laser consisted of a 2 cm long Ytterbium-Erbium-doped phosphate glass fiber and was pumped with a 370 mW laser diode in a linear cavity.

Fiber laser sources that own narrow linewidth property are required for enabling high capacity network, corresponding to the narrower optical beam inside a waveguide. In contrast, fiber lasers normally operate in multi-longitudinal modes due to small spacing between the emitted longitudinal modes. At the same time, to achieve narrow optical laser emission spectrum or single frequency fiber laser operation is a challenging task.

Several techniques has been introduced to achieve narrow linewidth operation of fiber lasers such as using a compact and short linear cavity to broaden the spacing of between the longitudinal modes and eradicate multi-longitudinal modes fiber laser oscillation (Zyskind, J.L. *et al.*, 1992). However, the short length of the fiber laser cavity limits the output power. An alternative proposed method is to use a long fiber laser cavity and additional optical components. For instance, ultra-narrow bandpass filter based on phase-shifted fiber Bragg grating, to remove the multi-longitudinal

mode laser operation and mode competition triggered by the long fiber laser cavity length. This results in the narrow longitudinal mode spacing (Yu Yao *et al.*, 2006). Other methods such as using fiber Bragg grating based Fabry–Perot (FP) filter (Sun Szkopek and Smith, 2003; Cheng *et al.*, 2008), a saturable absorber based Sagnac loop (Zhang and Kang, 2008), a fiber Bragg grating based Fabry-Perot filter together with a narrow-band fiber Bragg grating and a fiber-based saturable absorber have been established to providing an excellent mode selection for a fiber laser. Feng T. *et al.* reported a combination of a narrow-band fiber Bragg grating based Fabry-Perot filter, a section of un-pumped Erbium-doped fiber (EDF) as a saturable absorber, and an all-fiber polarizer (Feng *et al.*, 2014).

In this project, an advanced Q-switching approach in Erbium-doped fiber lasers is proposed and experimentally investigated. Improvement and optimization in term of the design and the use of suitable devices to develop Q-switched Erbium-doped fiber laser systems are targeted. Fiber laser characteristics that yields peak power, time duration, output power stability, extinction ratio, narrow linewidth, robustness and simplicity required for potential applications motivate this research project. In addition, another importance of this research is the development of a customized numerical model to validate the new Q-switching technique proposed this project. A refined numerical technique to simulate the Q-switched fiber laser characteristics, peak power and time duration is suggested. Effects of fiber laser cavity parameters

such as pump power, Erbium-doped fiber length and repetition rate of pulses are evaluated.

1.3 Research objectives

Q-switched fiber lasers have been extensively and actively studied for its concept, designs, and various physical phenomena involved in its operation. The purpose of the research presented in this thesis has been focused on proposing and demonstrating an innovative Q-switching mechanism in fiber lasers. Hence, the experimental and simulation results obtained from this study are important as a reference source for the future experiments and implementations. Therefore, this research includes both theoretical and experimental contributions. The project objectives are:

- ❖ Design and build all-fiber Q-switched Erbium-doped lasers which exploit the spectral overlapping mechanism between the reflection spectrum of a fiber Bragg grating and the transmission spectrum of a tunable fiber Fabry-Perot filter.
- ❖ Test and characterize the Q-switched fiber lasers in both linear and ring cavity arrangement.
- ❖ Perform experiments in continuous wave and pulsed regime to study the fiber laser output features, peak power, time duration, output stability, extinction

ratio and linewidth as function pump power, repetition rate, doped fiber concentration, doped fiber length and coupling ratio.

- ❖ Explore and implement techniques to stabilize the output power and narrow the linewidth the investigated fiber lasers.
- ❖ Explore and implement linewidth measurement technique suitable for the fiber lasers.
- ❖ Develop a customized numerical method to simulate the Q-switching approach introduced in this project.
- ❖ Explore various physical mechanism involved in Q-switched fiber laser and their effects on the peak power and time duration of pulse output.
- ❖ Validate simulation results against the obtained experiments results.

1.4 Research methodology

Prior to the experimental investigation, literature studies, as well as the understanding of the working principle of the Q-switched fiber lasers are first presented. Subsequently, reviews on the state of art in all-fiber Q-switched fiber laser configuration are discussed. Advantages and shortcoming of leading all-fiber active Q-switching techniques are highlighted to identify new avenues to improve characteristics and system design of all-fiber Q-switched fiber laser systems.

Furthermore, fiber laser characteristic such as output power stability and linewidth are underlined.

Upon completion of the literature review, the design of Q-switching approach proposed in project is presented. The design of the all-fiber active Q-switched fiber laser is described and experimentally characterized in both ring cavity and linear cavity configurations. Erbium-doped fiber is chosen as gain medium in fiber laser cavities. The choice of Erbium-doped fiber is motivated by its emission spectrum in the C band of telecommunication (around 1550 nm), where the telecommunication fibers exhibit a low loss characteristic. We first characterized the fiber laser systems in the continuous wave regime to determine optimal cavity parameters such as pump power, Erbium ion concentrations, fiber laser cavity length and output coupling ratio. The fiber lasers are then characterized in pulsed (Q-switching) regime to determine peak power and time duration of pulses as a function of the cavity parameters.

With Q-switched fiber lasers fully characterized, we proceed with the output power stability and linewidth characterisation of the fiber lasers systems, for both ring and linear fiber laser cavity configurations. Brief highlights on key physical phenomena that lead to multimode laser operation in fiber laser are provided. Techniques to stabilize the output power and narrow the linewidth are discussed. Important linewidth measurement techniques are reviewed. Delay self-heterodyne technique is chosen as being the best suited technique for the range of linewidth measured in this project.

Because the existing literature does not address the Q-switching approach experimentally demonstrated in this project, we complete this project with well elaborated numerical model to simulate the Q-switched Erbium-doped fiber ring laser. We validate the model by comparing simulation results against obtained experimental results.

1.5 Layout of the dissertation

There are seven Chapters in this thesis. Chapter 1 covers the opening description of this research which comprised of brief history and background of the all-fiber Q-switched fiber laser and its characteristics requirement for various applications. The project motivation, objectives and significance of this research are also incorporated in this Chapter.

In Chapter 2, literature review pertaining to this research is presented. Basic concepts related to rare-earth doped fiber lasers are outlined. Short pulse generation based on Q-switching is fully discussed. A state-of-the-art review on all fiber active Q-witched lasers is presented to put in perspective the experimental results achieved in this research.

The design and working principle of the Q-switching mechanism introduced in this project is described in Chapter 3. The proposed Q-switching approach in fiber laser is based on the spectral overlapping of two optical fiber filters to modulate the intra-cavity loss in the fiber laser. The Q-switching technique is implemented in Q-switched fiber ring laser system and experimentally characterized. Peak power and pulse duration of the fiber laser pulses are evaluated as a function of cavity parameters such as Erbium-doped fiber length, Erbium ions concentration in the doped fiber and output coupling ratio. The extinction ratio of the fiber laser, which is an important characteristic of fiber laser for potential sensor application, is measured and parameters affecting it are discussed.

In Chapter 4, the implementation of the Q-switching technique in a linear cavity configuration is presented. A well-elaborated description of the experimental set-up and comprehensive characterisation are provided. Obtained characteristics of the fiber laser pulses, as well as the fiber laser extinction ratios, are discussed.

In Chapter 5, the linewidth and output power stability of the fiber laser sources implemented in Chapter 3 and Chapter 4 are measured. Physical phenomena that lead to multimode fiber laser emission are first discussed. This includes the cause of output power instability in the fiber laser. Different techniques to measure the linewidth of the fiber laser are explored. Method to improve the output power stability and

linewidth are discussed in this Chapter. The significance of the experimental results is finally highlighted.

In Chapter 6, a detailed computer model to reproduce the physical phenomena involved in Q-switching and their effects on the temporal response of the pulse output is described. Dependence of Q-switched fiber laser output pulse characteristic on various fiber laser cavity parameters such as pump power, cavity length and repetition rate is established through simulation.

Chapter 7 Sums up the project with concluding remarks and research output that answered the projected objectives. Results discussions and recommendations for future work in all-fiber Q-switched fiber laser are provided in this Chapter.



Chapter 2

Fiber lasers and Q-switched fiber lasers



UNIVERSITY
OF
JOHANNESBURG

2.1 Introduction

An overview of the theory is presented in different sections of this Chapter. The main focus is on Q-switched Erbium-doped fiber lasers. First, basic concepts and characteristics of rare-earth-doped fiber laser systems are reviewed. We distinguish between continuous wave and pulsed Erbium-doped fiber lasers and concentrate more on active Q-switching techniques. The theory of the improved active Q-switched fiber laser systems is presented. The shortcomings of Q-switched laser systems using optical bulk components like acousto-optic modulators and electro-optic modulators, as compared to all-fiber based active Q-switching fiber lasers are discussed. Finally, a state of arts review on all-Q-witched fiber lasers is presented.

2.2 Rare-earth doped fibers

Since its invention in the mid-20th century, fiber optics has been a very important technological achievement. In 2009, Charles K. Kao shared the Nobel Prize in physics with George E. Smith and Willard Boyle for his pioneering work in optical communication. In 1966, Kao published a joined research paper with George A. Hockham recommending the utilization of optical fiber for low-loss guiding of light

(Kao, K. C. and Hockham, G. A. , 1966). From that point forward, optical fibers have been used to transport laser light in optical telecommunication networks

A typical structure of optical fiber is illustrated in Figure 2.1, which is fundamentally a cylindrical dielectric waveguide made from silica glass.

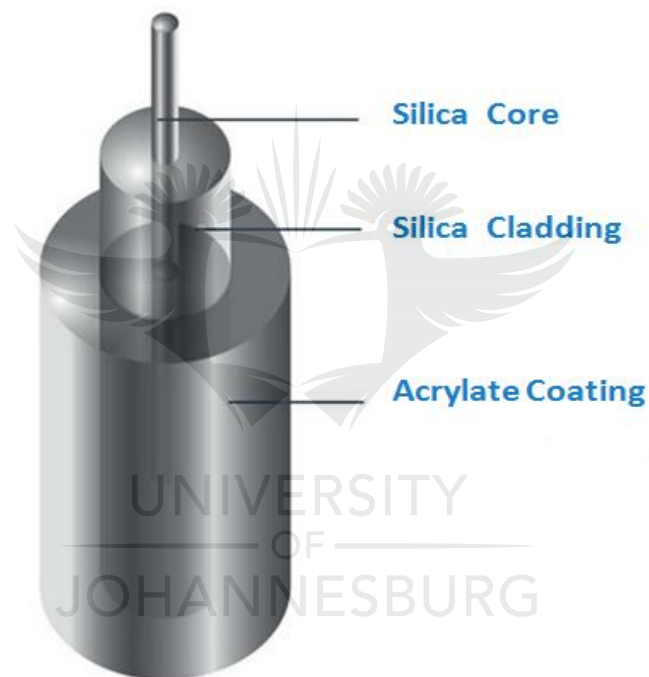


Figure 2. 1: Optical fiber structure.

An optical fiber comprises of a core with a refractive index n_1 , surrounded by a cladding with a slightly lower refractive index n_2 . An external coating made out of

polymer provides mechanical strength and protection to the fiber (Guenther, 1990; Verdeyen, 1995; Agrawal, 2013)

By doping optical fiber with rare-earth elements, amplification can be achieved directly inside the optical fiber without electronic manipulation of the signal. There exist two groups of rare-earth atoms, namely the lanthanides and actinides. These atom groups contain 14 elements each. The lanthanides fill the 4f shell and have atom numbers from 57 to 71. The actinides fill the 5f shell and the atomic numbers range from 90 to 103. A considerable part of rare-earth doped fibers is doped with lanthanides ions. Rare-earth-doped fibers are usually employed as amplifying medium in fiber lasers. Depending on the desired operating wavelength of a fiber lasers, an appropriate rare-earth doped fiber is chosen. The most common rare-earth-doped ions used in fiber laser are Praseodymium, Neodymium, Europium, Holmium, Ytterbium, Thulium and Erbium (Digonnet, 2001; Paschotta, 2009).

2.3 Erbium-doped fiber

In a silica or glass matrix, Erbium is embedded as trivalent ions $[\text{Er}^{3+}]$ with a $4f^1 5s^2 5p^6$ (Paschen notation) electronic structure (Bellemare, 2003). A number of Erbium transitions start from the 4f state, as illustrated in Figure 2.2.

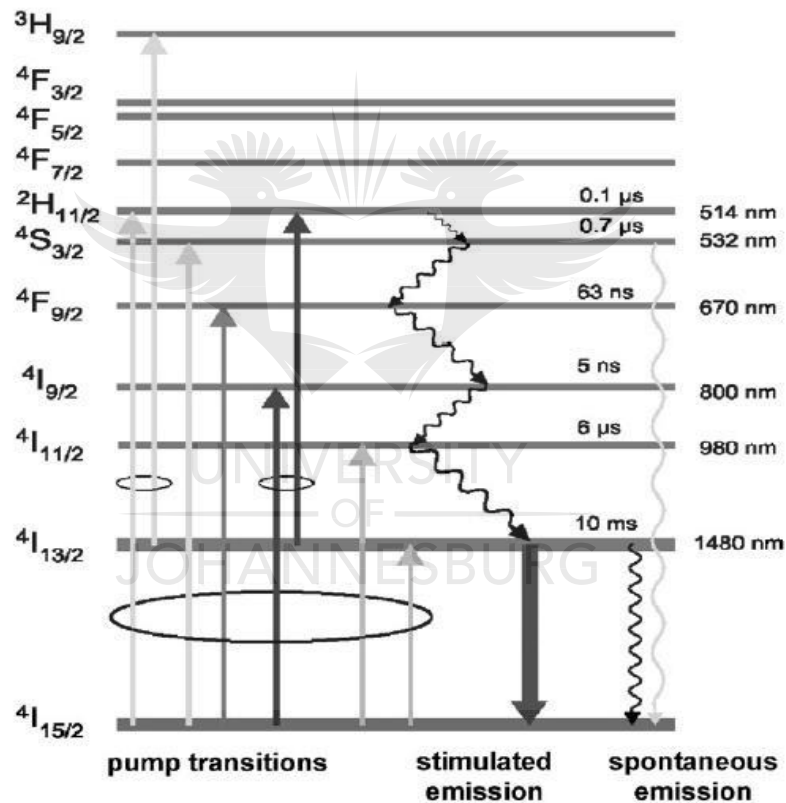


Figure 2.2: Lifetimes and absorption wavelength for Erbium energy levels (Bellemare, 2003).

Since the 4f state is partially isolated from the 5s and 5p states, the Erbium emission and absorption spectra are relatively unaffected by the type of the host material. However, the photons energies influence the lifetimes of the excited energy levels of the host material (Myslinski *et al.*, 1992).

The main energy levels of the Erbium ions together with pump wavelengths and lifetimes are also illustrated in Figure 2.2. The excited energy levels can be pumped by different laser wavelengths, e.g. the $^4F_{9/2}$ level can be pumped by 670 nm. The excited energy levels decay quickly and non-radiative to the metastable level $^4I_{13/2}$. Metastable level means that this level has a very long lifetime. The lifetime of the Erbium-doped fiber metastable is about 10 ms.

2.3.1 Emission and absorption cross-section

The intensity distribution of emission and absorption spectra in an Erbium-doped fiber as a function of the wavelength is illustrated in Figure 2.3. An Erbium-doped fiber displays a broad emission spectrum around 1550 nm. This wavelength range is known to be suitable for low loss characteristic of transmission fibers used in a telecommunication network.

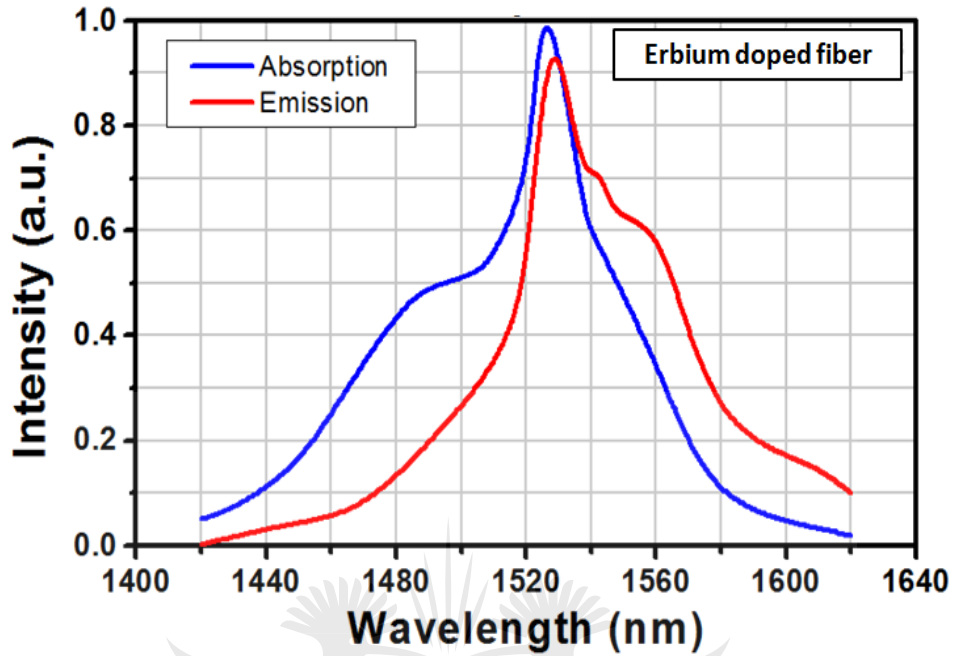


Figure 2.3: Intensity distribution for emission and absorption spectra of an Erbium-doped fiber as a function of the wavelength.

The Erbium-doped fiber absorption cross-section is given by:

$$\sigma_{abs} = \frac{W_p}{\frac{P_p}{h\nu_p} A} \quad (2.1)$$

where W_p is the probability per second of pump absorption efficiency of each ground state carrier that is pumped to the metastable. P_p is the optical pump power. $\frac{P_p}{h\nu_p}$ is the number of incoming pump photons per second, ν_p is the optical pump frequency and A is the effective fiber core cross-section area.

The emission cross-section of Erbium-doped fiber is given by:

$$\sigma_{em} = \frac{W_s}{\frac{P_s}{A} \cdot h\nu_s}, \quad (2.2)$$

where, P_s and ν_s are the emitted laser power and frequency, respectively. W_s is the stimulated emission efficiency or the probability of each carrier in the metastable state that recombines to produce a photon within each second.

Emission and absorption cross-sections are related by the McCumber formula (Desurvire, 1995; Becker, Olsson and Simpson, 2003).

$$\sigma_{em}(\nu) = \sigma_{abs}(\nu) \exp\left(\frac{\epsilon - h\nu}{kT}\right) \quad (2.3)$$

where, h is the Plank constant, k the Boltzman constant, ν is the frequency and ϵ the net free energy required to excite one Erbium ion from the $^4I_{15/2}$ state to the $^4I_{13/2}$ state at the absolute temperature T .

2.3.2 Lifetimes of the Erbium-doped fiber levels

The population of excited levels in Erbium-doped fiber depletes exponentially with a time constant corresponding to the lifetime of the energy level. Transition probability rate of excited levels is inversely proportional to the lifetime of each respective energy

level. The depletion of population follows two main pathways, which include the radiative and non-radiative depletion pathways. The total transition probability is given by the sum of the probabilities of each depletion path as (Desurvire, 1995) :

$$\frac{1}{\tau} = \frac{1}{\tau_r} + \frac{1}{\tau_{nr}} \quad (2.4)$$

where τ is the total lifetime, τ_r the radiative lifetime and τ_{nr} the non-radiative lifetime.

The composition of the glass affects the lifetimes of the Erbium-doped fiber levels. The lifetime of the radiative transition mainly depends on the transitions probability between an excited level and all lower energy levels. The typical radiative lifetime of the metastable level of Erbium-doped fiber is about 10 ms.

The non-radiative lifetimes depend mostly on the concentration of the doped fiber (Lidgard, Simpson and Becker, 1990). One important non-radiative transition is pair induced quenching. This non-radiative interaction is extensively discussed in the literature (Lidgard, Simpson and Becker, 1990; Miniscalco, 1991; Digonnet, 2001; Paschotta, 2009). Quenching effect manifests in energy transfer between ions in the same energy level due to high doping concentrations in the Erbium-doped fiber. For instance, a donor ion in metastable level ${}^4I_{13/2}$ can transfer its energy to another metastable ion (acceptor) and decay to the ground state ${}^4I_{15/2}$. The ion receiving the energy is excited to ${}^4I_{9/2}$ level and decays later via radiative transitions. The quenching

effect in Erbium-doped fiber reduced lifetime of metastable ions and alter the amplification characteristic of the Erbium-doped fiber (Payne and Reekie, 1988; Urquhart, 1988; Giles and Desurvire, 1991; Horowitz *et al.*, 1994; Voo *et al.*, 2005). Figure 2.4 illustrates quenching effect in Erbium-doped fiber.

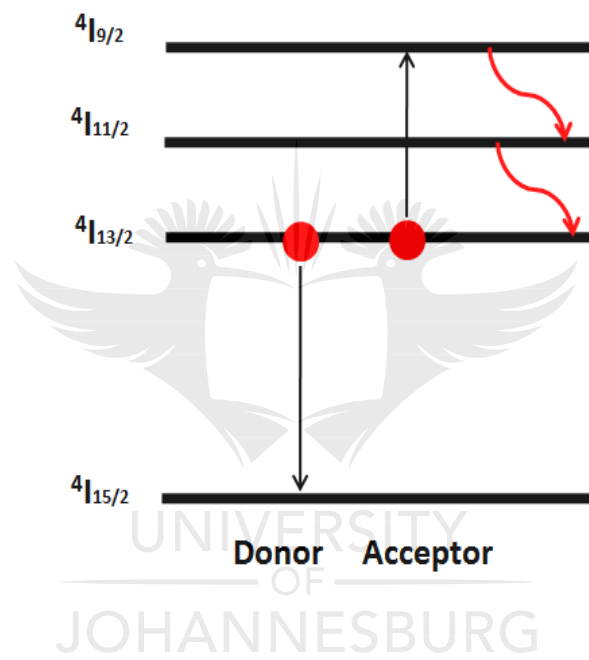


Figure 2.4: Illustration of the quenching effect in Erbium-doped fibers (Snitzer, 1964).

2.4 Basics of fiber lasers

Consider an atomic system (rare-earth doped fiber) with corresponding discrete energy levels annotated here as E_b and E_a . An atom can absorb or emit photons when

electrons make an upward or downward transition between its discrete energy levels. The frequency of the absorbed or emitted radiation is described by Bohr's relation given by

$$\nu_{ab} = \frac{E_b - E_a}{h}, \quad (2.5)$$

where h is the Planck's constant and ν_{ab} is frequency.

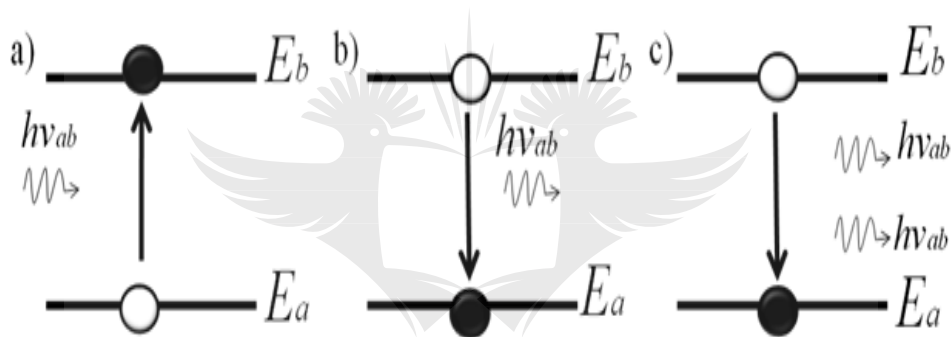


Figure 2.5: Two energy levels representations illustrating: (a) Stimulated absorption, (b) Spontaneous emission and (c) Stimulated emission.

An electromagnetic wave with frequency ν_{ab} corresponds to an energy band gap between two energy levels of an atomic system (Figure 2.5). Three processes can take place in this interaction, which include stimulated absorption, spontaneous emission and stimulated emission.

In the presence of a radiation field, the probability for stimulated absorption transition and stimulated emission transition is the same. These two processes take place at the

same time. However, according to the Boltzmann distribution, stimulated absorption is a dominant process as majority of the electrons occupies the lower energy levels (ground level).

Stimulated absorption takes place when the energy of an incident photon of specific frequency is absorbed by the atom and an electron is promoted from the lower energy level to an excited energy level. The population of lower energy level decay at a rate proportional to both the total population N_a of the lower energy level and the energy density $q(\nu)$ of photons per unit frequency.


$$\frac{dN_a}{dt} = -B_{ab}q(\nu) N_a, \quad (2.6)$$

where B_{ab} is the constant of proportionality.

Stimulated emission becomes a dominant process when a large amount of the electrons occupy higher energy levels. *Stimulated emission* happens when an incoming photon stimulates excited electrons to relax. This process results in the emission of another propagating photon, having the same polarity, and same energy as the incident. The rate of depletion of the excited level is given by:

$$\frac{dN_b}{dt} = -B_{ba}q(\nu) N_b, \quad (2.7)$$

where B_{ab} is the constant of proportionality and N_b is the population of the excited level.

Spontaneous emission occurs when an excited electron make a transition to the lower energy level and spontaneously emits a photon with energy equal to the energy difference between the two energy levels. The depletion of the population of the excited level is proportional to its initial population N_b and the proportionality constant A_{ba} expressed as:

$$\frac{dN_b}{dt} = -A_{ba} N_b. \quad (2.8)$$

Spontaneously emitted photons have no phase relationship to each other and propagate in random directions.

It is important to note that in radiative transitions, stimulated emission, stimulated absorption and spontaneous emission are always present at the same time. To construct a lasing gain medium, situation which favor stimulated emission over spontaneous emission and stimulated absorption have to be found. Therefore, both the correct gain medium and sufficient conditions must be fulfilled to produce the laser effect.

To make stimulated emission the prevailing process, **population inversion** process is required. This means the situation where the equilibrium of the atomic system, provided by Boltzmann distribution, is inverted by having fewer atoms in the lower

energy level (N_a) compared the upper energy level (N_b). The population inversion condition is achieved through a process known as pumping by actively exciting the atoms at a lower energy level to a higher energy level.

It is clear that population inversion is mandatory for laser operation; however, this process cannot be achieved in a two energy-level system (Figure 2.5). In fact, any method by which the atoms are continuously excited from the lower energy state to the excited state (such as optical absorption) will eventually reach equilibrium with the de-exciting processes of spontaneous and stimulated emission. At best, an equal population of the two states $N_a = N_b$, can be achieved, resulting in optical transparency but no population inversion. To accomplish a population inversion resulting in an optical gain, three or four level systems must be used.

A fiber laser is composed of main components: The gain medium, the laser cavity and the pumping system as shown in Figure 2.6.



Figure 2.6: Basic laser configuration: The feedback is accomplished with the help of two mirrors.

The ***pump system*** enables population inversion to take place; by providing the necessary energy to the gain medium and excites molecules, atoms, or ions to make a transition from lower to higher energy level. For efficient optical pump system, it is required that the emission spectrum of the pump source closely matches the absorption spectrum of the gain medium, and therefore transfers the radiation with a minimum loss from the pump source to the absorbing gain medium of the laser. Laser diodes are commonly used as pump sources for fiber laser systems.

The ***gain medium*** is basically a rare-earth-doped fiber in which population inversion is established and stimulated emission occurs. The structure of energy level of the gain medium dictates both the required emission wavelength of the pump and the emission spectrum of laser source.

The working principle of a fiber laser is based on a dynamic balance between the competitive processes of gain and loss in the cavity. When the laser process starts, as the pump source supplies energy to the gain medium, the gain of the active medium of the fiber laser start to increase exponentially (small signal gain). If the gain of the active gain medium of the fiber laser is still increased, the energy in the fiber laser cavity would also grow exponentially to point where one of the components of the

fiber laser would be damaged. However, because of the obvious limitations of the fiber laser such as limited pump power, or absorbing feedback elements, the gain does not increase indefinitely in the amplifying medium of laser. Instead, at some point, the fiber laser reaches a condition of gain saturation which leads to the amplifier gain reduction. In addition, if the loss is larger than the available gain in the fiber laser cavity, propagating photons in the cavity are lost on each successive round trip. Consequently, no significant output is produced from the fiber laser. The condition where the gain of the fiber laser is exactly equal to the net loss of the laser is known as a threshold.

2.4.1 Erbium-doped fiber laser configurations

Erbium-doped fiber lasers can be designed with a variety of cavity configurations. The most popular are the linear cavity and ring cavity (Ter-Mikirtychev, 2014). In this section, we discuss the characteristics, advantages and disadvantages of these two fiber laser cavity configurations.

2.4.1.1 Linear cavity fiber laser

The linear cavity, also known as a Fabry-Perot cavity, consists of a gain medium placed between two reflecting mirrors as shown in Figure 2.7. Fiber Bragg gratings are usually used as fiber laser mirrors placed at the opposite ends of the fiber laser

cavity. The gain medium is based on Erbium-doped fiber. Other intra-cavity optical components may be included in the fiber laser to control the spectral and temporal properties of the fiber laser.

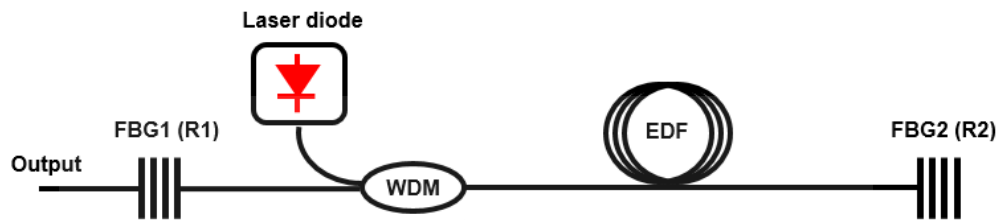


Figure 2.7: Example of a linear cavity fiber laser.

The use of two gratings results in an all-fiber laser linear cavity which makes the system more robust and reduces the cavity losses. The additional advantages of the linear cavity include its simplicity and the possibility to make very short fiber laser cavities (Ball, Morey and Glenn, 1991). In linear cavity fiber laser, the lasing frequencies or resonator modes consist on a superposition of two counter-propagating electromagnetic waves between the fiber laser cavity mirrors. The lasing frequencies of the linear fiber laser cavity are given by the following by (Barnard et al., 1994):

$$f = M \times \left(\frac{c}{2 \times n \times L_c} \right), \quad (2.9)$$

with M being an integer representing the number of lasing mode. n and L_c represent the refractive index of the length of the fiber laser cavity, respectively.

2.4.1.2 Ring fiber laser cavity

The ring fiber laser cavity is an alternative type of fiber laser resonator. This type of fiber laser cavity is preferred for unidirectional light propagation in the fiber laser. This is achieved by inserting optical component such as optical circulator or optical isolator into the cavity (Bellemare *et al.*, 2001; Chen *et al.*, 2005).

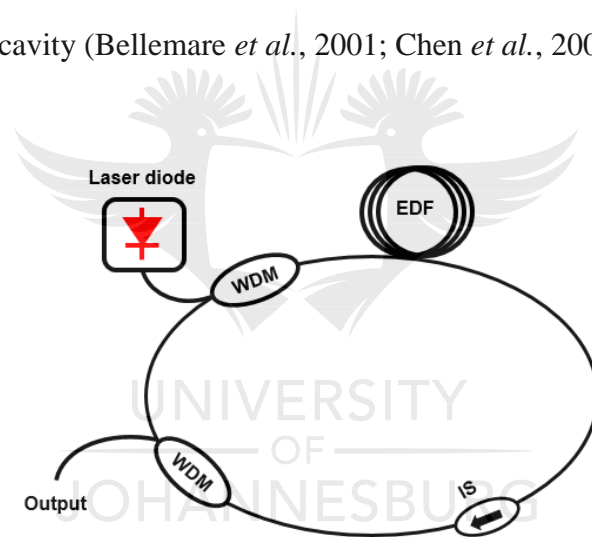


Figure 2.8: Example of a ring fiber laser cavity.

Figure 2.8 shows the schematic structure of a fiber ring laser. The advantages of a fiber ring laser are low cavity loss, low pump thresholds and high conversion efficiencies. The expression for lasing frequency is given as follows (Barnard *et al.*, 1994):

$$f = M \times \left(\frac{c}{n \times L_c} \right), \quad (2.10)$$

2.4.2 Pumping process in Erbium-doped fiber lasers

Laser diodes emitting at a wavelength of 1480 nm or 980 nm are commonly used as a pumping source for Erbium-doped fiber laser systems. The pumping light is usually coupled into Erbium-doped fiber laser using a wavelength division multiplexer (WDM) coupler. The pumping wavelength of 1480 nm does not produce non-radiative transitions between $^4I_{11/2}$ and $^4I_{13/2}$. This makes it relatively more efficient than the 980 nm pumping wavelength. Hence, the laser diode emitting at a wavelength of 1480 nm is preferred for high-power optical amplifiers and laser systems. However, amplifiers with 1480 nm pumping wavelength are usually associated with higher noise levels than 980 nm pumping wavelength. Consequently, the choice between 1480 nm and 980 nm pumping wavelength is not always obvious since each pumping wavelength hold its merit. For a practical development of Erbium-doped fiber amplifiers and lasers, both pumping wavelengths have been utilized (Zhang and Kang, 2008).

2.5 Theoretical model of Erbium-doped fiber lasers

The analytical model describing Erbium-doped fiber laser characteristics is derived in this section. The efficiency of Erbium-doped fiber lasers depends on the cavity design. A fiber laser cavity design includes the choice of the fiber laser cavity configuration and cavity parameters such as pump power, output coupling ratio, Erbium-doped fiber length and overall cavity loss (Agrawal, 2013).

The small signal gain of an Erbium-doped fiber laser can be written as

$$g(z) = \sigma_{em}(N_2(z) - N_1(z)), \quad (2.11)$$

where $N_1(z)$ and $N_2(z)$ are the populations of the lower and upper energy states as a function of the propagating distance along the fiber laser cavity. σ_{em} is the stimulated emission cross-section.

The threshold condition of any laser is reached when the gain is equal to the loss. If we consider a linear cavity, formed by two fibers Bragg grating used as mirrors at the two ends of an Erbium-doped fiber of length L , the threshold condition is given by:

$$G^2 R_1(\lambda) R_2(\lambda) \exp(-2\alpha_{int}L) = 1, \quad (2.12)$$

where $R_1(\lambda)$ and $R_2(\lambda)$ representing the wavelength dependent reflectivity of the first and second fiber Bragg grating, respectively. G is the single-pass amplification factor and α_{int} is the total intra-cavity loss within the cavity.

The single-pass amplification factor is linked to the small signal gain via the relation

$$G = \exp \left[\int_0^L g(z) dz \right]. \quad (2.13)$$

By substituting equation 2.13 and equation 2.11 into equation 2.12, the threshold condition becomes

$$\frac{1}{L} \int_0^L g(z) dz = \alpha_{gratings} + \alpha_{int} = \alpha_{cav}, \quad (2.14)$$

where $\alpha_{gratings} = -\frac{\ln(R_1(\lambda)R_2(\lambda))}{2L}$ is the effective grating loss and α_{cav} is the total cavity loss.

The population difference $N_2(z) - N_1(z)$, from equation 2.11, depends on considered energy level for the gain medium and pump power. To achieve threshold condition, a pumping power to produce the desired population inversion is required.

Given that the pump power is exponentially absorbed along the fiber laser cavity as:

$$P_{abs} = P_p [1 - \exp(-\alpha_p L)], \quad (2.15)$$

where P_p is the pump power and P_{abs} is the absorbed pump power.

The pump threshold is expressed by.

$$P_{Threshold} = \alpha_{cav} L \left(\frac{\alpha_p}{\alpha_s} \right) P_p^{sat}, \quad (2.16)$$

where P_p^{sat} is the pump power saturation and α_s and α_p are the absorption coefficient at the lasing wavelength and pumping wavelength, respectively.

The pump threshold is also expressed in terms of the pump overlap Γ_s by the expression:

$$P_{Threshold} = \alpha_{cav} L \left(\frac{\alpha_p h \nu_p}{\tau \sigma_s \Gamma_s} \right) P_p^{sat}, \quad (2.17)$$

where τ is the lifetime of the ions in the metastable level of the Erbium-doped fiber.

It is clear, from Equation 2.17, that the pump threshold of the laser depends on parameters associated with the fiber laser cavity and the gain medium. In practice, it has been demonstrated that the reflectivity of fiber Bragg gratings are high enough so as the power at lasing wavelength, P_s , is considered as constant. This lead to a simplified expression of the output power given by

$$P_{out} = P_P^{sat} \left(\frac{P_{abs}}{P_{Threshold}} - 1 \right) = P_S^{sat} (P_{abs} - P_{Threshold}) \quad (2.18)$$

and the output power, from the output mirror R_1 of the fiber laser, is given by

$$P_{out} = P_S(1 - R_1(\lambda)) = P_S^{sat} (P_{abs} - P_{Threshold}), \quad (2.19)$$

The output power of the laser increases linearly with the absorbed pump power. The

slope efficiency η_s is defined as the ratio $\frac{dP_{out}}{dP_{abs}}$, and it is given by

$$\eta_s = \frac{1 - R_1(\lambda)}{\alpha_{cav}L} \left(\frac{\alpha_s h \nu_s}{\alpha_p h \nu_p} \right). \quad (2.20)$$

In fiber lasers, with a linear cavity the output power, the pump threshold and the noise level are relatively high. This is because spontaneous emissions are amplified twice in a linear cavity but only once in a ring cavity. The higher spontaneous emission level in linear configurations may induce a severe decrease in gain and absorption at 1550 nm in the Erbium-doped fiber laser.

2.6 Q-Switched Erbium-doped fiber laser

So far, Erbium-doped fiber lasers operating in continuous wave (CW) has been described. The intra-cavity loss of the Erbium-doped fiber laser is constant. In this section, Erbium-doped fiber laser operation in pulsing regime using Q-switching technique is introduced. Unlike continuous wave fiber laser, Q-switched fiber laser operates on the principle of intra-cavity loss modulation. Q-switched fiber lasers produce energetic laser pulses of nanoseconds with repetition rates of a few hertz to several kilohertz. The basic configuration of a Q-switched Erbium-doped fiber laser is illustrated in Figure 2.9.

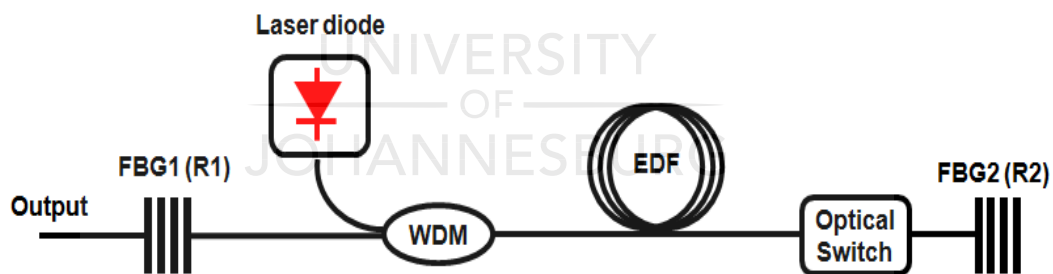


Figure 2.9: Schematic illustration of a Q-switched Erbium-doped fiber linear cavity.

The optical switch allows the changes of the cavity loss, by opening and closing the fiber laser cavity.

2.6.1 Q-Value of a fiber laser cavity

The Q-value (or Quality factor) of a fiber laser cavity is the ratio between the amount of energy stored in the cavity and the amount energy lost per round trip. The Q-value of a fiber laser cavity can be expressed as (Ter-Mikirtychev, 2014).

$$Q = \frac{2\pi L}{\lambda\alpha_{cav}}, \quad (2.21)$$

where L is the cavity length, λ is the laser wavelength, and α_{cav} is the cavity loss coefficient.

In linear fiber laser cavities, the cavity loss coefficient can be expressed as

$$\alpha_{cav} = 2l - \ln R_1(\lambda)R_2(\lambda), \quad (2.22)$$

where l is the fractional loss of the gain medium in the laser cavity. $R_1(\lambda)$ and $R_2(\lambda)$ are the wavelength dependent reflectivities of the two mirrors, respectively as shown in Figure 2.9. The modulation of the cavity loss results in the generation of laser pulses.

2.6.2 Principle of Q-switching in fiber laser

A typical sequence of events during laser Q-switching is shown in Figure 2.10. Q-switching is accomplished by introducing large losses, low Q-value in the fiber laser during pumping. This prevents the onset of the laser emission.

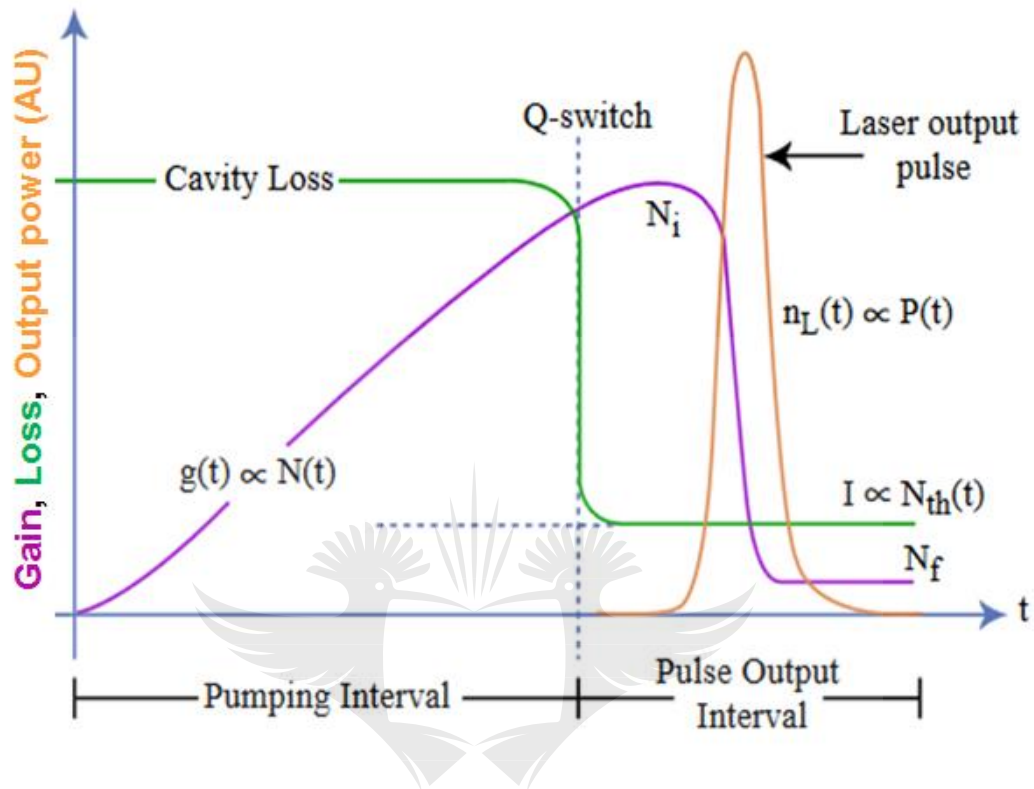


Figure 2.10: Formation of a Q-switched fiber laser pulse. N_i is the population inversion at the beginning of the Q-switched pulse; N_t is the population inversion at the threshold and N_f is the population inversion at the end of the Q-switched pulse.

The energy is stored in the fiber laser cavity as the gain is increased. The population inversion builds up to values far above the threshold required for normal lasers. The cavity loss is then reduced to its lowest value, high Q-value, resulting in a gain that greatly exceeds that which is possible in continuous wave operation.

The stored energy is suddenly released in the form of a large short laser pulse. This laser pulse then begins to deplete the inverted population, thereby reducing the available gain. As the gain decreases below the cavity loss, the laser oscillation rapidly dies out. This entire process results in Q-switched laser pulses with time duration of a few nanoseconds and peak powers that can be several orders magnitudes above normal CW laser output powers.

Q-switched pulse trains can be generated by periodically switching the cavity loss. Q-switching can be realized either passively or actively. In passive Q-switching, the losses are modulated using a component like saturable absorber. Active Q-switching needs an active control element, such as an acousto-optic modulator (AOM), electro-optic modulator (EOM), or a rotating mirror. The advantages of active Q-switching are easy to control the pulse repetition rate, pulse time duration and peak power of pulses.

2.7 Q-switched fiber laser pulse characteristics

In this section, the mathematical description of a Q-switched fiber laser is reviewed to understand output pulses characteristics. Gaeta, C. J. et al. (1987) proposed a numerical model to investigate the pulse characteristics of a Q-switched fiber laser. The proposed model highlighted the influence of the characteristics of the doped-fiber

(gain medium) and the fiber laser cavity parameters on the time duration, peak power and energy of the output pulses using the mode overlapping approach. Shang et al (2006) used the model proposed by Gaeta, C. J. et al. to introduce effective methods to optimize and analyze a Q-switched Ytterbium-doped double cladding fiber laser.

The general assumptions made to study the behavior of a Q-switched fiber laser are: The length of the Q-switched fiber laser cavity is equal to the length of the Erbium-doped fiber. The time between the low Q-value and high Q-value of the fiber laser cavity is shorter than the pulse build-up time. The spontaneous emission is neglected during the emission of the output pulse. The effects of optical pumping are neglected during the emission of the output pulse. Finally, the model assumes a uniform concentration profile along the Erbium-doped fiber. Under these assumptions, the photon lifetime in the fiber laser cavity is defined by

$$\tau_c = \frac{2Ln}{c\delta_i} \quad (2.23)$$

where c is the velocity of light in vacuum, L is the length of the Erbium-doped fiber laser cavity, n is the index of refraction of the Erbium-doped fiber at the lasing wavelength. δ_i is the cavity round trip loss of fiber laser for the i^{th} transverse mode when the Q factor is high.

At the beginning of the Q-switching process, the initial population inversion N_i in the amplifying medium of the Q-switched fiber laser is given by

$$N_i = \left(\frac{\tau}{h\nu_p} \right) P_p [1 - \exp(-\alpha_p L)]. \quad (2.24)$$

N_i is a function of the pump power P_p , the length of the Erbium-doped fiber and the lifetime τ of the photons in the metastable level.

Assuming a fiber laser cavity loss is δ_i , the population inversion at the laser threshold $N_{t,i}$ for the i^{th} mode is expressed by (L J Shang *et al.*, 2006).

$$N_{t,i} = \delta_i \frac{A^2}{2\sigma_{em}}, \quad (2.25)$$

with $A = \pi r^2$ the fiber core area. r is the fiber core radius.

At the end of the Q-switching process, the photon density is once zero. The final population inversion N_f can be calculated from:

$$\frac{N_f}{N_{in}} = \exp\left(\frac{N_f - N_i}{N_{t,i}}\right). \quad (2.26)$$

The instantaneous output power can be related to the photon number by (Koechner W., 1976)

$$P_i = S_i h\nu_s \frac{cT_{OC}}{2L}, \quad (2.27)$$

where T_{OC} is the output coupler transmittance; with S_i , being the photon distribution function for i^{th} transverse laser mode given by

$$S_i = \left[N_{t,i} \ln \frac{N}{N_{in}} - (N - N_i) \right], \quad (2.28)$$

with N representing the total population inversion in the Erbium-doped fiber.

Substituting equation 2.28 into equation 2.27 leads to the following expression

$$P_i = h\nu_s \frac{cT_{OC}}{2L} \left[N_{t,i} \ln \frac{N}{N_i} - (N - N_i) \right]. \quad (2.29)$$

By setting $\frac{dP_i}{dN} = 0$, the maximum output peak power is obtained when $N = N_{t,i}$. The maximum output peak power can be written as:

$$P_{i,max} = h\nu_s \left(\frac{cT_{OC}}{2L} \right) \left[N_{t,i} \ln \frac{N_{t,i}}{N_i} - (N_{t,i} - N_i) \right]. \quad (2.30)$$

2.7.1 Output pulse energy

The total energy in a single output pulse is obtained by integrating the instantaneous power P_i over the time from the beginning (time $t = t_i$) to the end (time $t = t_f$) of pulse as

$$E_i = \int_{t_i}^{t_f} P_i dt = \int_{N_i}^{N_f} \frac{P_i}{dN/dt} dN, \quad (2.31)$$

where dN/dt is expressed in terms of output power instead of photon number by the expression:

$$\frac{dN}{dt} = -\left(\frac{2L\sigma_{em}}{nT_{OC}}\right)\left(\frac{\Gamma_i}{h\nu_s}\right)NP_i. \quad (2.32)$$

Substituting equation 2.32 into equation 2.31 and performing the integration over the population inversion N results in the following expression for the output pulse energy:

$$E_i = \left(\frac{nT_{OC}}{2L\sigma_{em}}\right)\left(\frac{h\nu_s}{\Gamma_i}\right) \ln\left(\frac{N_i}{N_f}\right). \quad (2.33)$$

Equation 2.33 can be rewritten in a form that is more convenient for physical interpretation with the help of equations 2.27 and 2.30:

$$E_i = h\nu_s \frac{T_{OC}}{\delta_i} (N_i - N_f). \quad (2.34)$$

The energy of the a single output pulse is proportional to the difference between the initial and the final population inversion, the photon energy at the fiber laser emission wavelength, and the ratio of the transmittance of the output coupler to the total round trip loss.

2.7.2 Pulse time duration

Assuming that the output pulses from the fiber laser are square shaped, the pulse time duration t_d is:

$$t_d = \frac{E_i}{P_{i,max}}. \quad (2.35)$$

Substituting equation 2.33 and 2.29 into equation 2.34 gives

$$t_d = \tau_c \frac{N_i - N_f}{N_{t,i} \ln \frac{N_{t,i}}{N_i} - (N_{t,i} - N_i)}. \quad (2.36)$$

The time duration of the output pulses is proportional to photon lifetime in the laser cavity, which is defined by the cavity length. Equation 2.36 also illustrates the dependency of the time duration of a Q-switched pulse with respect of the population

inversion at each phase of the Q-switching process; at the beginning, at the threshold and at the end of Q-switching process.

2.7.3 Peak power characteristic for a train of Q-switched fiber laser pulses

To determine the peak power from the average power and time duration of a pulse, we start with the average power as the total energy divided by the time.

$$P_{ave} = \frac{E}{t} \quad (2.37)$$

The pulse energy is power integrated over time. The energy of one pulse is the power integrated over the period T_p .

$$E = \int P(t)dt = E_{pulse} = \int_{t=0}^{t=T_p} P(t)dt \quad (2.38)$$

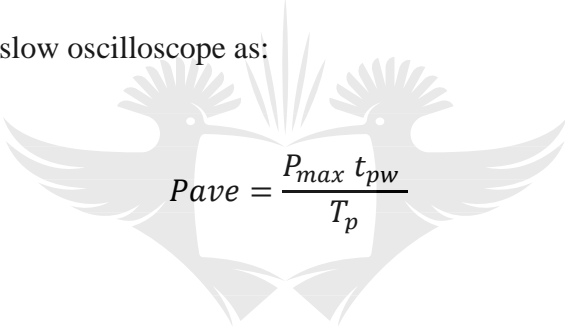
In general, Q-switched fiber lasers produce a train of pulses. Assuming a single pulse in each switching period, the integration only needs to be carried out over the pulse width, and not the entire period. Therefore the average power will be given by the energy received in a single pulse divided by the time between the two consecutive pulses as

$$P_{ave} = \frac{1}{T_p} \int_{t=0}^{t=t_{pw}} P(t) dt, \quad (2.39)$$

where t_{pw} is the duration of a pulse and P_{ave} is the average power.

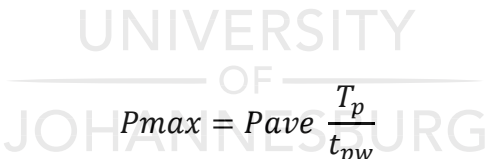
For a square output pulse, the power is equal to the maximum when the pulse is on and zero when the pulse is off.

This results to an estimation of the peak power (P_{max}) which is relatively easy to calculate using a slow oscilloscope as:



$$P_{ave} = \frac{P_{max} t_{pw}}{T_p} \quad (2.40)$$

or



$$P_{max} = P_{ave} \frac{T_p}{t_{pw}} \quad (2.41)$$

A more accurate Q-switched pulse approximation is done by using a Gaussian pulse shape instead of a square pulse. The average power can be obtained as follow:

$$P_{ave} = \frac{1}{T_p} \int P_{max} e^{-(\omega t)^2} dt \quad (2.42)$$

Assuming that the peak power is constant for each pulse, P_{max} can be moved outside the integral. We can use the closed form solution for Gaussian integrals.

$$P_{ave} = \frac{P_{max}}{T_p} \frac{1}{2} \sqrt{\frac{\pi}{\omega^2}} \quad (2.43)$$

It is technically easier to determine the full width at half maximum of the pulse, or FWHM using an oscilloscope. Accordingly, it is essential to convert the formula into a form in which the measured quantities can be directly used. We first set the value of the power at half width equal to half the power as:

$$P\left(\frac{1}{2}t_{FWHM}\right) = \frac{1}{2}P_{max} \rightarrow e^{-\left(\frac{\omega}{2}t_{FWHM}\right)^2} = \frac{1}{2} \quad (2.44)$$

Taking the logarithm of both sides simplifies the exponential, and eliminates the negative sign.

$$\left(\frac{\omega}{2}t_{FWHM}\right)^2 = \ln 2 \rightarrow \frac{\omega}{2}t_{FWHM} = \sqrt{\ln 2}, \quad (2.45)$$

and

$$\omega = \frac{2}{t_{FWHM}} \sqrt{\ln 2} \quad (2.46)$$

Finally, the pulse repetition rate, which is the inverse of the pulse period T , is the quantity set by the laser operator. This gives us the final form for the peak power of a Gaussian pulse:

$$P_{max} = \frac{P_{Ave} t_{FWHM}}{f_{RR}} 2 \sqrt{\frac{\ln 2}{\pi}}. \quad (2.47)$$

where t_{FWHM} is the full-width at half maximum of the pulse, and f_{RR} is the pulse repetition rate.

Contrary to the assumption of a pulse with a square shape, the Gaussian shape effectively provides a more practical pulse approximation. In addition, the output peak power obtained using average power and pulse duration generally agree with the experimental results obtained using a photodiode.

2.8 State of the art of all-fiber actively Q-Switched lasers

Earlier research and development of active Q-switching based fiber lasers were based on the utilization of bulk free-space modulators, namely electro-optic or acousto-optic modulators (Schmidt *et al.*, 2007). The use of bulk modulators led to important

drawbacks. On one hand, they may not satisfy the requirements for mechanical stability that is needed in practical systems; on the other hand, they increase the cavity losses which cause a reduction of the laser efficiency (Canning, 2006). An alternative solution for these limitations is all in-fiber based optical modulators which in turn promote the design of all-fiber-based laser systems.

The fundamental requirement for successful development of all-fiber Q-switching approach is to develop fast, low loss and in fiber-based optical modulator. All-fiber Q-switched laser are proposed in the literature and offer increased simplicity and robustness. These fiber lasers are implemented in both linear and ring laser cavity configuration.

Traditional all-fiber Q-switched lasers are categorized in three different methods that have been proposed: The first approach is based on direct interaction with the evanescent field of the fundamental lasing mode to modulate the cavity of the fiber laser. Chadonnet *et al.* (1993) demonstrated the first all-fiber Q-switched laser using a side-polished coupler as an efficient intra-cavity switching element. Active Q-switching by interaction with the evanescent field was developed by oscillating a microsphere in and out of contact with a taper. It is possible to modulate the fiber transmission by controlling external coupling to the evanescent light field. This Q-switching approach requires an accurate mechanical control of the positioning of the fiber since the evanescent field extends only few microns away from the fiber. In

addition, a specific environmental control needs to be taken into consideration as the system is sensitive to vibrations (Kieu and Mansuripur, 2006).

The second approach consists on a fast mechanical tuning of the reflection spectrum of a fiber Bragg gratings (FBG) and the last technique is based on in-fiber acousto-optic interaction. In this technique, two fibers Bragg grating are use as cavity mirrors to construct a linear cavity fiber laser. It is possible to develop simple cavity loss modulators by tuning the refection spectrum of one of the gratings. The use of mechanical and piezoelectric transducers has been proposed to control the Q-switching of a fiber laser. One of the gratings can be fixed to a mechanical stretcher or a piezoelectric transducer, modulated by an electrical signal, to tune its reflection spectrum. When the reflection spectra of the two gratings do not overlap, the cavity exhibit a low Q-factor, while a high Q-factor is obtained when both reflection spectra overlap. In this simple Q-switching approach, the characteristics of the stretcher are crucial (Takeshi Imai *et al.*, 1997; Russo, N. A. *et al.*, 2002; Andrés, M. V. *et al.*, 2007). For instance, the vibration introduced when using piezoelectric transducer imposes important disadvantages on the working frequencies and on the waveform of the modulation signal.

The third approach takes advantage of the acoustic waves guidance in an optical fiber. Efficient acousto-optic interaction with the fundamental lasing mode in the fiber is achieved by modulating the cavity loss in fiber laser. With this Q-switching method,

the propagation of flexural waves permits a direct control of the attenuation generated in a short section of fiber optimized to achieve active Q-switching of fiber lasers. Ding *et al.* (2000) reported an acoustically modulated fiber Bragg grating to Q-switch a fiber laser. Kaneda *et al.* (2005) and Matthew *et al.* (2007) reported similar technique of constructing an all-fiber Q-switched laser using fiber birefringence induced by stress. Perez M, *et al.* (2005) demonstrated a Q-switched all-fiber laser, in which the magnetostrictive-based modulator (MM) is used to modulate the Q-value of the fiber laser cavity. Diez, A. *et al.* (2006) reported an all-fiber laser Q-switched using a fiber Bragg grating based acousto-optic modulator. In this configuration, Q-switching is performed by tuning the reflection spectrum a fiber Bragg grating with an external acoustic wave.

All these all-fiber modulators include a fiber Bragg grating and exploit the specific interaction mechanism of magnetostrictive materials or acoustic waves with the fiber Bragg grating itself. In some of the reported experiments, the fiber Bragg gratings were written into the active fiber to avoid the presence of any splice within the cavity. Fan-Wen and Jung-Jui, (2007) described an actively Q-switched fiber laser tuned by a pair of temperature controlled fiber Bragg gratings. X. P. Cheng et al (2008) proposed an all-fiber Q-switched laser by integrating an apodized fiber-Bragg-grating (FBG) reflector and a Fabry-Perot (FP) etalon constructed from cascaded chirped fiber Bragg gratings into the fiber laser cavity (Figure 2.11). The Q-switching operation is achieved by periodically tuning the chirped fiber Bragg grating Fabry-Perot (CFBG

FP) and shifting the relative positions of these multiple peaks to the stop-band of the fiber Bragg gratings (FBG) reflector. Using this technique, laser pulses of 3.5 μJ and 3.5 kHz of repetition rate were demonstrated for a pump power of 70 mW.

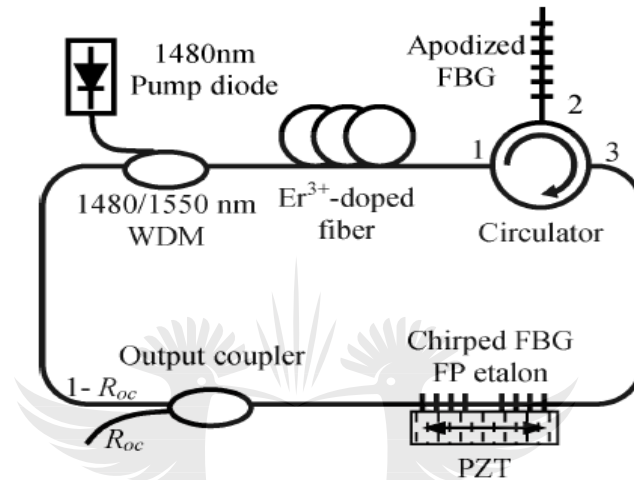


Figure 2.11: Illustration of an all-fiber Q-switched fiber ring laser (X.P Chang et al. (2008).

Another all-fiber Q-switched Erbium-doped laser has been proposed (Cheng X. P. et al, 2008). It consists of a phase-shifted fiber Bragg grating (FBG) and an apodized FBG reflector (Figure 2.12). By using the piezoelectric transducer (PZT) to periodically stretch the apodized FBG and detune it with the phase-shifted FBG, the cavity loss of the fiber ring laser is switched between high and low states to achieve Q-switching.

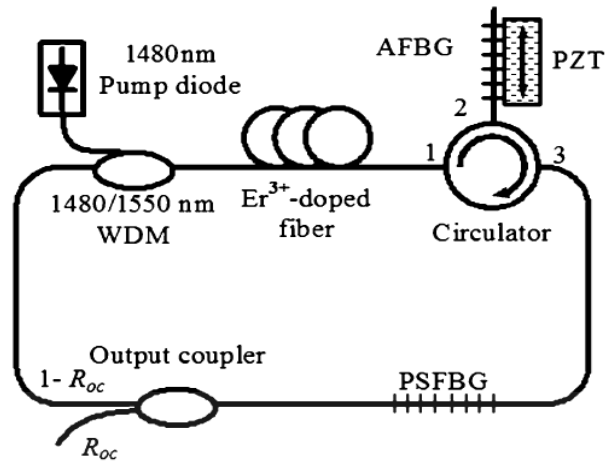


Figure 2.12: Illustration of an all-fiber Q-switched fiber ring laser (X.P Chang et al. (2008).

However, as the fiber Bragg grating is tuned, the above methods of Q-switching are limited by the tuning speed. It is very easy to crack the fiber grating when it is stretched and relaxed in high speed. Another limitation is that the center wavelength of the laser output will also be oscillating slightly during the process of tuning the fiber Bragg grating (FBG) back and forth.

Alternative concepts to develop Q-switched fiber laser systems that maintain robustness and simplicity of all-fiber Q-switched laser is suggested. This time the Q-value of cavity is not achieved by a mechanical stress applied on a fiber Bragg grating. Sousa, J. M. and Okhotnikov, O. G. (1999) proposed a Q-switched fiber laser by combining a scanning Fabry- Perot filter and Fabry-Perot etalon illustrated in Figure

2.13. The modulation of the Q-factor of the fiber laser cavity is achieved by controlling the wavelength of the scanning Fabry-Perot filter with respect to the fixed wavelength of the Fabry-Perot etalon.

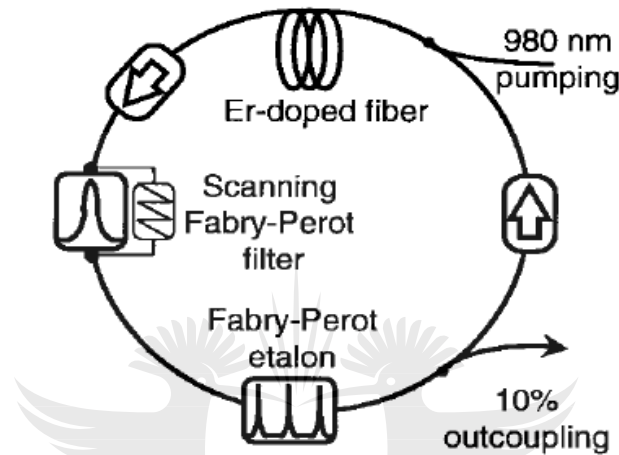


Figure 2.13: All-optical Q-switched laser using a Fabry-Perot etalon and a scanning Fabry-Perot filter.

Delgado-Pinar M. et al. (2006) proposed an active Q-switched fiber laser using a Bragg grating based on an acousto-optic modulator (Figure 2.14).



Figure 2.14: All-fiber Q-switched laser using an acousto-optic modulator of a fiber Bragg grating linear cavity (Delgado-Pinar M. et al., 2006).

The Q-switching process is performed by modulating a fiber Bragg grating with an extensional acoustic wave. The acoustic wave modulates periodically the effective index profile of the fiber Bragg grating (FBG) and changes its reflection features. This allows controlling the Q-value of the fiber laser cavity. This technique has been also implemented in the ring configuration (Miguel V. Andrés et al., 2006). The ring configuration is illustrated in Figure 2.15.

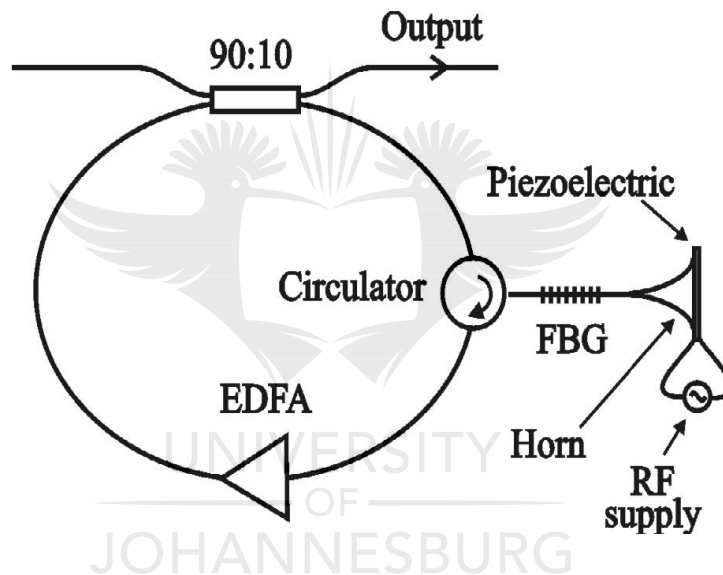


Figure 2.15: All-fiber Q-switched laser using an acousto-optic modulator of a fiber Bragg grating ring cavity (Miguel V. Andrés et al., 2006).

An optically tuneable Q-switched fiber laser was demonstrated by Robert et al. (2010). This all-optical Q-switching mechanism incorporated an optically-tuneable fiber-Bragg grating into a fiber laser, as illustrated in Figure 2.16. The Q-switching is obtained by repetitively tuning the high reflector (HR) on and off-resonance with a

stabilized output coupler (OC) grating. The output laser pulses from this Q-switched fiber laser configuration was characterized by a time duration of 5 μ s of time duration, 3.5 mW of average power for 35 kHz of repetition rate.

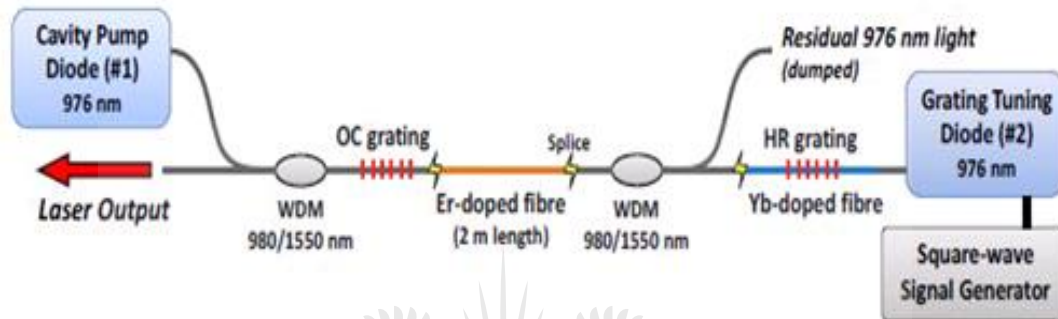


Figure 2.16: Illustration of all-optical Q-switched fiber lasers using an optically-tunable fiber Bragg grating in a fiber laser (Robert et al. (2010)).

Recently, a new technique of an all-optical Q-switched fiber laser has been proposed by Zhi-Zheng et al. (2010). A high extinction ratio abrupt-tapered Mach-Zehnder (MZ) filter and Fabry-Perot (FP) tunable filter are incorporated into a fiber laser cavity to establish or to destroy the laser resonance (Figure 2.17). When the pass-band wavelength of the Fabry-Perot (FP) filter is tuned to equal the stop band wavelength of the Mach-Zehnder (MZ) filter, the resonance fails, which corresponds to a low Q-factor of the fiber laser. When both of the pass-band wavelengths of Mach-Zehnder (MZ) and Fabry-Perot (FP) filters overlap, resonance occurs and the Q-factor is high.

Using this switching technique, tunable pulse time durations of Q-switched Erbium-doped fiber lasers ranging from 78 ns to 23 ms were demonstrated.

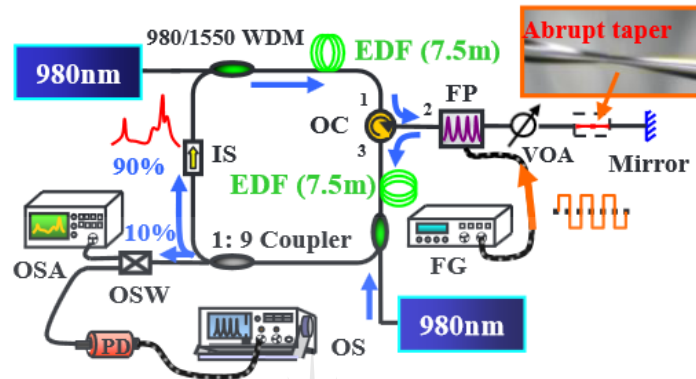


Figure 2.17: Experimental set-up of a pulse time duration tunable Erbium fiber laser (Zhi-Zheng et al., 2010).

Based on the advantages and limitations of each Q-switching technique presented earlier, a simple, robust and unique all-fiber Q-switching approach in fiber laser is proposed and experimentally demonstrated in this thesis. The proposed Q-switching mechanism includes two wavelength dependent optical components, namely fiber Bragg grating and fiber Fabry-Perot tunable filter. The modulation of the quality factor in the fiber laser is based on the overlap spectrum between the transmission spectrum of a fiber Fabry-Perot tunable filter and a reflection spectrum of a fiber Bragg grating. To the best of our knowledge, this is a first time that such Q-switching technique has been introduced and successfully implemented in both linear and ring cavity configuration.

2.9 Summary

We have presented a theoretical survey of the relevant theory of fiber lasers and Q-switched fiber lasers. In particular, we have reviewed the mathematical description of an Erbium-doped fiber laser to highlight the key output laser characteristics, which are laser threshold, laser output power and slope efficiency. We have described the basic theory of an actively Q-switched fiber laser with an emphasis on the output pulse characteristics. We have also presented a brief review of techniques employed for developing actively Q-switched fiber lasers. The limitations of these techniques have been presented to motivate the development of all-fiber based optical modulators. The progress of the development of the previous all-fiber actively Q-switched fiber lasers is presented. We have reviewed techniques demonstrated experimentally by other research groups to achieve actively Q-switched fiber lasers. These techniques have shown merit in terms of robustness and simplicity. Contributing to the existing Q-switching techniques, in the next chapters, we introduce and demonstrate a simple, robust and innovative Q-switching approach in fiber laser.

Chapter 3

Implementation all-fiber Q-witched Erbium-doped ring laser

UNIVERSITY
OF
JOHANNESBURG

3.1 Introduction

The experimental investigation on a Q-switched fiber laser is discussed in this Chapter. A new Q-switching mechanism approach in fiber laser is introduced. The fiber laser is a ring based configuration using Erbium-doped fiber as gain medium. To modulate the cavity loss of the fiber laser, a Q-switching mechanism based on the spectral overlap between a tunable fiber Fabry-Perot filter and a fiber Bragg grating is proposed. To characterize the Q-switched fiber laser system, we first studied the system in continuous wave mode in order to optimize the fiber cavity parameters such as Erbium ion concentrations, Erbium-doped fiber length, output coupling ratio of the fiber laser and extinction ratio. Then we introduced the spectral characteristics of a fiber Bragg grating and the fiber Fabry-Perot tunable filter to illustrate the overlap utilized in this Q-switched fiber laser. We finally present and discuss the experimental results characterizing the Q-switched fiber laser.

3.2 Construction of an all-fiber Erbium-doped fiber ring laser

As mentioned earlier, the experimental configuration of the actively Q-switched fiber laser investigated in this thesis is based on the spectral overlap between the reflection

of a fiber Bragg grating and the transmission spectrum of a fiber Fabry-Perot tunable fiber. In this section, the Q-switching mechanism is described and the overlapping mechanism experimentally demonstrated.

3.2.1 Fiber Fabry-Perot tunable filter

The Fabry-Perot filter is an optical resonator discovered by Charles Fabry and Albert Perot in 1898. In the past decades, a great number of different Fabry-Perot tunable filters (F-PTFs) have been proposed and developed. The most popular F-PTFs are micro-electromechanical systems F-PTF, bulk Fabry-Perot tunable filter, liquid crystal F-PTF and fiber Fabry-Perot tunable filters (FF-PTF). These Fabry-Perot tunable filters have achieved great success for example in wavelength division multiplexing (WDM) telecommunication networks and tunable fiber laser systems. Among all the tunable optical filters, fiber Fabry-Perot tunable filters have become the most attractive ones, and are broadly used in both scientific research and technical applications (Miller and Janniello, 1990; Stone and Stulz, 1987). The major advantages of fiber Fabry-Perot tunable filters are the simple and robust design, which includes a lensless configuration, low loss, and high isolation.

A Fabry-Perot filter is basically a combination of two highly reflecting mirrors R_A and R_B facing each other, separated by some distance “ L ” which defines the cavity of the interferometer as illustrated in Figure 3.1.

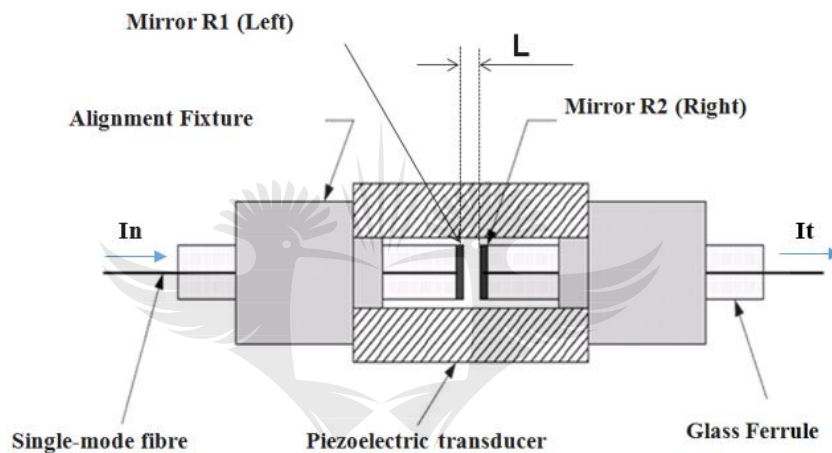


Figure 3.1: Schematic configuration of a fiber Fabry-Perot tunable filter.

Light enters through the back of left mirror is reflected by the right mirror and again reflected by the left mirror. The light wave is transmitted through the cavity only when a certain condition for the wavelength of the laser and the geometry of the resonator cavity are satisfied. The spectral transmission of a tunable filter is tuned by applying a sinusoidal electrical signal to the piezoelectric transducer (PZT) attached to it. When

the electrical signal is applied to the piezoelectric transducer, a mechanical stress is generated to move the filter mirrors and modify the cavity length L .

Let us assume a monochromatic light wave of intensity I_{in} enters the Fabry-Perot cavity filter (Figure 3.1), and is reflected inside the cavity several times. If the refractive index n of the medium separating the two mirrors is 1, in the absence of light absorption from the mirrors, the fractional transmission response of the filter ($T_f = \frac{I_{in}}{I_t}$) is given by (R. D. Guenther, 1990).

$$T_f = \frac{(1 - R)^2}{1 + R^2 - 2R \cos \left[2\pi \frac{v}{c/2L} \right]}, \quad (3.1)$$

when $nL = m \frac{\lambda}{2}$, with m being an integer, equation (3.1) has a maximum corresponding to the resonance condition within the Fabry-Perot cavity. v and c represent the frequency and speed of light in vacuum, respectively.

The transmission function T_f , is periodic in frequency (wavelength). The difference between the two consecutive resonance frequencies (wavelength) is called the tuning range or free spectral range given defined by the Fabry-Perot cavity length as

$$FSR = \frac{c}{2L} \quad (3.2)$$

Another important characteristic of a Fabry-Perot tunable filter is its finesse. It is a quantitative measure of the interferometer's ability to resolve closely spaced transmission peaks. The finesse fundamentally characterizes the width of the resonant frequencies defining the sharpness of the maxima.

3.2.2 Experimental characterisation of the fiber Fabry-Perot tunable filter

In this project, a fiber Fabry-Perot tunable filter (F-FPTF) from Micron Optics is used. The experimental arrangement to characterize the filter is illustrated in Figure 3.2. A wide spectrum superluminescent diode, (SLD-761), is connected to the input port of the fiber Fabry-Perot tunable filter. The other output port of the tunable filter is connected to the optical spectrum analyzer (AQ-6315A) used to record the output spectrum. To avoid instability of the Fabry-Perot filter, an optical isolator is placed between the SLD and the filter to prevent light back reflection to the source.

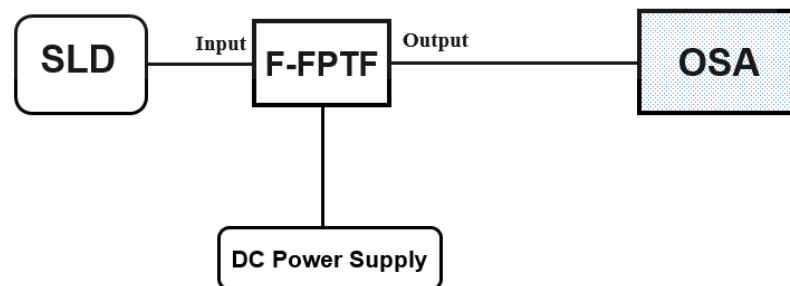


Figure 3.2: Experimental setup used to characterize the fiber Fabry-Perot tunable filter

The electrical bias of the fiber Fabry-Perot tunable filter is connected to a variable direct current (DC) power supply. The spectral position of the Fabry-Perot filter transmittance band is controlled by the applied voltage. The tuning is achieved by changing the spacing of the gap between the mirrors with the attached piezoelectric element. The continuous voltage from the DC voltage is varied manually from 0 V to 10 V to tune the fiber Fabry-Perot tunable filter. The transmission wavelength of the fiber Fabry-Perot tunable filter versus the applied voltage is shown in Figure 3.3.

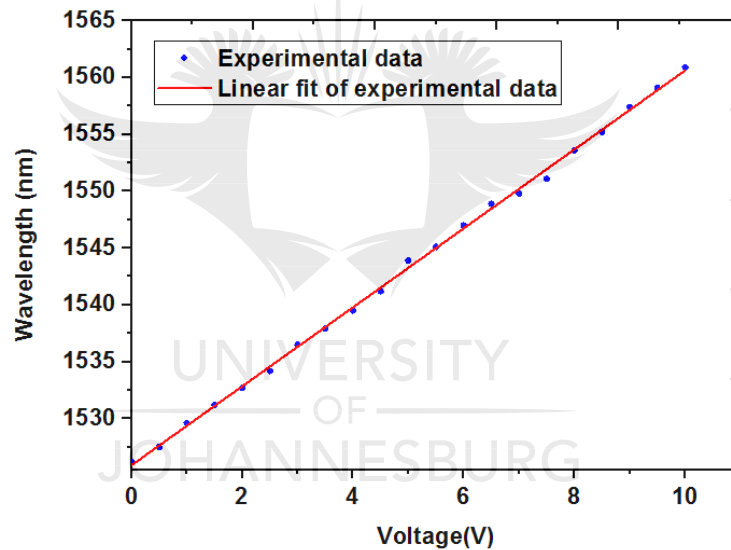


Figure 3.3: Dependence of the transmission wavelength of the fiber Fabry-Perot tunable filter versus the applied voltage.

The transmission wavelength increases linearly with the applied voltage. A transmission line of 1550 nm is obtained when 8 Volts are applied to the filter. This value is used to design the Q-switching device. The transmission spectrum of the fiber

Fabry-Perot tunable filter used in this project is illustrated in Figure 3.4. The transmission spectrum is a periodic function consisting of narrow resonant bands. The Fabry-Perot filter has a characteristic bandwidth ($\delta_\nu=200$ pm) and a free spectral range (FSR=40 nm), as shown in figure 3.4.

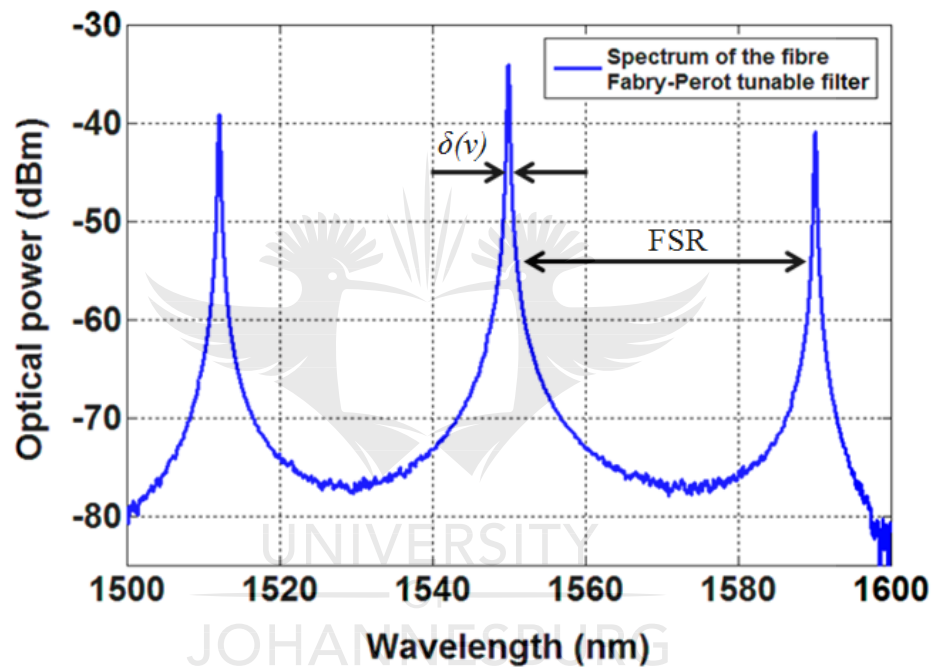


Figure 3.4: Transmittance spectrum of the Fabry-Perot filter, optical power versus the wavelength.

3.2.3 Fiber Bragg grating

The refractive index of any material is dependent on a range of factors including material density, temperature, and the molar refractivity. In particular, the alterations in the refractive index in the core of an optical fiber are obtained upon exposure to high energy radiation (Poumellec *et al.*, 1996). By spatially and periodically modifying such refractive index along the length of an optical fiber, it is possible to fabricate a device capable of reflecting light propagating within the core. These devices, which are known as fiber Bragg gratings (FBGs) are currently and broadly available and have extensive application in communication and sensing of strain and temperature. The fiber Bragg grating (FBG) was discovered by Ken Hill and co-workers in Canada, nearly four decades ago. The manufacturing of fiber Bragg gratings has also been critical to the development of all-fiber lasers systems. The modification of refractive index in fibers is widely established to occur by means of two-photon absorption at visible frequencies followed by dissipation of the absorbed energy into the glass matrix. It is also possible to obtain excitation through single-photon absorption at ultraviolet frequencies (G. Meltz *et al.*, 1989), which in turn decreasing the irradiance and exposure time necessary to induce a stable refractive index change within the core of the fiber.

The schematic diagram of a fiber Bragg grating is illustrated in Figure 3.5.

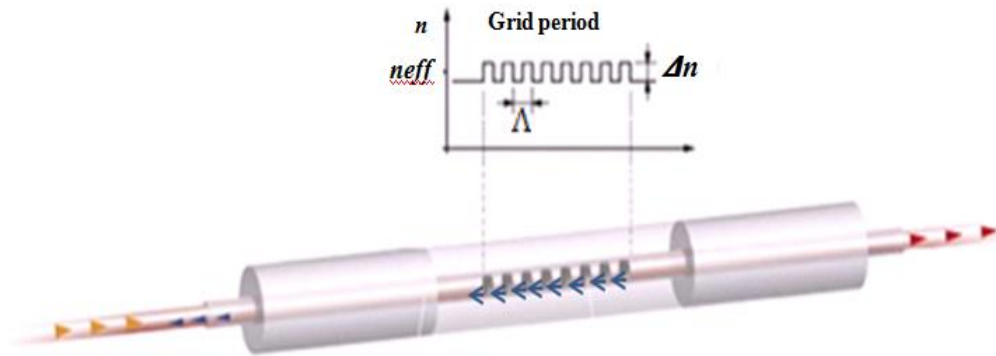


Figure 3.5: Schematic diagram of a fiber Bragg grating. Λ : grating period, n_{eff} : effective core index.

The wavelength of maximum reflection, also known as Bragg wavelength is a function of the period of the refractive index perturbation Λ and the effective modal index n_{eff} in the fiber core:

$$\lambda_B = 2 n_{eff} \Lambda , \quad (3.3)$$

In addition to the fiber parameters in a single mode fiber, the reflectivity of the grating at the Bragg wavelength depends mostly on the amplitude of the index perturbation and the grating length as follows (Yariv A., 1997; Lam D. K. W. and B. Garside K., 1981; HoSze, 2007):

$$R(\lambda_B, L) = \tanh^2 \left(2 \frac{\partial n}{\lambda} \eta L g \right) \quad (3.4)$$

Where Lg is the grating length, ∂n is the magnitude of the index perturbation and η is the modal overlap factor.

3.2.4 Characterisation of a fiber Bragg grating

In this section, the fiber Bragg grating used in the fiber laser experiment is characterized. The optical fiber used to print the fiber Bragg grating supports single mode operation at a wavelength of 1550 nm. To characterize the fiber Bragg grating, the experimental set-up shown in Figure 3.6 is used.

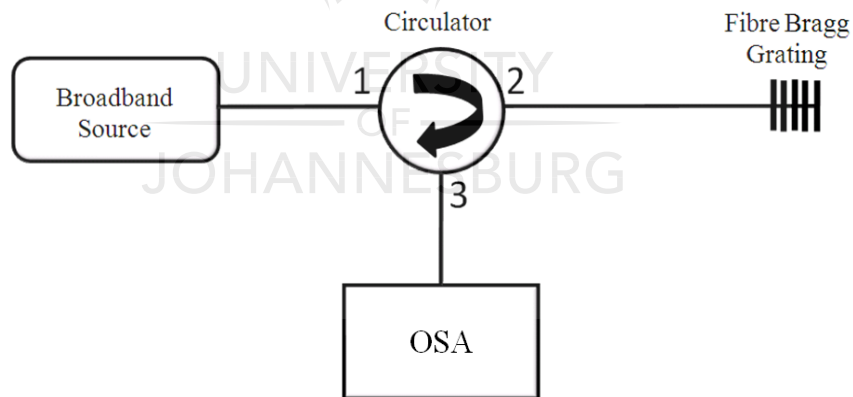


Figure 3.6: Experimental set-up used to characterize the fiber Bragg grating.

Light from the broadband source (superluminescent diode) is directed to the FBG via port 1 and port 2 of the circulator. The reflected wavelength from the fiber Bragg grating is directed through port 3 of the circulator and displayed on an optical spectrum analyzer. The reflection spectrum of the fiber Bragg grating is shown in Figure 3.7.

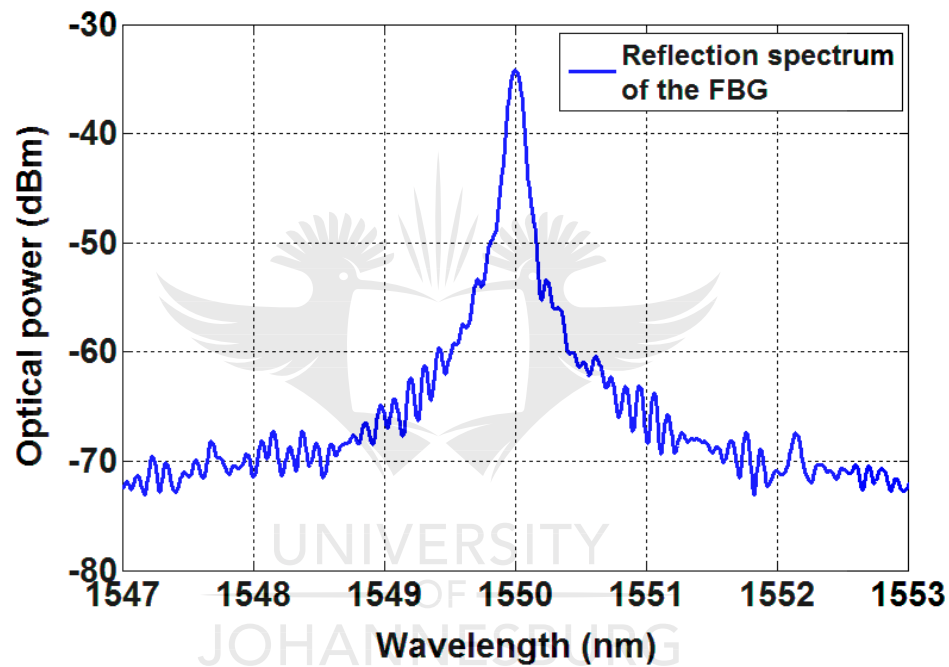


Figure 3.7: Reflection spectrum of a fiber Bragg grating.

The reflection of the fiber Bragg grating is 98% at 1550 nm, and the spectral width of the reflected wavelength is 150 pm.

3.2.5 All-Fiber Q-switching device

The all-fiber-based Q-switch modulator introduced in this project relies on the wavelength modulation in the fiber laser cavity that incorporates two wavelength-dependent elements, namely fiber Bragg gratings and fiber Fabry-Perot tunable filter. The fiber laser cavity losses and wavelength switching is achieved by modulating the spectral position of the transmission spectrum of the fiber Fabry-Perot tunable filter with respect to the fixed reflection spectrum of the fiber Bragg grating. The switching principle is illustrated in Figure 3.8.

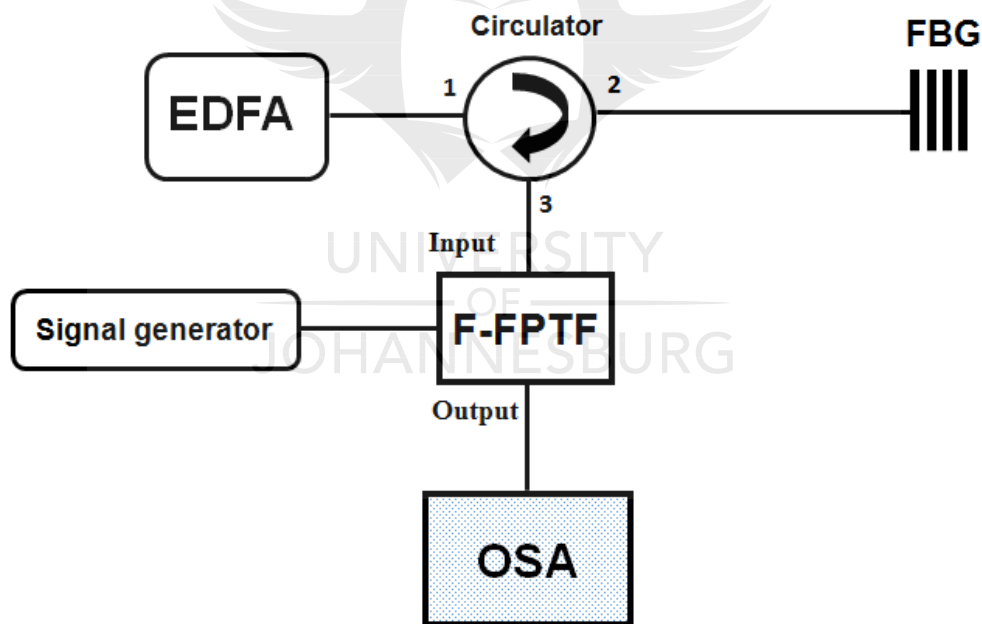


Figure 3.8: Illustration of all-fiber Q-switching device.

The spectral transmission of a tunable filter is tuned by applying a sinusoidal electrical signal to the piezoelectric transducer (PZT) attached to it. The spectrum of light emitted via spontaneous emission from the Erbium-doped fiber is directed to the fiber Bragg grating via port 1 and 2 of the circulator. The reflected light from the fiber Bragg grating is directed toward the fiber Fabry-Perot tunable filter through port 3 of the circulator.

The fiber Fabry-Perot tunable filter is used to induce a periodic cavity loss characteristic within the fiber laser cavity, determined by the variable transmission spectrum. As the transmission spectrum of the tunable filter moves towards the reflectivity spectrum of the fiber Bragg grating, the spectral overlap between the two filters increases and the fiber laser cavity loss decrease (Figure 3.9).

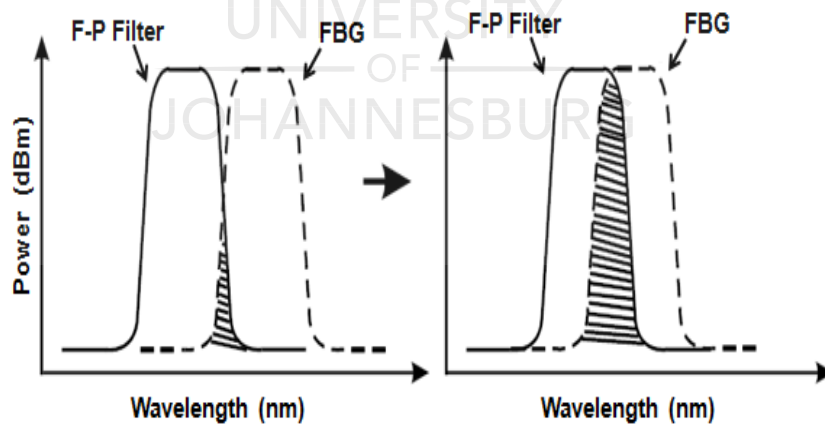


Figure 3. 9: Illustrations of the spectral overlap between the transmission spectrum of Fabry-Perot filter and reflection spectrum of fiber Bragg grating.

When the wavelength of a given reflected spectrum of the fiber Bragg grating and instantaneous transmission wavelength spectrum of the fiber Fabry-Perot tunable filter overlap, the fiber laser cavity switches from low to a high Q value.

3.3 All-fiber active Q-switched fiber laser

As mentioned earlier, the experimental investigation proposed here is based on the development of a simple and robust Q-switched fiber laser using the spectral response of two optical filters to modulate the fiber laser quality factor. Contrary to the bulk elements, used in traditional Q-switched fiber lasers, these optical components exhibit lower insertion losses. To the best of our knowledge, this is the first time that such Q-switching mechanism has been successfully demonstrated in fiber lasers. The results of this investigation were initially published by our research group (Manuel *et al.*, 2016). The experimental configuration of all-fiber Q-switched laser for the generation of 1550 nm pulse signal is shown in Figure 3.10.

The proposed fiber laser system consists of a laser diode emitting light at 980 nm which is used as pump source for the fiber laser. The pump light is coupled into the ring cavity using a wavelength division multiplexer (WDM). The gain medium of the laser consists of an Erbium-doped fiber (EDF). The unidirectional operation of the fiber ring laser is guaranteed by the three-port circulator with high isolation from port

3 to port 1. The fiber Bragg grating reflects and selects the emission wavelength of the fiber laser. The fiber Fabry-Perot tunable filter operates as cavity loss modulating device.

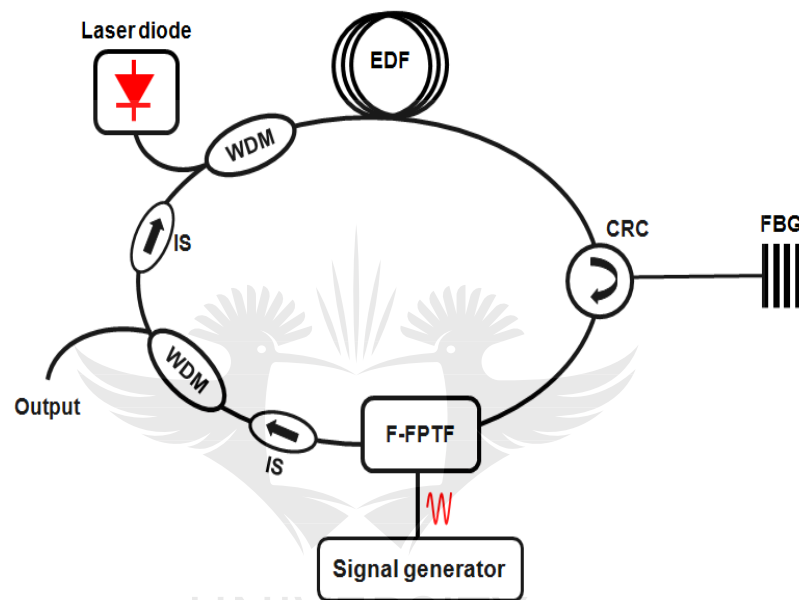


Figure 3.10: Experimental set-up of an all-fiber active Q-switched ring laser.

The output power is extracted with an output coupler. The optical isolator in the fiber laser cavity guarantees unidirectional propagation of the laser light. In this configuration, Q-switching in the fiber laser cavity is based on the dynamic spectral overlapping of two filters, the FBG-based filter (reflection spectrum) and fiber Fabry-Perot (F-P) tunable filter (transmittance spectrum). When the spectra of the two filters overlap, the filter system has maximum transparency; at this point, the laser cavity has

minimum losses and can release the stored energy in the form of a giant pulse. The fiber Fabry–Perot tunable filter changes the spectral transmittance and actively switches the Q-factor of the all-fiber ring cavity. Thus, stable and short pulses can be generated from the fiber laser. The spectral Fabry–Perot transmittance wavelength spectrum is controlled by the applied voltage and tuned by a signal from a standard low-power signal generator. In this way, the cavity Q-factor can be easily modulated. The output pulse was measured with a high-speed detector in combination with a digital oscilloscope.



3.4 Experimental Q-switched fiber ring laser

To fully explore the characteristics of the fiber presented in this Chapter, the continuous wave (CW) operation of the fiber laser was first investigated. In continuous wave regime, both the fiber Bragg grating and the fiber Fabry-Perot filter are included in the fiber laser cavity for consistency with the Q-switched fiber laser experiment. This is to take into account insertion loss of all components included in the Q-switched fiber laser system. In continuous wave operation, an appropriate DC (direct current) voltage is applied to the fiber Fabry-Perot tunable filter to make its transmission spectrum overlap with the reflection spectrum of fiber Bragg grating.

The output spectrum of the fiber laser is plotted in Figure 3.11 when the two spectra do not overlap. The reflected light from the fiber Bragg grating is attenuated, by more than 20 dB, by the filter to prevent stimulated occurring in the fiber laser. At the reflected Bragg grating wavelength, the cavity loss is higher than the gain. The obtained output power results in two wavelength peaks corresponding to the transmission spectrum of the tunable filter and the reflection spectrum of the fiber Bragg grating.

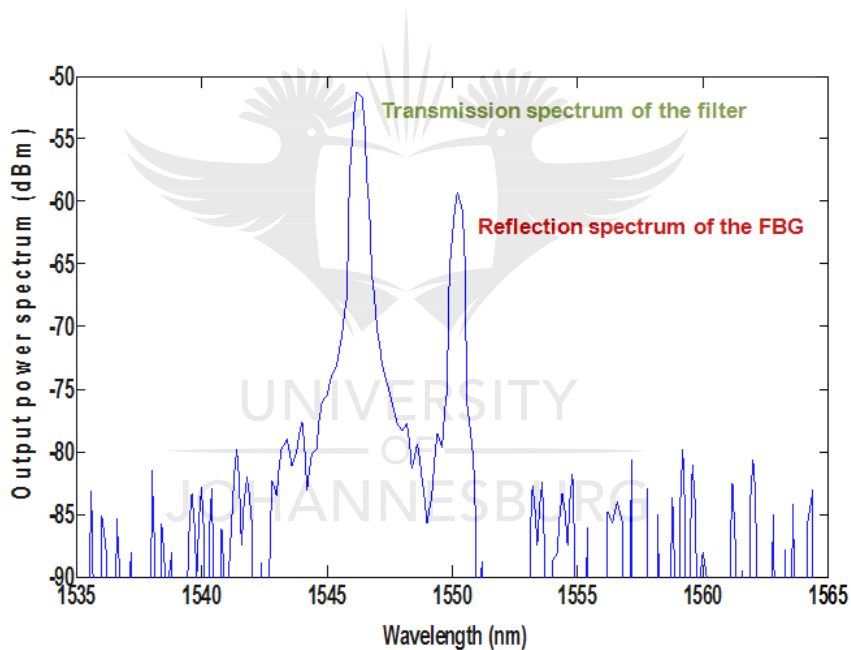


Figure 3.11: Power spectrum when the spectra of the fiber Bragg grating and Fabry-Perot filter do not overlap.

The continuous-wave fiber laser light is produced only when the reflection spectrum of the fiber Bragg grating and transmission spectrum of the tunable fiber Fabry-Perot

filter overlap. This is achieved by choosing an appropriate voltage to tune the transmission spectrum of the Fabry-Perot filter. A total overlap between the two spectra was obtained for 8 volts applied to the filter. The fiber laser output is shown in Figure 3.12.

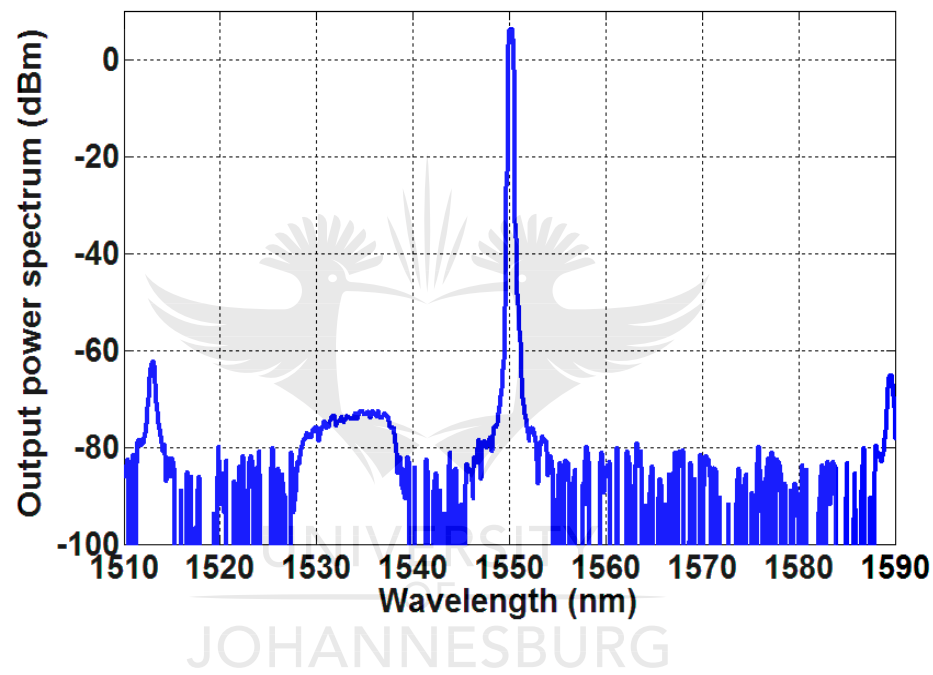


Figure 3.12: Illustration of the emission spectrum of the fiber laser when the reflected spectrum of the fiber Bragg grating and the transmission spectrum of Fabry-Perot filter overlap.

In the following sections, a series of experiments were performed to optimize the all-fiber laser in term of output power. Two different Erbium-doped fibers laser system having different Erbium ion concentration are used in this experimental investigation.

The first doped fiber, EDF1, with an Erbium ion concentration of 2200 ppm and pump absorption of 23.4 dB at 980 nm is referred to as “*high concentration*” and the second, EDF2, with an Erbium ion concentration of 960 ppm and pump absorption of 12.4 dB at 980 nm is referred to as “*low concentration*”. The contribution of fiber laser cavity parameters to the performance of the fiber laser such as the length of the Erbium-doped fiber, the output coupling ratio, the repetition rate of pulses and the concentration of the Erbium-doped fibers were explored.

3.4.1. Optimal output coupling ratio

In order to increase the output power of an Erbium-doped fiber laser, without increasing the pump power, the optimization of the output coupling ratio is of great importance. The amount of laser light one can couple out depends on the gain. The output peak power as a function of the output coupling ratio is shown in Figure 3.13.

To perform this experiment, a 3.5 m M-12 (980/125) Fibercore Erbium-doped fiber with ion concentration of 960 ppm was used as a gain medium. A variable coupler was used to modify the coupling ratio of the fiber laser system. The maximum fiber laser out power was obtained when 87 % (approximately 90 %) laser light was coupled out.

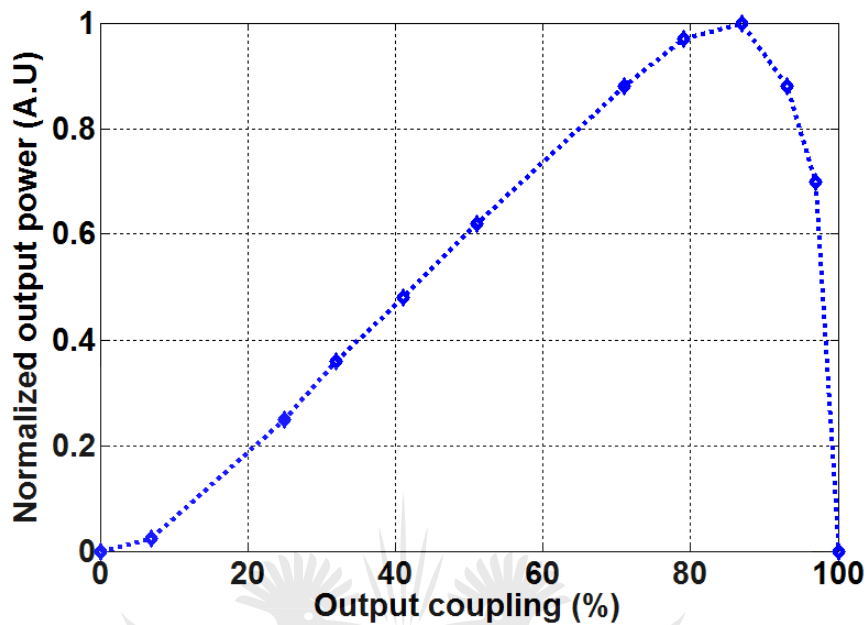


Figure 3.13: Normalized output power versus output coupling ratio.

The output coupling ratio is part of the round trip loss and defines the optimal amount of light to be fed back in the fiber ring laser. It has been observed that for less than 50 % and more than 96 % of light coupled out of the fiber laser, the output power was less than half of the maximum. If the output coupling ratio is too high, the power fed back into the laser cavity cannot sustain the lasing process. In addition, when output coupling is too low, the amount of light feedback in the cavity tend to saturate the gain medium and reduce the laser output power. The gain determines the maximum laser output power. It was shown by various authors that the slope efficiency of a fiber laser is directly related to the ratio of the output coupling losses to the total round-trip losses,

which include the cavity losses (Digonnet, 2001). It has been observed that the output coupling ratio is determined by the characteristics of the gain medium used (Shang *et al*, 2006; Hambali N.A.M.A. *et al*, 2009; Gong-Ru Lin *et al*, 2006). For the same amount of pump power, the maximum output power of a low gain fiber laser is obtained when 20 % to 40 % of light is coupled out. Output coupling ratios between 80 % and 90 % were observed for high gain Erbium-doped fiber lasers. Our experimental results demonstrated clearly that our laser is efficient when 90 % of the light is coupled out

3.4.2 Optimum Erbium-doped fiber Length

For fiber laser cavity optimization, the optimum fiber length of Erbium-doped fiber for a given pump power and the output-coupling ratio is important. In this experiment, the optimum length of the Erbium-doped fiber leading to the highest output power of the fiber laser was recorded when fiber laser is pumped using a laser diode emitting 100 mW at 980 nm. The output power was measured for Erbium-doped fiber lengths between 0.25 m and 5 m. A constant length interval of 0.5 m was kept in the experiment between 0.5 m and 5 m. In Figure 3.14 the output powers of the fiber lasers using two different Erbium-doped fibers (EDF1 and EDF2) is shown. The maximum output power for the laser with an EDF1 was 16 mW when the fiber was 1.5 m long. The fiber laser with an EDF2 fiber achieved 17 mW maximum output power with a 3.5 m long fiber. From these results, it is clear that, since the gain of Erbium-doped

fiber amplifier increases with length, the slope increases as the length also increases, approaching the quantum efficiency for a lossless fiber laser cavity. However, it can be observed, the laser output power is maximum output power at an optimal length (1.5 m for EDF1 and 3.5 m for EDF2), and when the Erbium-doped fiber length is longer than the optimal, the output power progressively drops due to the intrinsic absorption of the Erbium-doped-fiber. When the loss due to absorption is stronger in the cavity, the pump threshold is larger, the output power is smaller, and the change of the output power is sharper with the Erbium-doped fiber length. In other words, the pump power is absorbed in the first section of the Erbium-doped fiber to produce stimulated emission which is then reabsorbed in the second section of the Erbium-doped fiber.

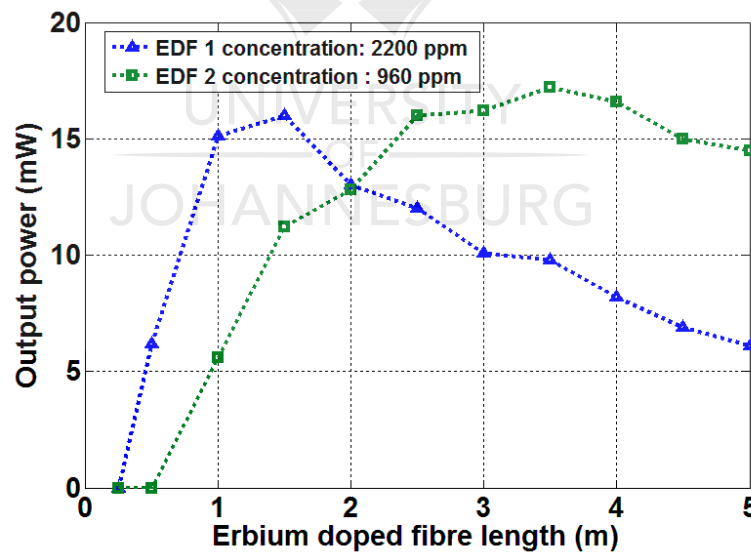


Figure 3.14: The output power of the fiber ring laser as a function of Erbium-doped fiber length and different Erbium concentration.

In Figure 3.15, the optical output power at 1550.160 nm versus pump power is illustrated. The lasing threshold is around 10 mW. No saturation of the output power was observed for pump powers up to 160 mW. The slope efficiency was 10.4 %. The slope efficiency admitted in Erbium-doped fiber lasers range between 10 % and 20 %. In our experiment, the slope efficiency is limited by the insertion loss of 3 dB introduced by the fiber Fabry-Perot tunable filter around 1550 nm of the transmission spectrum.

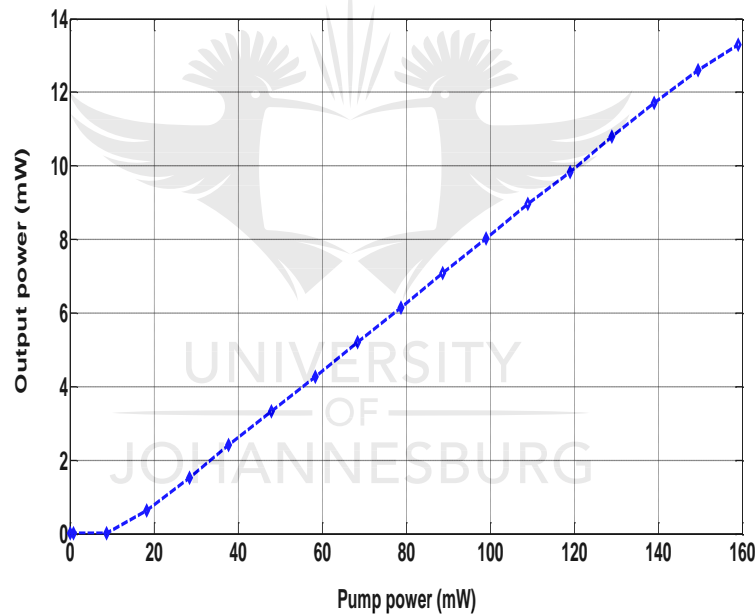


Figure 3.15: Output power versus pump power in continuous wave fiber ring laser.

3.4.3 Pulsed regime of fiber laser

The characterisation of the Q-switched fiber system illustrated in Figure 3.10 was achieved by applying harmonic signals to the filter at different frequencies, but with the same amplitude. An example of a train of generated light pulses is shown in Figure 3.16. The standard deviation of the Q-switched fiber laser output peak power was less than 1 %.

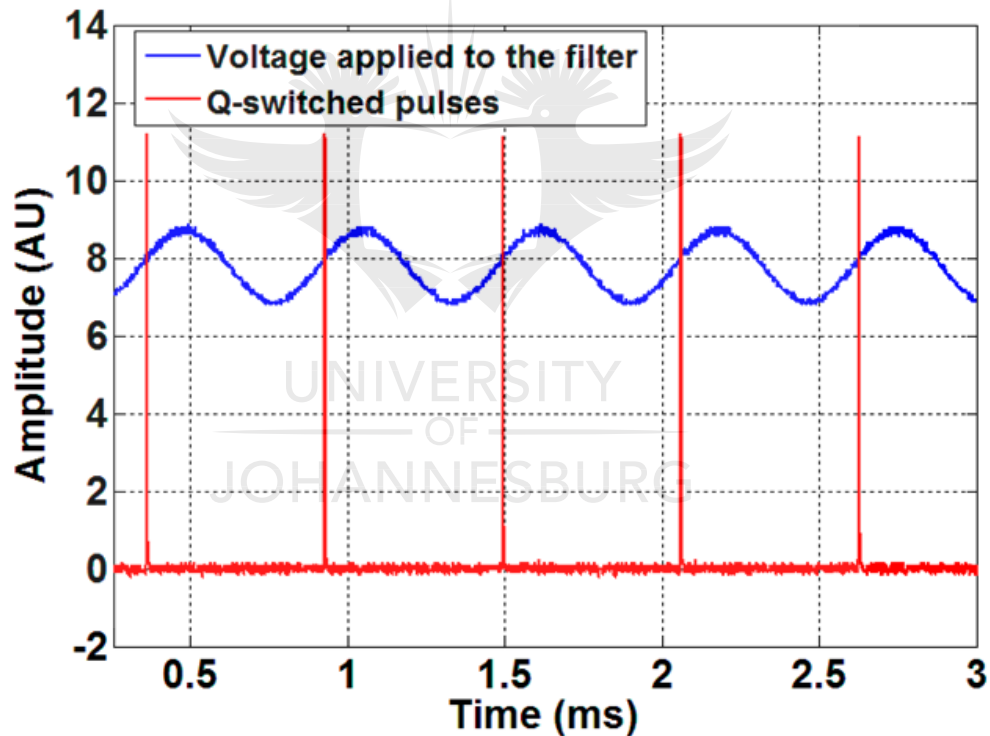


Figure 3.16: Train of the generated light pulses.

For any change in the amplitude of the applied sinusoidal signal to the tunable filter, the DC voltage offset should be adjusted accordingly to ensure a periodic and stable waveform recorded in the oscilloscope. To determine the time duration of the pulses, the full width half maximum (FWHM) of the pulse is measured directly from the oscilloscope. The output peak power of the pulse was determined by the relative peak voltage of the pulse recorded in the oscilloscope. The unit of output peak power of the fiber laser is mW. However, the output of the laser is measured using an oscilloscope providing readings in volts. To determine the output peak power (in mW), the following steps were carried out.

Step 1: The fiber laser was first set to operate in the continuous wave regime by applying 8 volts direct current to the fiber Fabry-Perot filter, corresponding to the operating wavelength of 1550 nm.

Step 2: The voltage, V_{DC} , of the continuous wave laser output was measured with the oscilloscope. The output of the fiber laser is connected to the oscilloscope via a high-speed photo-detector.

Step 3: With the fiber laser in continuous, we measured the output power, P_{CW} , of the fiber laser using with an optical power-meter. The output of the fiber laser was directly connected to the optical power meter.

From the results obtained in step 2, step 3, the calibration relation between the output voltage (V) and the output power (mW) was established as:

$$V_{DC}(Volts) = P_{CW}(mW) \quad (3.5)$$

Step 4: The fiber laser was set to operate in pulsing regime by applying a sinusoidal electrical voltage to modulate the fiber Fabry-Perot tunable filter. The frequency, the peak voltage and the DC offset of the modulating signal were correctly chosen. The output of the fiber laser is connected to the photo-detector through a 30 dB attenuator to prevent saturation. The reading of output peak voltage, V_{Peak} , from the oscilloscope is recorded.

With this calibration relation, the output peak power of the all-fiber actively Q-switched Erbium-doped ring laser was calculated after taking into account the amount of attenuation introduced.

3.4.4 Effect of Erbium ion concentration and Erbium-doped fiber length

In this section, the output peak power of the Q-switched fiber laser with respect to the concentration of Erbium-doped fiber characterized. Two different Erbium-doped fibers are used in the experiment with characteristics described earlier in section 3.3. For each type of Erbium-doped fiber, the experiment is performed with a variable length from 0.5 m to 4.5 m by step of 1 m. The experimental results are presented in Figure 3.17.

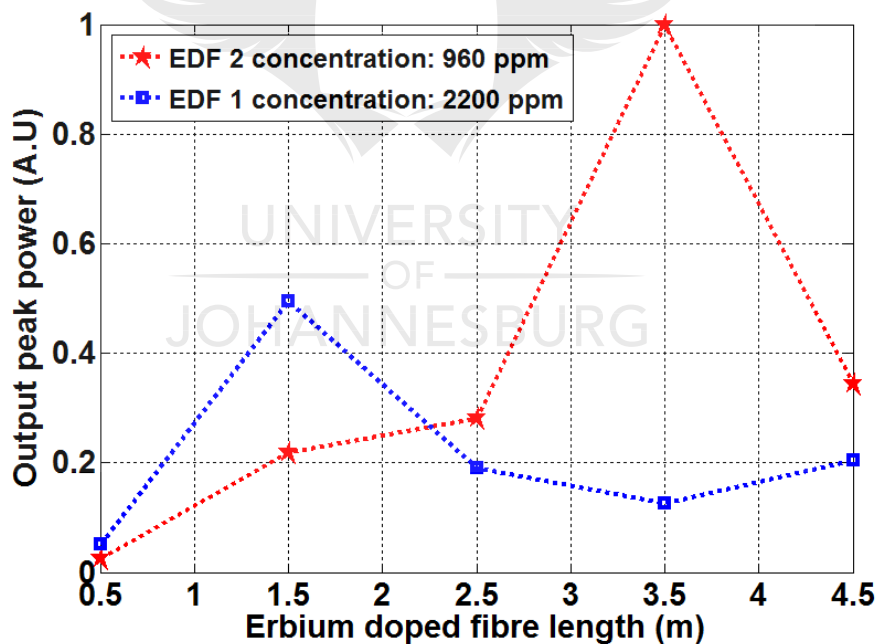


Figure 3.17: Dependence of the laser output peak power on the length of the Erbium-doped fibers with different ion concentration.

In this experiment, the output power of the pumping laser diode was set at 60 mW. The scanning frequency of the fiber Fabry-Perot tunable filter was kept at 1 kHz during the experiment. The highest output peak power was obtained with a 3.5 m using low concentration fiber Erbium-doped fiber (960 ppm). For 2.5 m of the same fiber the output peak power was only 25 % of maximum value. For 4.5 m of the same fiber, the peak power was reduced to 46 %. The maximum output peak power is obtained for short EDFs (1.5 m), when the concentration is high (2200 ppm).

Figure 3.17 shows that the decrease of the fiber laser efficiency caused by the increase of the cluster concentration. This physical phenomenon is known as quenching effect, and strongly manifest in high concentration Erbium-doped fibers. As the concentration of Erbium-doped fiber increases, ions clusters are formed. This leads to Erbium ions sharing energy to their neighbors in the same energy level. This reduces the lifetime of the excited Erbium ions contributing to the population inversion. This Quenching effect also reduces the gain of the Erbium-doped fiber and therefore increases the pump threshold of the fiber laser. The quenching effect is also responsible for the decrease of the output power of a fiber laser with a 2200 ppm Erbium-doped fiber compared to a laser with a 960 ppm Erbium-doped fiber (Paschotta, 2008). The length of the Erbium-doped fiber as well affects the output peak power. For the Q-switched fiber laser using EDF2, with small ions concentration compared to EDF1, a decrease of the output peak power is caused by the fiber lengthening and influence of the optical cavity losses.

3.4.5 Effect of scanning frequency of the fiber Fabry-Perot tunable filter

Using the 3.5 m fiber with the 960 ppm ion concentration in the laser cavity, the dependence of the peak power and pulse duration on the scanning frequency of the Fabry-Perot filter was measured. The results of these measurements are presented in Figure 3.18. The speed of the Fabry-Perot wavelength tuning depends on the frequency of the electrical signal.

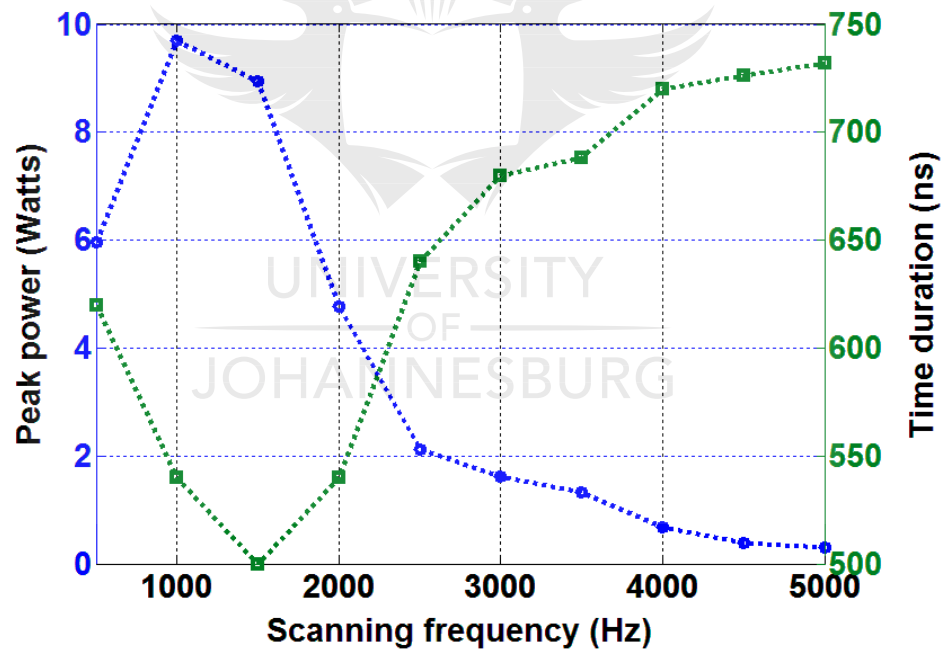


Figure 3.18: Output peak power and time duration of the light pulses as a function of the scanning frequency of the Fabry-Perot filter.

At low frequency, less than 1 kHz, the transmittance spectrum of the Fabry–Perot filter overlaps with the FBG spectrum too slowly. Lasing starts before the filter system achieves the maximum transmittance. The peak power of the pulses is less and pulse width wider. More than one pulse can be generated per scanning cycle. As the scanning rate increases, the peak power approaches maximum at a frequency of 1 kHz and then declines linearly. At the same time, the duration of light pulses reaches its minimum value of 500 ns at a frequency of 1.5 kHz and then the pulse width becomes wider. We attribute this to the low power of the pump diode laser.

At a high frequency, the period between pulses becomes shorter than the time required for the cavity gain to reach its maximum. The output coupling ratio in this experiment was 90 % of output radiation. Even with only 60 mW of pump power, the laser parameters such as pulse frequency, maximum peak power and minimum pulse duration are acceptable for some applications in fiber-optic sensors, (Bao X, 2012) where the length of the sensing fiber is a limiting factor for the pulse repetition rate.

The Fabry–Perot filter can support a scanning frequency of more than 5 kHz. However, in our configuration with a low-level pump power the output peak power decreases drastically when the scanning frequency is increased, as shown in Figure 3.19. Similarly, the scanning speed changes with the amplitude of the sine wave signal.

Figure 3.20 illustrates how the amplitude of the tuning sine wave signal contributes to the output peak power of the laser. For 60 mW pump power and an output coupling

ratio of 90 %, the peak power varies with the amplitude of the tuning voltage. At 1.5 kHz, about a 27 % increase in peak power is observed when the amplitude voltage increases from 2 to 3 Volts. A slight 14 % increase in peak power is observed when the amplitude voltage increases from 3 to 4 Volts. At higher frequencies, the amplitude of the sinewave is relatively small. These results show that the scanning speed associated with the switching dynamics contributes of the output power produced by Q-switched fiber laser fiber laser.

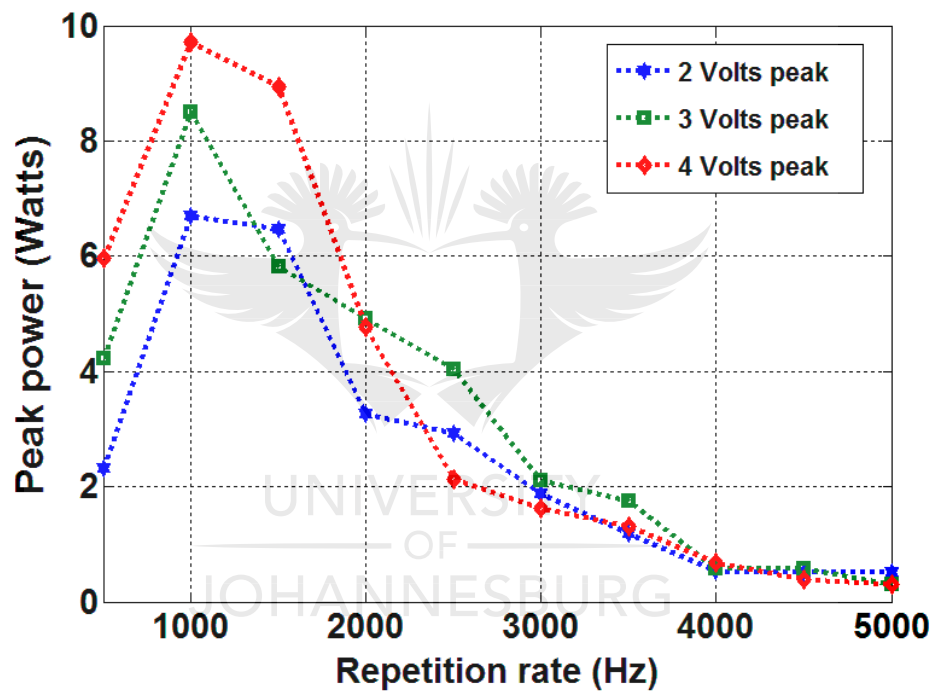


Figure 3.19: Dependence of the output peak power on the frequency and amplitude of the sinusoidal signal.

3.4.6 Extinction ratio

For distributed fiber sensors applications, especially when a long multi-kilometer sensing fiber is required, high extinction ratio in the output of Q-switched fiber laser is needed. In this section, the extinction ratio of the Q-switched fiber laser is measured. The experiment is performed with the continuous wave fiber laser operation. In this case the reflectance spectrum of the FBG overlaps with the transmission spectrum of the F-P filter (ON). When the F-P transmission line is tuned away from the FBG wave-length high losses are introduced into the laser cavity (OFF). The extinction ratio of the output laser was measured at more than 40 dB; the results are shown in Figure 3.21.

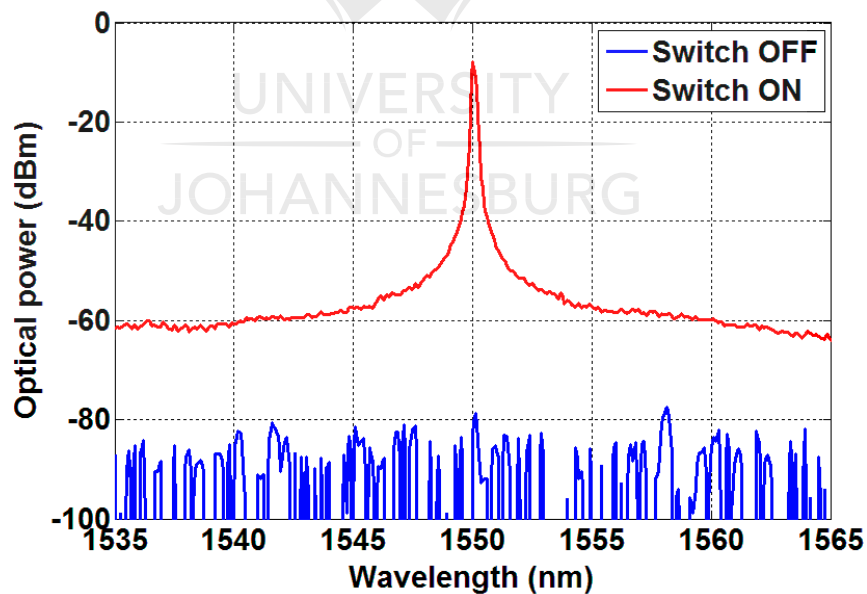


Figure 3.20: Spectra of the output laser light for switch-on and switch-off.

The optimized fiber laser cavity was used in this experiment. This includes a 3.5 m long Erbium-doped fiber with low Erbium ions concentration (960 ppm). For this experiment, 90 % of light was coupled out of the fiber laser system. The output power from the pumping laser diode was fixed at 60 mW. This high extinction ratio was achieved because of the high isolation in the ring cavity. If the optical isolator was removed, the extinction ratio was reduced to 20 dB. These results clearly show that a higher extinction ratio value is expected in the pulsing regime when the accumulated energy is released as a pulse.

3.5 Summary

We have proposed and experimentally investigated a simple configuration for an active Q-switched Erbium-doped fiber ring laser. A new concept of Q-switching in fiber laser based on the overlap between the transmission spectrum of tunable fiber Fabry-Perot filter and reflection spectrum of a fiber Bragg grating. The peak power and time characteristics of the Q-switched fiber laser have been characterized with respect to the length of the Erbium-doped fiber, the Erbium ions concentration, and the scanning frequency. Based on these experimental investigations, optimization of the laser configuration was performed to maximize the output peak power of the laser at a low pump power of 60 mW. It was shown that the peak power and pulse duration

are strongly dependent on the repetition rate frequency of pulse. The output peak power of 9.7 W was obtained using 3.5 m of Erbium-doped fiber with an ion concentration of 960 ppm, at 1 kHz of the pulse repetition rate and 90 % of light coupled out. The laser pulse duration of 500 ns at the wavelength of 1550 nm was obtained at the same pulse repetition rate. An extinction ratio up to 40 dB was obtained from fiber laser. This is the first time that such an all-fiber Q-switching approach has been experimentally implemented, and the Q-switched fiber laser fully optimized. The simplicity of this Q-switching technique and the principle of its operation make it suitable for being extended into more complex set-ups, including multi-wavelength fiber lasers for sensing applications.



Chapter 4

Implementation all-fiber Q-witched Erbium-doped laser in a linear cavity

UNIVERSITY
OF
JOHANNESBURG

4.1 Introduction

High peak power laser pulses with short pulse duration and high extinction ratio are essential for a variety of applications including coherent optical transmission and optical fiber sensing systems. In Chapter 3, a new concept of Q-switching based on the spectral overlap mechanism between the transmission of a fiber Fabry-Perot tunable filter and the reflection spectrum of a fiber Bragg grating was discussed. Successful Q-switching operations and pulse characteristics were then presented. The system was implemented and studied using a fiber laser ring cavity configuration. In addition to the successful Q-switching mechanism demonstrated in ring cavity, it was demonstrated that the extinction ratio is easily improved because of the unidirectional light propagation achieved with an optical isolator inside the fiber ring laser cavity. In this Chapter, a Q-switched fiber laser linear cavity configuration is designed and demonstrated experimentally. Contrary to the ring laser cavities, linear laser cavities do not allow the use of optical isolator inside the laser cavity to increase the extinction ratio of the fiber laser. However, it is established in this investigation that with a proper cavity design, a linear cavity performs with characteristics comparable to a ring fiber laser. To obtain the full benefit from the designed linear cavity Q-switched fiber laser, the laser system was first optimized and characterized in the continuous wave regime. The output pulses of Q-switched fiber laser are studied as a function of pump power and modulation frequency. To characterize the Q-switched fiber laser performance, a

3 m long Erbium-doped fiber was used. Fiber laser parameters, such as output coupling ratio, pump power and modulation frequency were optimized to obtain the output pulse time duration and peak power. This Q-switching technique maintains the intrinsic robustness and simplicity of an all fiber laser system. The results of this experiment were published earlier in (Kaboko *et al.*, 2017).

4.2 Design of the linear cavity Q-switched fiber laser

The Q-switching mechanism proposed in this project include both filters; fiber Bragg grating and Fabry-Perot tunable filter. A proper cavity design and optimization is required to achieve both continuous wave and Q-switched operation. The physical position of each optical component in the fiber laser cavity plays a crucial role in the trade-off between gain and loss of the fiber laser system. Scenarios of linear cavity arrangement are proposed to choose the best suited for archiving linear cavity fiber laser operating optimally in both continuous wave and Q-switching regime based on the spectral overlap between the reflection spectrum of the fiber Bragg grating and the transmission spectrum of the fiber Fabry-Perot tunable filter.

The first fiber laser configuration is shown in Figure 4.1. The fiber laser contains a 3 m long Erbium-doped fiber (EDF) as a gain medium. The Erbium-doped fiber is pumped a semiconductor laser diode emitting 100 mW at wavelength of 980 nm. The

pump light is coupled to the fiber laser cavity via a wavelength division multiplexer (WDM). The Erbium-doped fiber emits a broad spectrum of light in the 1550 nm region. The radiation from the Erbium fiber enters port 2 of the circulator, exits port 3 and reenters port 1. Finally it emerges from port 2 to be amplified by the Erbium-doped fiber. The Fabry-Perot filter is voltage modulated to select the lasing wavelength which is determined by the fiber Bragg grating. The fiber Bragg grating also acts as left mirror and is connected to a 90/10 output coupler; with 90 % of light coupled out of the fiber laser.

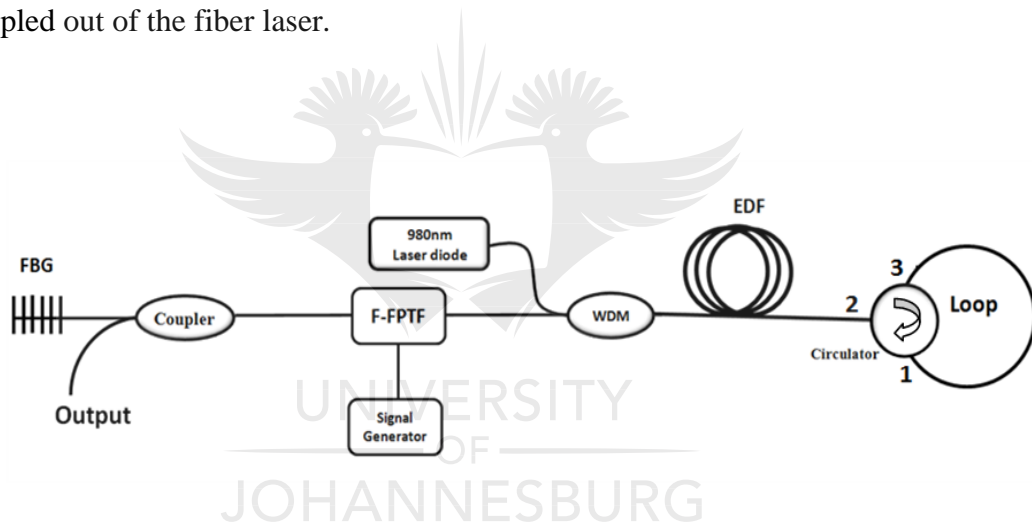


Figure 4.1: Linear cavity fiber laser using a fiber Bragg grating as left mirror and a looped circulator as the right mirror.

Figure 4.2 shows the recorded output spectra of the fiber laser using a spectrum analyzer. The transmission spectrum of the fiber Fabry Perot tunable filter is tuned using a DC voltage. Due to a small change in the cavity length of the fiber Fabry-Perot tunable filter, in this experiment, the transmission spectrum of the filter at 1550 nm is

obtained when 6.5 volts DC is applied to it; which corresponds to the reflection spectrum of the fiber Bragg grating.

In this experimental set-up, it is expected a high cavity loss, when 0 volts is applied to the filter; and fiber laser emission and total spectral overlap between transmission of the filter and the reflection spectrum FBG, when the filter is tuned with 6.5 DC voltage. However, due to the gain and loss completion within the fiber laser cavity, a weak multi-wavelength emission around 1600 nm is generated.

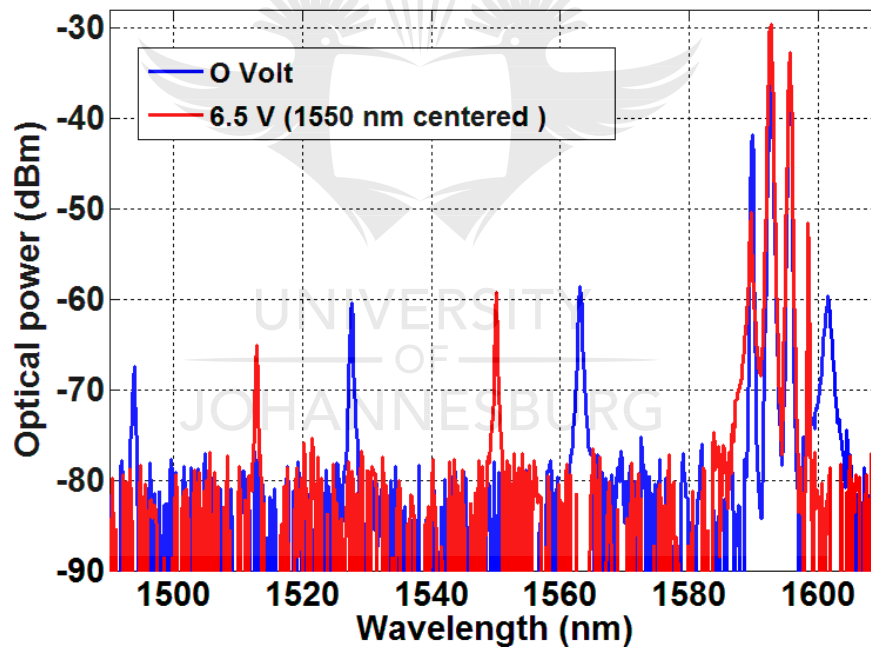


Figure 4.2: Multi-wavelength laser emissions in 1600 nm window.

In addition, from results in Figure 4.2, it is clear that the fiber laser output spectrum is independent of the applied voltage to the tunable filter. This mean it is not possible to

achieve the Q-switching of fiber laser in the 1550 nm range where the maximum reflection of the fiber Bragg grating is obtained. Nevertheless, this fiber laser configuration, if optimized, presents a potential for emits a multi-wavelength fiber laser emission. Additionally, with an appropriate fiber Bragg grating reflection wavelength spectrum, this configuration could possibly be optimized to produce longer wavelength.

In a second configuration, illustrated in Figure 4.3, the fiber Fabry-Perot tunable filter is placed between the FBG and the Erbium-doped fiber.

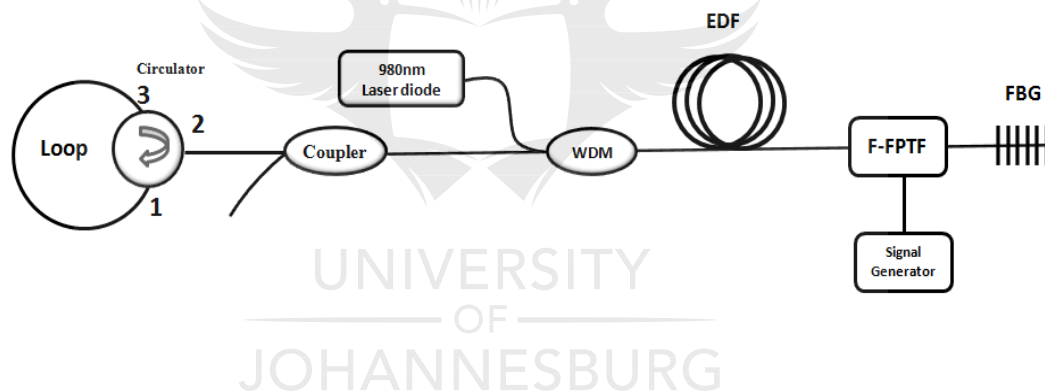


Figure 4.3: Linear cavity fiber laser using a fiber Bragg grating as right mirror and a looped circulator as left mirror. The tunable filter is inserted between the FBG and the EDF.

The measured output laser spectrum is shown in Figure 4.4 when 6.5 DC voltage is applied to the tunable filter. The result is an interference pattern generated by the different sub-cavities at 1560 nm with a spectral width of 7 nm. A fiber Fabry-Perot tunable filter is made of two parallel mirrors forming a cavity. A sub-cavity is also

formed between right mirror of the tunable filter and the fiber Bragg grating. The lasing mode of the fiber laser is a result of the superimposed interference patterns of the forming cavities. In this cavity configuration, the cavity loss could not be modulated to achieve laser emission at 1550 nm, fixed by the fiber Bragg grating.

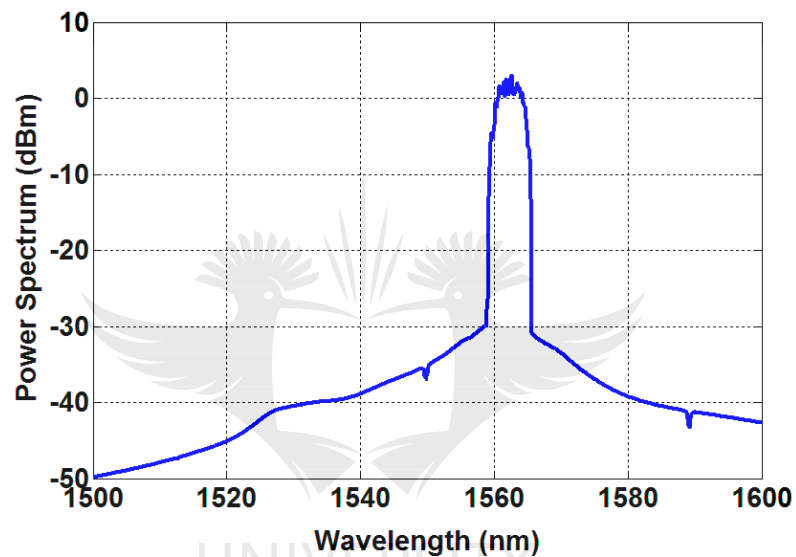


Figure 4.4: Broad spectrum emissions of the fiber laser in 1560 nm region.

4.3 Experimental set-up of linear cavity Q-switched fiber laser

To obtain Q-switching in linear cavity, the proposed all-fiber Q-switched laser is schematically shown in Figure 4.5. The pumping of the fiber laser is provided by a laser diode emitting light at 980 nm. The pump source is coupled to the fiber laser cavity using a wavelength division multiplexer (WDM). The gain medium of the fiber laser consists of a 3 m long Erbium-doped fiber (M-5-125 Fibercore). The high reflectivity fiber Bragg grating (FBG) and the looped optical circulator are used as left and right cavity mirror, respectively. The cavity loss is controlled with a modulated fiber Fabry-Perot tunable filter. The output power from the fiber laser is collected using an optical coupler.

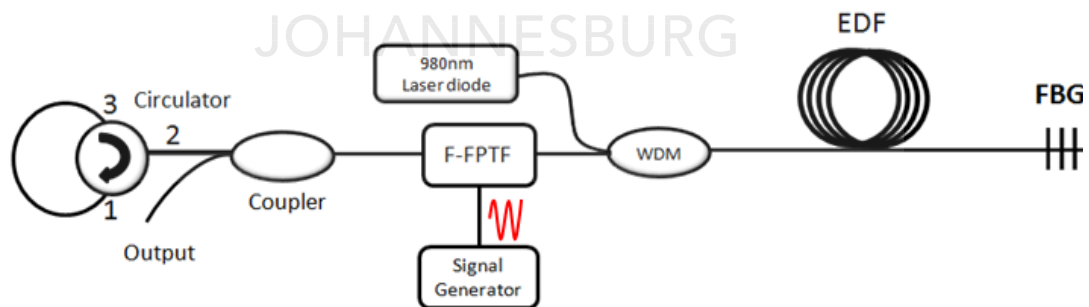


Figure 4.5: Experimental set-up of the linear cavity Q-switched fiber laser.

The pump light absorbed by the Erbium-doped fiber (EDF) generates spontaneous emission at 1550 nm. This light is reflected by a fiber Bragg grating, used as right mirror. The reflectivity of the Fiber Bragg grating is approximately 98%. The Full wave half maximum (FWHM) of the reflection spectrum of the fiber Bragg grating is 150 pm at 1550 nm, as shown in Figure 3.7. The reflected radiation propagates towards the fiber Fabry-Perot tunable filter. The measured spectral width of the transmission spectrum Fabry-Perot filter is 200 pm, as illustrated Figure 3.4. The modulated fiber Fabry-Perot filter controls the intra-cavity loss of the laser resonator. If the reflection spectrum of the FBG overlaps with the transmittance spectrum of the fiber Fabry-Perot tunable filter, the light reflected from the FBG can pass through the filter. Part of it is coupled out through an optical coupler and the rest is reflected back into the cavity via and looped circulator used as a mirror.

Q-switching is obtained in the following way: Firstly, the transmission spectrum of the fiber Fabry-Perot (F-P) tunable filter and the reflection band of the FBG do not overlap. The Q-switch is off (cavity open) and blocks the intra-cavity beam. Stimulated emission is suppressed because photons are not circulating in the gain medium. This allows the population inversion to grow to a very large value. Then, the transmission spectrum of the fiber Fabry-Perot (F-P) tunable filter is tuned to overlap with of the reflection spectrum of the FBG. In this case, the cavity the Q-switched laser is closed (Q switch on) and the accumulated energy of the fiber laser is then released in one a large pulse.

In Figure 4.6, the transmission spectrum of the fiber Fabry-Perot filter and the reflection spectrum of the fiber Bragg grating is shown.

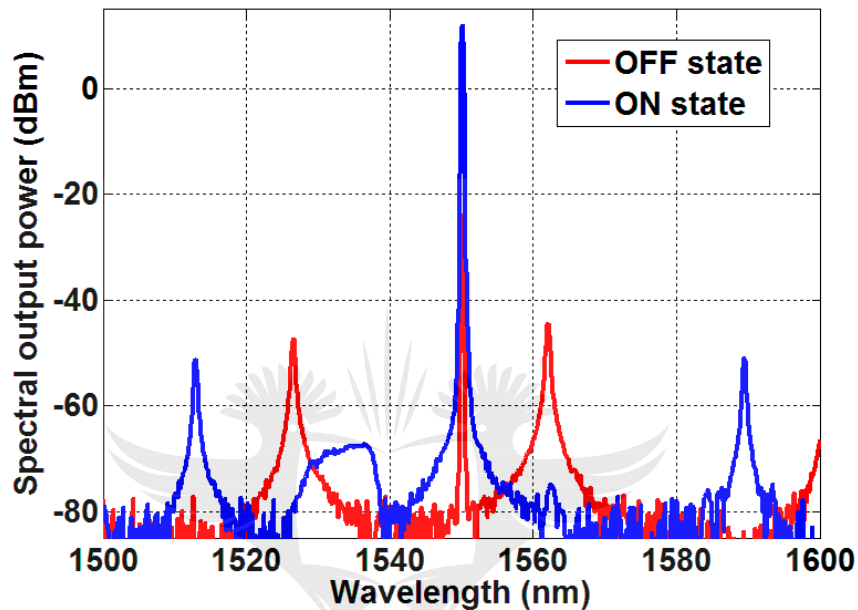


Figure 4.6: Illustration of the transmission spectrum of fiber Fabry-Perot tunable filter and reflection spectrum of the fiber Bragg grating.

In this experiment, the spectral position of the Fabry-Perot transmittance band is dynamically tuned using signal from a standard low-power sinusoidal signal generator. In this way, the intra-cavity loss is easily modulated. To avoid random spectral shifts of both fiber Bragg grating and tunable filter, the fiber laser cavity are kept in a controlled temperature environment. This is a requirement when using this type of fiber laser as source for sensing application.

A variable coupler is initially used to determine the optimal coupling ratio of the fiber laser. The output coupling ratio contributes to the overall cavity loss in fiber laser. In other word, it defines the minimum Erbium-doped fiber gain to achieve lasing. The maximum output power of the fiber laser is obtained for 90/10 coupling ratio, with 90 % of light coupled out of the fiber laser.

In Figure 4.7 the optical output power versus pump power is displayed. The lasing threshold is 15 mW. No saturation of the output power was observed. The slope efficiency is 12 %.

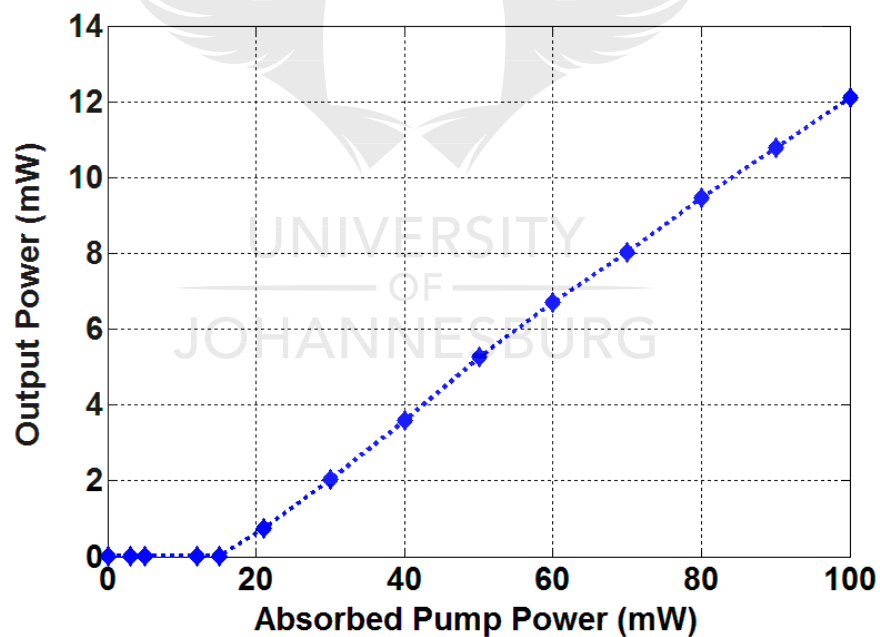


Figure 4. 7: Output power versus absorbed pump power.

4.4 Experimental results of Q-switched fiber laser

The Q-switched fiber laser pulses were measured with a photo-detector and a digital oscilloscope. A Sinusoidal signal at different frequencies and fixed amplitudes were used to characterize the system. The DC voltage offset of the applied sinusoidal signal is determined, prior the Q-switched fiber laser characterisation. The tunable Fabry-Perot filter is first tuned using a DC voltage to ensure maximum spectral overlap between the reflection spectrum of the FBG and the transmission spectrum of the Fabry-Perot filter. When these two spectra are tuned to 1550 nm, the fiber laser starts to oscillate with a narrow spectrum. The cavity loss then periodically modulated with a 4 volts peak sinusoidal wave. In this experiment, the pump power was varied from 40 mW to 100 mW and there repetition rate is kept constant at 1 kHz.

The peak power and the width of the Q-switched pulses as a function of the modulation frequency of the fiber Fabry-Perot filter are shown in Figure 4.8. With the pump power fixed at 100 mW, the pulses widen as the peak power decreases for frequency above 1 kHz. The decrease in peak power with increased repetition rate is due to the limited recovery time of the population inversion in the pumped Erbium-doped fiber. If the Q-switching of the laser cavity occurs faster, less energy is stored.

The pulse build-up and decay take longer, resulting in longer pulses with decreased peak power.

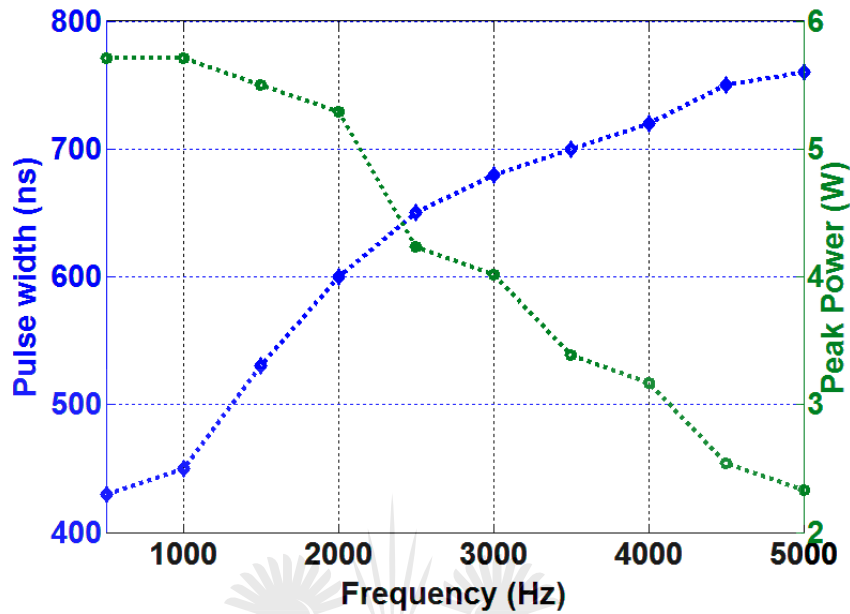


Figure 4. 8: Output peak power and time duration of the Q-switched fiber laser pulses as a function of repetition rate.

The population inversion build-up is determined by the lifetime of the metastable energy level. The typical lifetime of Erbium-doped fibers is about 10 ms corresponding to a frequency of 100 Hz. However, because of possible non-radiative decay processes in the atomic structure of Erbium-doped fiber such as amplified spontaneous emission, quenching effect, this lifetime is reduced ten times. This results in Q-switched fiber laser producing narrower pulses and higher peak power at around 500 Hz. However, there we observed parasitic and unstable pulses, below 500 Hz, which would be a shortcoming for sensing applications.

The peak power and time duration of Q-switched fiber laser pulses as a function of the pump power is displayed in Figure 4.9. For low pump power, around the threshold, the pulse width is wide and the peak power low. With an increase in pump power, far from the threshold, the pulses shorten and the peak power rises. An increase in pump power of Q-switched fiber leads to an increase in pump absorption and there a rise in the accumulated population inversion. In this lasing condition, the Q-switched pulse width tends to be equal to the photon lifetime in the cavity.

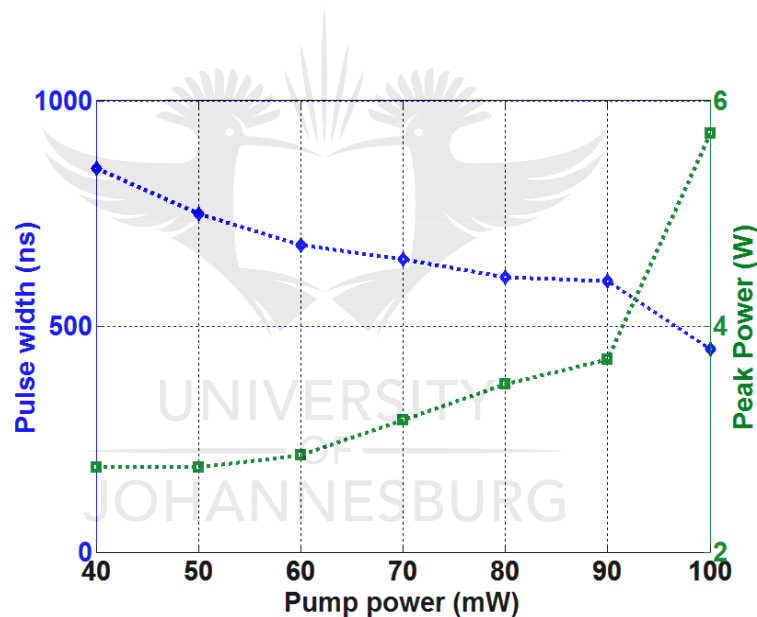


Figure 4.9: Output peak power and time duration of Q-switched pulses as a function pump power.

The spectral output power was measured using an optical spectrum analyzer (OSA). The recorded output spectra, illustrated in Figure 4.10, were taken with the OSA set at

0.05 nm resolution. The measurements were performed in the continuous wave regime with the fiber laser fiber Fabry-Perot tunable filter on and off modulation status. If the reflectance spectrum of the FBG overlaps the transmission spectrum of the Fabry-Perot filter, the Q-switch is on and the cavity losses are low. If the Fabry-Perot filter transmission spectrum does not overlap the FBG spectrum the Q-switch is off and the losses are high. The obtained extinction ratio is about 36 dB. The limited achieved extinction ratio is due to the laser cavity configuration. The linear cavity does not allow the use of an isolator to prevent unwanted light reflections when the two filter spectra do not overlap.

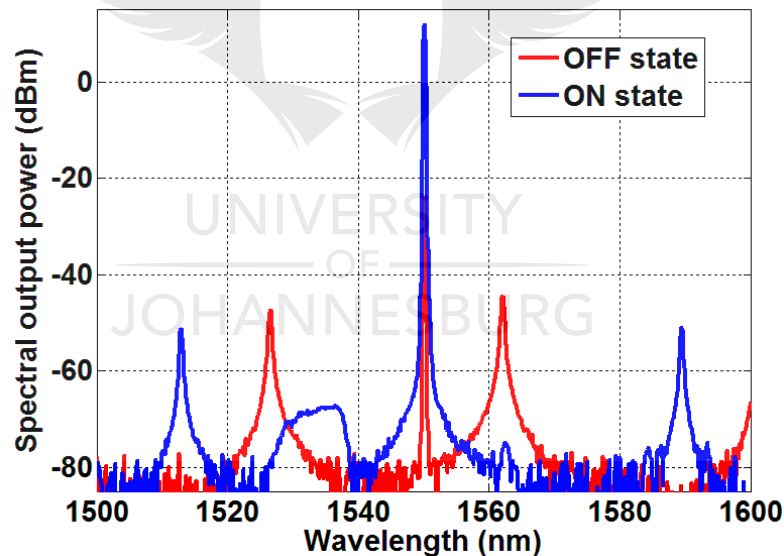


Figure 4. 10: Spectra of the output laser light for Q-switch-on and Q-switch-off.

4.5 Summary

In this Chapter we have presented the experimental optimization of the linear actively Q-switched Erbium-doped fiber laser. We have successfully and experimentally demonstrated a Q-switched Erbium-doped fiber laser based a spectral overlap between the transmission spectrum of a tunable filter and the reflection spectrum of a fiber Bragg grating. We have demonstrated that the proposed Q-switching approach is compatible with a linear cavity configuration. However, for this Q-switching technique to be successfully implemented in linear cavity, a proper fiber laser cavity designed is required, and all cavity parameters such as pump power, Erbium-doped fiber length, and output coupling ratio adequately optimized. The pulse characteristics of the Q-switched fiber laser, peak power and time duration, were characterized with respect to the frequency of the applied scanning frequency of the tunable filter and the pump power. Laser output peak power of 5.6 W with a 450 ns pulse time duration at a wavelength of 1550 nm was obtained at 1 kHz repetition rate; with 3 m long Erbium-doped fiber pumped with a 100 mW at 980 nm. The optimal coupling of 90 % light out the fiber laser was used. Additional, we have demonstrated that, though the linear cavity does not allow unidirectional light propagation inside the cavity, it is possible to achieve an extension ratio up a 36 dB, when the fiber laser cavity is optimized.

Chapter 5

Output stability and linewidth of fiber lasers

UNIVERSITY
OF
JOHANNESBURG

5.1 Introduction

Fiber lasers have demonstrated to be an important tool for experimentation in fields of pure scientific research, applied physics and engineering. To maintain the quality and accuracy of experiments, it is required a stable output power and well-defined frequency from the fiber laser source. In particular, for experiments where the temporal coherence of the light source plays a role, frequency stability and the linewidth characteristic of fiber laser are important factors. For instance, in modern fiber-optic communications, a spectral linewidth of the light source constitutes an important characteristic specification as it defines the signal dispersion and bit rate in long-haul optical communications. Moreover, fiber optic sensors based upon interferometric technique make use of narrow linewidth laser sources to improve the actual resolution of the sensor system.

To meet these requirements, the need to develop fiber laser systems with narrow linewidth arises. Accordingly, effective techniques to experimentally measure fiber lasers spectral linewidth are needed. Hence, in this Chapter the linewidth of the Q-switched fiber lasers, experimentally demonstrated in previous Chapters, are investigated. The background related to the linewidth and factors contributing to the broadening of the linewidth in these fiber lasers are first presented. Different methods to narrow the linewidth are discussed. In order to accurately measure the linewidth of the fiber lasers, a clear and effective experimental procedure is provided. We

implement here a linewidth narrowing technique based on using un-pumped Erbium-doped fiber. The experimental characterisations of spectral linewidth in both linear and ring Erbium-doped fiber laser systems are described and obtained results are discussed in sections of this Chapter.

The output power stability of Erbium-doped fiber laser sources is also required for applications such as high-resolution spectroscopy, photonic generations of microwave signals (Pérez-Herrera *et al.*, 2010). In this Chapter, the experiment is extended to explore the output power stability of fiber laser systems, as a function of output coupling ratio. Techniques to improve the output power stability in both ring and linear cavity are discussed.

5.2 Background of single longitudinal mode fiber laser

The spectral content of the fiber laser light is measured by its spectral linewidth. The linewidth characteristic of a fiber laser is defined as the full width at half-maximum (FWHM) of its optical power spectral density in terms of frequency or wavelength. Theoretically, the linewidth $\Delta\nu$ of any laser source is only limited by the Schawlow-Townes equation (A. Schawlow and C. Townes, 1958).

$$\Delta\nu = \frac{\pi h\nu(\Delta\nu_{res})^2}{P_{out}} \quad (5.1)$$

where $\Delta\nu_{res}$ is the full width at half maximum of the fiber laser cavity bandwidth, $h\nu$ is the photon energy and P_{out} is the output power.

Normally, the linewidth of a fiber laser is usually much broader than Schawlow-Townes limit due to various sources noise such as variations of the pump power, fluctuation in the pump wavelength, mechanical vibrations of the optical resonator, temperature fluctuations inside the fiber laser cavity, amplified spontaneous emission in the gain medium (Ball G. A. *et al.*, 1994; Rønnekleiv E., 2001; Horak P. *et al.*, 2006; Paschotta R. *et al.*, 2006). In other words, the Schawlow-Townes equation linewidth limit can only be obtained in a situation where one build a laser which has very small temperature fluctuation, has very stable pump source (in amplitude and emission wavelength), and has homogeneously broadened gain active media (Philip Goldberg, 1991; Arnaud J., 1996; Paschotta R. *et al.*, 2008).

The linewidth of a fiber laser depends on the time period over which it is observed. For short observation periods, like microseconds or nanoseconds, the linewidth is influenced by population density fluctuations in the gain medium, pump power fluctuations, spontaneous emission, the quality factor (Q) of the laser cavity, and the coupling between the phase and amplitude of the lasing field (Fox R.W., et al., 1997). For longer observation periods, from microseconds to milliseconds, mechanical and

thermal instabilities in a fiber laser result in frequency a fluctuation which widens the linewidth. For even longer observation periods, from seconds to days, temperature variations or changes in the pumping current result in frequency instabilities and also affect the laser output power stability.

Fiber lasers are known to emit light in more than one cavity longitudinal mode simultaneously. This multimode process is the major reason for a broad wavelength or frequency spectrum. Not only does multimode lasing cause the broadening of the fiber laser linewidth but it also makes the laser extremely unstable as the power is continually shifted from one mode to another. Because of the natural sensitivity of fiber lasers to temperature, fiber length, and vibrations, the output power of conventional fiber lasers is unstable. These perturbations induce competition among the different longitudinal modes of the fiber laser which results in mode hopping and output power variations.

The linewidth of a fiber laser depends on the gain medium and the laser cavity. The linewidth in a rare-earth-doped fiber laser is influenced by homogeneous and inhomogeneous broadening (Paschotta, 2006; Thiel C.W., 2011). In the homogeneous broadening, all the individual ions in the doped fiber are broadened in the same way. The homogeneous linewidth in Erbium-doped fiber can be expressed as the sum of several contributions given by (Hams, 2001):

$$\Gamma_{hom} = \Gamma_{pop} + \Gamma_{Er-Er} + \Gamma_{phonon} + \Gamma_{Er+host} + \Gamma_{ISD} \quad (5.2)$$

where, Γ_{pop} is population decay from the excited state which corresponds to the fundamental linewidth; Γ_{Er-Er} is the contribution from mutual transitions between Er^{3+} ions (Mims, 1979), and Γ_{phonon} represents a variety of phonon contributions. $\Gamma_{Er+host}$ is the contribution from nuclear and electronic spin fluctuations of the host crystal, and Γ_{ISD} originates from the local environment due to the optical excitation of neighbouring ions.

Imperfections such as impurities and defects cause local stresses and strains within the doped fiber. These stresses and strains cause the centre of the homogeneous linewidth of individual optical centres to shift slightly in frequency (Thiel C.W., 2011). The combination of many homogeneously broadened lines, each with a Lorentzian absorption profile centered at its own resonant frequency, results in an inhomogeneous linewidth which is much broader and has a Gaussian profile.

For Erbium-doped fiber, known as having a homogeneously broadened laser transitions, the lineshape for the stimulated emission cross-section as a function of wavelength or frequency, is constant and equal for all atoms in the laser gain medium (W. S. Rabinovich, 1989). This implies the gain profile of Erbium-doped fiber at any frequency depends just on the population inversion, resulting in a constant lineshape. In the event that the gain of an ideal homogeneous laser is enlarged, the longitudinal

mode nearest to the peak of the lineshape will lase given that the intra-cavity losses are wavelength independent.

In situation where the intra-cavity losses in the fiber laser are wavelength dependent, a single longitudinal mode operation may still be obtained. Nonetheless, the lasing mode may not be the one with the biggest stimulated emission. This means, during steady-state lasing operation, the gain of the lasing mode is equal to the cavity losses, in the meantime, all other longitudinal modes encounter comparable loss but have a net gain lower than the required minimum limit.

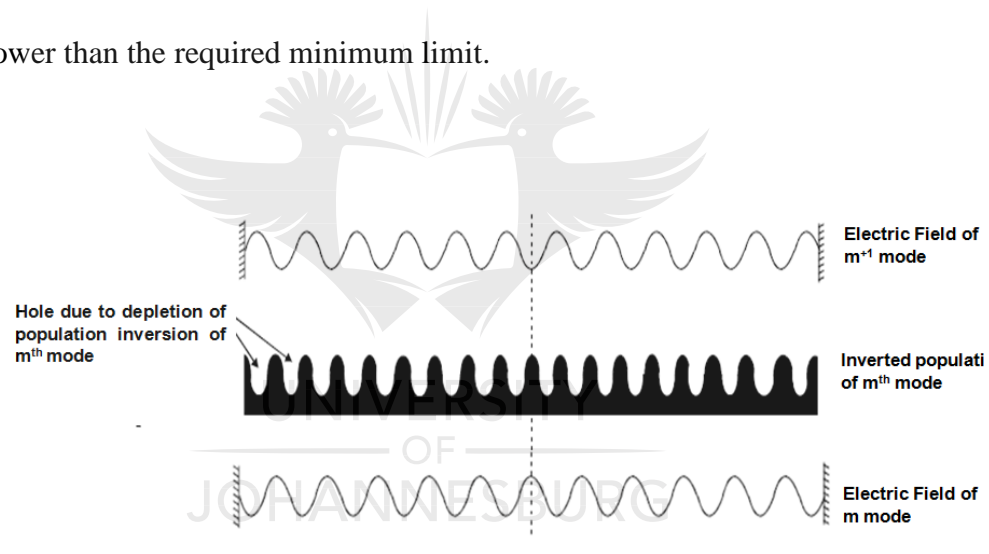


Figure 5.1: Field distribution of two adjacent modes and population inversion of the initial oscillation.

The fiber laser cavity configuration also contributes to multimode lasing operation. For instance, the forward and backward propagating waves in a linear cavity interfere to form a standing-wave which in turn depletion of the gain in the cavity. The gain

will be depleted at the peaks of the standing-wave and not at the nodes as illustrated in Figure 5.1. The population inversion increases at the nodes, resulting in spatial inhomogeneity of the gain. Consequently, neighboring modes may experience an overall gain large enough to initiate lasing. This phenomenon is not observed in a ring laser cavity, where we have unidirectional light propagation, which is further enforced by inserting components like isolators, circulators, polarization controller.

5.3 Methods of achieving narrow linewidth fiber laser operation

Because of the wide range of applications, narrow linewidth fiber lasers have been developed intensively over the last decades (Dong X L *et al.*, 2012; SchÄulzgen A *et al.*, 2007; Zhang W N *et al.*, 2012). Techniques for achieving stable, narrow linewidth fiber lasers are extensively discussed in the literature. These techniques include mode-selection and suppression of standing wave formation.

In the suppression of standing wave formation method, the laser cavity is designed in such a way that the formation of standing-waves is prevented. Unwanted lasing modes are suppressed by increasing the spacing between adjacent modes such that all the other modes lie outside the gain bandwidth. This is possible by designing a short linear

fiber laser cavity with fiber Bragg gratings (FBG) as reflecting cavity mirrors. The advantage of fiber Bragg gratings is low insertion loss, passiveness, high selectivity, and low cost. For conventional short linear laser cavities which use only two FBG reflectors for cavity feedback and wavelength selectivity, the laser cavity needs to be only a few centimeters long so that the laser mode spacing becomes comparable with the FBGs' bandwidth and single mode operation can be ensured (Xu O *et al.*, 2009). The drawback of this technique is that the scalability to high power is limited because of low pumping absorption efficiency (Zhao M *et al.*, 2009; Shijie Fu *et al.*, 2017). To extend the active fiber length for higher laser output power, ring cavity fiber lasers embedded with narrowband filters were developed. When operating far above the pumping power threshold, a travelling-wave in a ring-cavity is more suitable for single mode operation than a short linear cavity. Such a cavity avoids the formation of standing waves. In a unidirectional travelling wave laser the gain is depleted uniformly. However, this laser requires more intra-cavity components (Zhang J L, 1996). Among them, the FBG-based Fabry–Perot etalon (A. Polynkin *et al.*, 2005), saturable absorber (F. D. Muhammad *et al.*, 2012), and short sub-cavity (T. Wang *et al.*, 2014) approach to obtain single-frequency lasing in a ring cavity. However, in each case, additional loss is also introduced to the laser cavity and the complexity of the laser system has been increased.

In the mode-selection method, the laser cavity is constructed in such a way that the closest modes to the lasing mode reach threshold later because they have a large

difference in gain. To select longitudinal modes two cascaded fiber Fabry-Perot filters with different free spectral ranges are integrated into the fiber ring (Park N. *et al.*, 1991). This can also be accomplished by incorporating an equivalent phase-shifted FBG (Chen X F *et al.*, 2005) or by employing an FBG-based Fabry-Perot etalon (Cheng X P *et al.*, 2009) which acts as an ultra-narrow bandpass filter. Additionally, researchers suggested a passive multiple-ring (Lee C C *et al.*, 1991) or used a multiple cavity (Polynkin A *et al.*, 2005) in the fibre laser cavity to achieve mode selection. A gain fiber as saturable absorber was also utilized to act as a very narrow filter (Cheng Y, 1995; T Feng *et al.*, 2013). Injection locking technique in fibre was proposed to achieve single mode fiber laser oscillation (Lee C C and Chi S, 2000, Gong-Ru and Shih-Kai, 2003; Xin Zhang, 2007).

5.4 Linewidth measurement techniques.

To determine the suitability of a fiber laser for a specific application, the information regarding its spectral linewidth is essential. A number of research orientations have been devoted to measuring the exact value of the spectral linewidth of fiber laser systems (P. Yu, 2013; Huang, S. *et al.*, 2016). It is well known that fiber Bragg grating-based optical spectrum analyzer do not have the required resolution for laser linewidth measurement. The same is true for scanning filter methods. These traditional linewidth

measurements methods can only provide a resolution of several megahertz (M. W. Fleming and A. Mooradian, 1981), which is inadequate for kHz linewidth range expected for fiber laser. For this reason, measurement techniques such as homodyne and heterodyne based detection are proposed to achieve several kilohertz resolution measurement (Okoshi, 1998; Ludvigsen, H., 1998). These techniques are based on coherent detection approach. Coherent detection is achieved by combining the optical signal with a continuous wave (CW) laser in a coupler as shown in Figure 5.2.

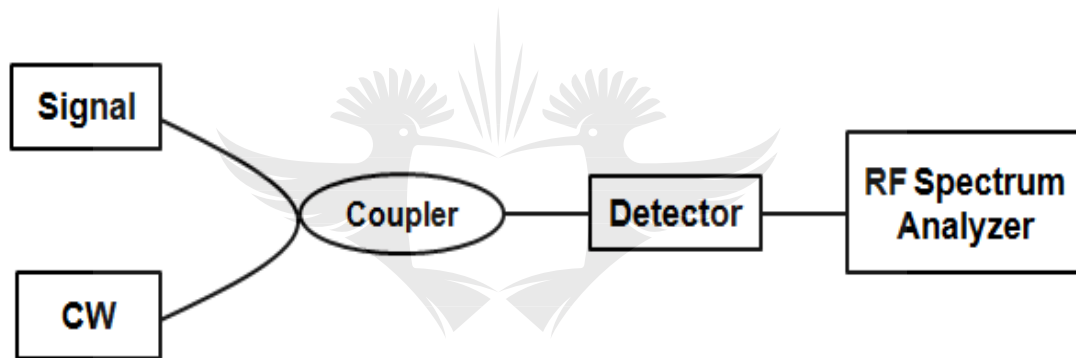


Figure 5.2: Coherent detection technique for linewidth measurements.

The resulting beat signal is detected with a photodetector and an RF spectrum analyzer. The continuous wave laser used, which is referred to as local oscillator, must have a stable and narrow linewidth. The central frequency of the local oscillator must be tuned to the signal laser frequency so that the beat frequency falls within the bandwidth of the electronic detection system.

The laser linewidth is determined from the width of the beat spectrum. Assuming that the two fields are identically polarized the optical signal can be written as

$$E_s = A_s \exp[-i(\omega_0 t + \varphi_s)], \quad (5.3)$$

in which ω_0 , A_s , and φ_s are the angular frequency, amplitude and the phase of the signal, respectively.

The optical field of the local oscillator is expressed as

$$E_{LO} = A_{LO} \exp[-i(\omega_0 t + \varphi_{LO})], \quad (5.4)$$

Given that the photodetector responds to the optical intensity, the incident optical power at the photodetector is shown by:

$$P(t) = k|E_s + E_{LO}|^2 = P_s + P_{LO} + 2\sqrt{P_s P_{LO}} \cos(2\pi\nu_{IF} t + \Delta\varphi), \quad (5.5)$$

where $P_s = kA_s^2$, and $P_{LO} = kA_{LO}^2$, are the powers of the signal and the local oscillator, respectively. $\Delta\varphi = \varphi_s - \varphi_{LO}$ is the phase difference of the two sources.

$\nu_{IF} = \frac{\omega_s - \omega_{LO}}{2\pi}$ is the intermediate frequency (ν_{IF}).

If the power P_{LO} of the local oscillator is much larger than the signal power P_s , the first term can be ignored. The second term P_{LO} is a large continuous signal which carries no information but contributes to shot noise or white noise. The third term is the

important mixing term. The actual optical signal frequency does not appear explicitly, only the difference between the signal and local oscillator frequency (ν_{IF}).

Depending on whether or not ν_{IF} is equaled zero; there are two types of coherent detection methods, the homodyne and heterodyne detection. We discuss here the delayed self-heterodyne detection.



5.5 Delay self-heterodyne measurement technique.

The delayed self-heterodyne detection technique is a well-established method for measuring the linewidth of fiber lasers (Albert Canagasabey *et al.*, 2011). The detection of the laser linewidth with the delayed self-heterodyne technique is based on the conversion of optical phase or frequency fluctuations of the laser into variations of light intensity in a Mach-Zehnder interferometer as shown in Figure 5.3.

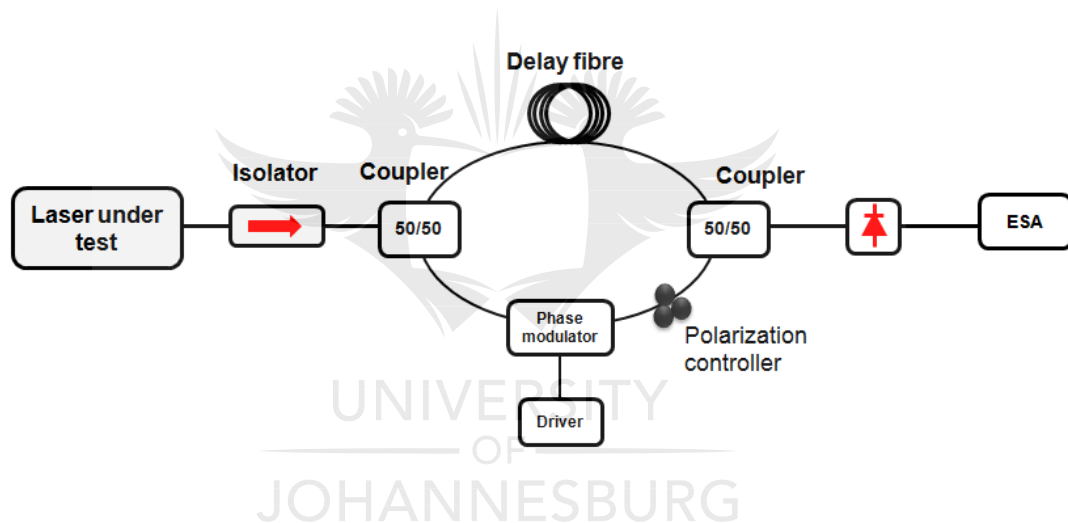


Figure 5. 3: Delayed self-heterodyne interferometer (DSHI) technique using a Mach-Zehnder interferometer (MZI).

The single longitudinal mode laser beam propagates through an optical isolator (ISO), and then split into two beams by a 1×2 coupler (C1). One beam is delayed by a single mode fiber. The other beam propagates through a phase modulator (PM). The phase modulator is used as frequency shifter to reject the DC signal in the detection system and measures only the photocurrent fluctuations. The two beams are recombined by

the coupler (C2) and their beat signal is detected by a photodetector (PD) and recorded by an electric spectrum analyzer (ESA). The laser light from the two arms interfering at the detector produces a spectrum with width and shape that depend on the linewidth laser under test.

The interferometer delay must be chosen carefully. A large delay gives a large signal because the slope of the Mach-Zehnder transfer function scales with the delay. A large delay narrows the bandwidth over which the interferometer transfer function is linear. This corresponds to a third of the interferometer spectral period (Chen, X et al., 2011). The optical signal delay is chosen to be longer than the coherence length of the laser. This simplifies the interpretation of the measured spectral power because interfering fields become uncorrelated on the detector. However, the length of the required optical delay line may become impractically long (Chen, X et al., 2011).

If the delay time, τ_d , of the beam one path exceeds the coherence time, τ_c of the source, the two combining beams interfere as if they originated from two independent lasers with an offset in frequency by δf . Thus the system performs similarly to optical heterodyne detection. The delay time τ_d and the resolution of the interferometric method $\Delta\nu_{res}$ are related by

$$\tau_d = \frac{nL_d}{c} \cong \frac{1}{\Delta\nu_{res}} \quad (5.6)$$

in which L_d is the length of the fiber delay line.

The interpretation and analysis of the laser linewidth resulting of the measured spectrum are twofold: one for lasers with a short coherence length or equal to the interferometer delay, and another for lasers with longer coherence length. Ideally, Lasers light with a shorter coherence length than the path length imbalance of the interferometer will produce a Lorentzian spectrum with a half width at half max equal to the laser light spectral linewidth. The Lorentzian-shaped linewidth at 3 dB can be inferred from the displayed linewidth by using the relationship shown in Table 5.1.

Table 5.1: Delayed self-heterodyne linewidth relations (Dennis Derickson , 1998).

Measured Full-Width Point	Displayed Width
-3dB	$\Delta\nu_{s,hom} = 2\Delta\nu_L$
-10dB	$\Delta\nu_{s,hom} = 2\sqrt{9}\Delta\nu_L$
-20dB	$\Delta\nu_{s,hom} = 2\sqrt{99}\Delta\nu_L$

On the other hand, for lasers with a significantly longer coherence, as compared to interferometer delay path length, the lineshape function, when using self-heterodyne, deviates considerably from the Lorentzian lineshape function. This is justified by the coherent interference of light from the two arms of the interferometer. In this case, the lineshape function results in a combination of a Dirac delta function at the frequency of modulator used in one arm of the interferometer with the interferometer transfer

function, where the depth of the ripples is determined by the laser linewidth. The linewidth is obtained by properly fitting data to the measured lineshape function.

5.6 Experimental procedures and results

In Figure 5.4 the experimental arrangement is illustrated. The system consists of two parts. The fiber laser which is the Erbium-doped fiber ring laser discussed in Chapter 3 and the linewidth measurement system based on the delayed self-heterodyne technique. We characterize the fiber laser in the continuous wave regime.

The fiber Fabry–Perot (FFP) tunable filter is a critical component in the Q-switched fiber laser systems developed in this project. The fiber Fabry-Perot tunable filter has a narrow transmission spectrum, making it suitable for narrow linewidth cavity development. However, because of its piezo-electric transducer (PZT) driven configuration, the transmission spectrum of the fiber Fabry-Perot tunable filter easily drifts from the target. For this reason, fiber laser setup is placed in a controlled environmental condition to guarantee both output power and linewidth stability.

The experimental set-up consists of an Erbium-doped fiber ring laser connected an isolator to prevent unwanted reflections from the fiber. The fiber laser is set to operate in continuous wave mode by tuning the transmission spectrum of the tunable filter to

a maximum overlap with the corresponding spectrum of the fiber Bragg grating. An additional un-pumped Erbium-doped fiber “EDF2” is spliced between the circulator and the fiber Bragg grating. This un-pumped Erbium-doped fiber plays a role of a saturable absorber for the linewidth narrowing purpose.

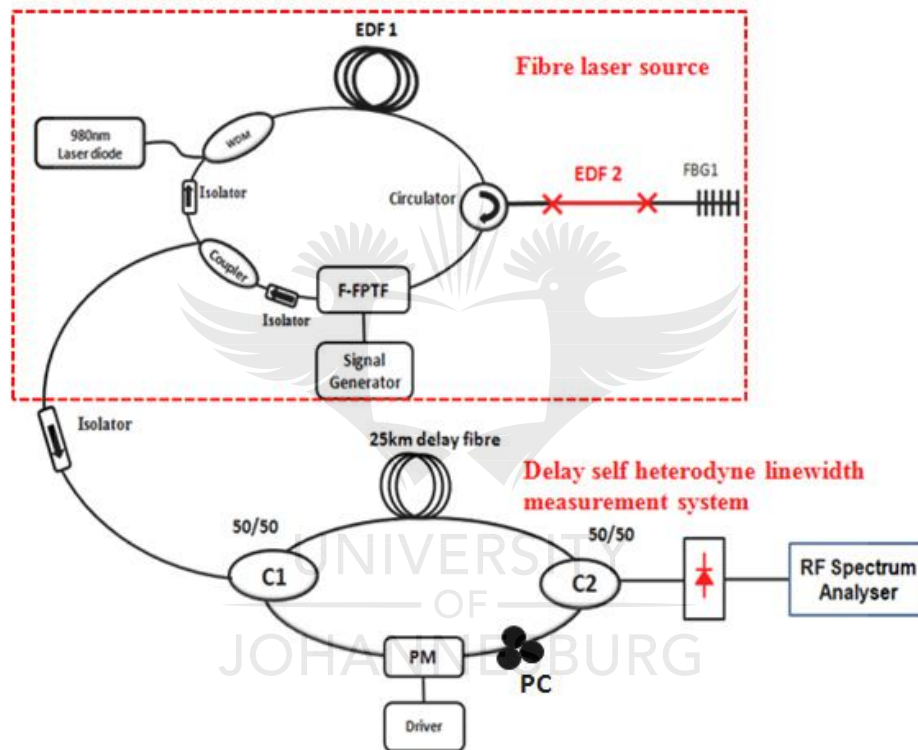


Figure 5.4: Erbium-doped fiber ring laser with linewidth measurement system.

Immediately after the isolator, the beam was split into two beams by a 50/50 optical coupler. One arm of the coupler is connected to a second 3 dB coupler via a phase modulator and a polarization controller (PC). A polarization controller was used to

maximize the heterodyne signal. The other arm of the coupler is connected to a 25 km long single mode fiber delay line connected to a second 3 dB coupler. The phase modulator (JDSU SN524022F) is used to generate a frequency shift. The phase modulator is driven by a modulator driver (MX10A) and a radio frequency (RF) signal generator (Agilent E8257C). The signal generator produces an analog signal of 400 mV at 80 MHz. The beat signal with a bandwidth of 250 MHz (FPD 510) is injected into a photodetector and measured by a radio frequency spectrum analyzer (Agilent E4407B, 9 kHz-26 GHz). In order to measure the spectral linewidth of the fiber laser, the central sweep frequency and span of the RF spectrum analyzer were set at 80 MHz and 600 kHz, respectively.

Other important parameters of the spectrum analyzer setting are the resolution bandwidth (RBW) and the video bandwidth. (VBW) The resolution the bandwidth determines how well closely spaced signals can be separated. The video bandwidth determines how the resolution of very weak signals can be improved in the presence of noise by smoothing out the signal of interest. In our experiment the RBW and VBW were set at 3 kHz and 30 kHz, respectively. The radio frequency (RF) spectrum is shown in Figure 5.5.

The experimental, characterisation of the linewidth is done in two phases. First, the fiber laser is built without the additional un-pumped Erbium-doped fiber (EDF2). This is to determine the actual linewidth of the fiber laser. Then after, the un-pumped

Erbium-doped fiber is spliced as per experimental setup in Figure 5.4. For each experiment, the linewidth and output stability of the fiber laser is measured. This experimental methodology will be followed in the experiments based on Figure 5.8

From the RF beat signal, we observe a 3 dB linewidth of ~32 kHz, corresponding to a Lorentzian fiber laser linewidth of 16 kHz for ring fiber laser system without un-pumped doped fiber.

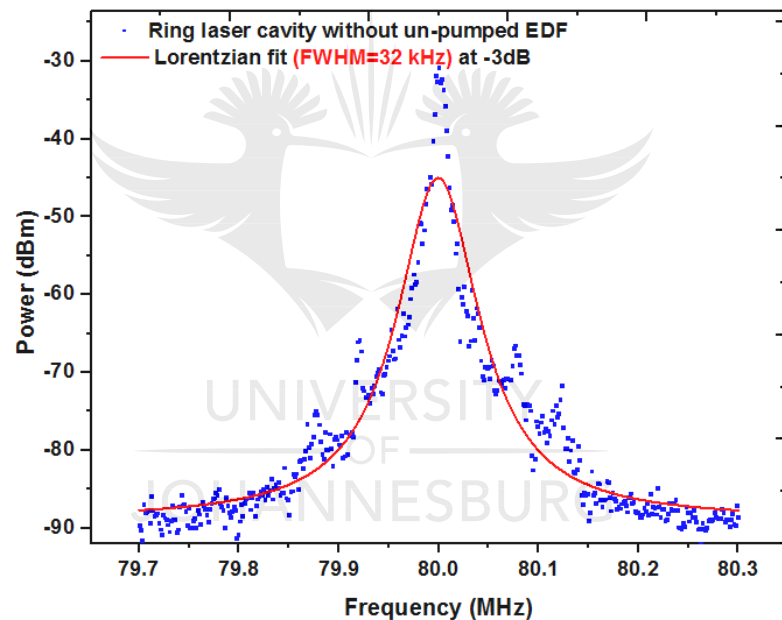


Figure 5.5: Beat spectrum of Erbium-doped fiber ring laser measurements averaged 100 times without un-pumped fiber (blue) experimental collected data (red) Lorentzian fitting for the beat spectrum.

To determine the stability of the laser we measured the output power over a period of 120 min, taking a reading every 5 min. The result is plotted in Figure 5.6. The room temperature was kept constant during the testing period to avoid wavelength shift of

the two optical filters. We studied the output power stability of the fiber laser for different output coupling ratios, as indicated in Figure 5.6 (a). The highest output power fluctuations of 7.52 %, corresponding to 0.24 dB were observed for output coupling ratios of 10 %. The lowest power fluctuations of 0.71 % were observed for output coupling ratios of 90 %, corresponding to 0.08 dB. For 20 % and 80 % output coupling ratios, the recorded power fluctuations were 3.06 % and 0.8 %, respectively.

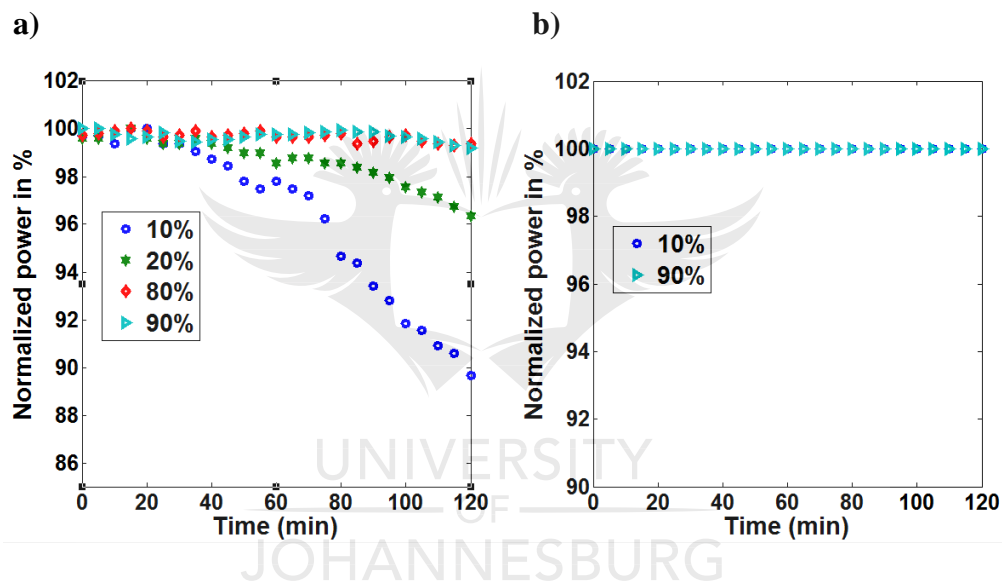


Figure 5.6: Output power stability for Erbium-doped fiber ring cavity fiber laser: (a) Normalized power stability versus time with output coupling ratios as parameters and without an un-pumped fiber for different coupling ratio (b) Normalized power stability versus time for 10 % and 90 % output coupling ratios with an un-pumped fiber.

As shown, at low output coupling ratios, the output power stability of the fiber laser is poor. So, higher output coupling ratios are necessary to achieve both, maximum output power and stability. To improve the stability and narrow the linewidth of the Erbium-doped fiber laser, an additional 1.5 m long M5-980-125 un-pumped Erbium-doped

fiber (EDF2), was spliced between the circulator and the fiber Bragg grating as depicted in Figure 5.4. This piece of fiber acted as a saturable absorber. In Figure 5.5 (b) the Erbium-doped fiber laser stability performance for 10 % and 90 % output coupling were compared. In both cases, excellent power stability was observed for the duration of the experiment. However, an additional power loss was introduced by the saturable absorber Erbium-doped fiber.

The measured RF beat spectrum at 80 MHz with the 1.5 m long un-pumped Erbium-doped fiber is shown in Figure 5.7. The Lorentzian shaped bandwidth at 3 dB below the maximum is about 20 kHz, which gives the spectral linewidth of 10 kHz. In this lasing condition, the linewidth is reduced by 38 %.

Because the existing reflections in the fiber laser cavity originating from splicing points, connectors and cavity components, standing waves in the Erbium-doped fiber would form, and spatial hole burning effect would be generated, leading in poor laser output power stability and broad linewidth characteristic. To overcome this setback, a section of un-pumped EDF is incorporated into the fiber laser. The linewidth narrowing in the un-pumped doped fiber is based on the grating formed by interfering two counter-propagating light waves (Zhiyong Dai, 2010), resulting in smaller absorption for the higher-power lasing longitudinal mode. Therefore, the unwanted competitive modes receive smaller loop gains, which would be suppressed because of the strong gain competition in the Erbium-doped fiber.

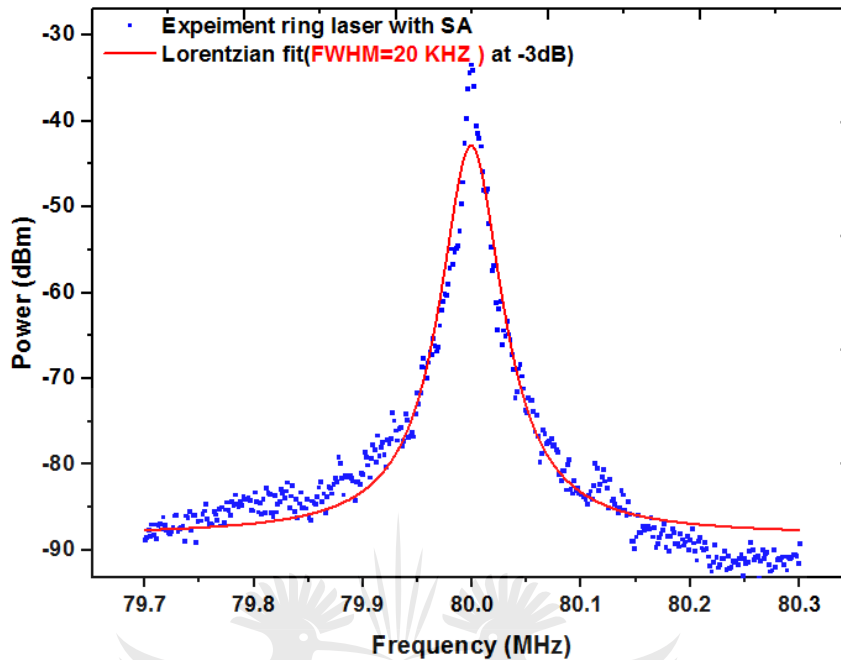


Figure 5.7: Beat spectrum of Erbium-doped fiber ring laser measurements averaged 100 times with un-pumped EDF fiber; (blue) experimental collected data (red) Lorentzian fitting for the beat spectrum.

We have also investigated the output power and spectral linewidth of the linear cavity Erbium-doped fiber laser discussed earlier in Chapter 4. The experimental set-up is illustrated in Figure 5.8.

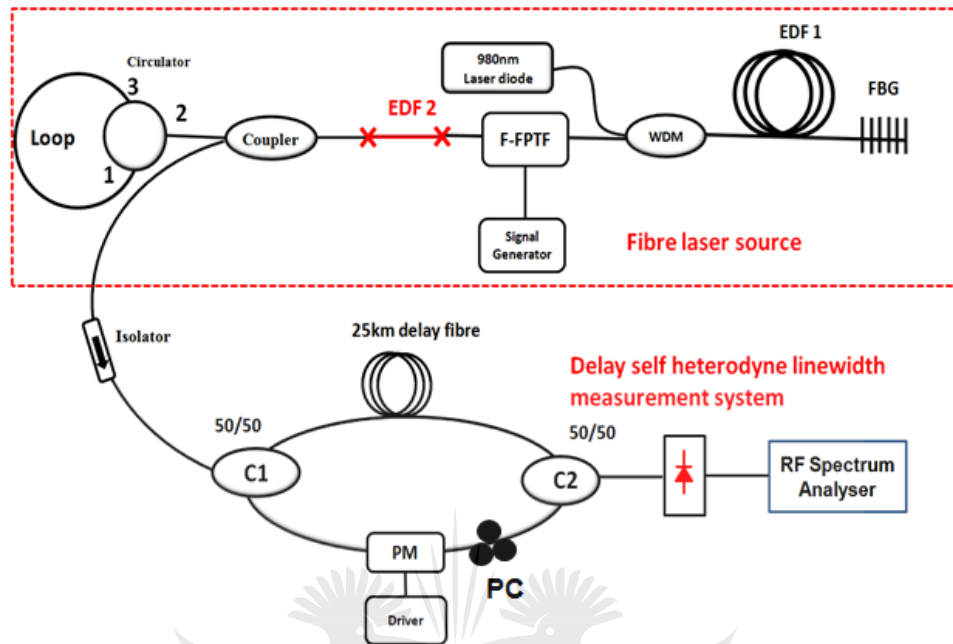


Figure 5.8: Erbium-doped fiber ring laser with linewidth measurement system.

By tuning the transmission spectrum of the tunable filter to overlap the fiber Bragg grating spectrum, the continuous wave regime is obtained. Taking into account the output coupling ratio contribution to the output power stability, 90 % output coupling ratio is used in the experiment. The laser output power of about 14 dBm without saturable absorber un-pumped Erbium-doped fiber was achieved for a pumping power 100 mW at 980 nm. For the same pumping power, an output power of about 10 dBm is attained when a 1.5 m long un-pumped Erbium-doped fiber (M5-980-125) is spliced between the fiber Fabry-Perot filter and the output coupler.

We have measured the stability of the output power over a period of 120 min. Figure 5.9 illustrates the result of this experiment. We have held the ambient temperature constant during the experiment and the interferometer isolated from both temperature change and vibration.

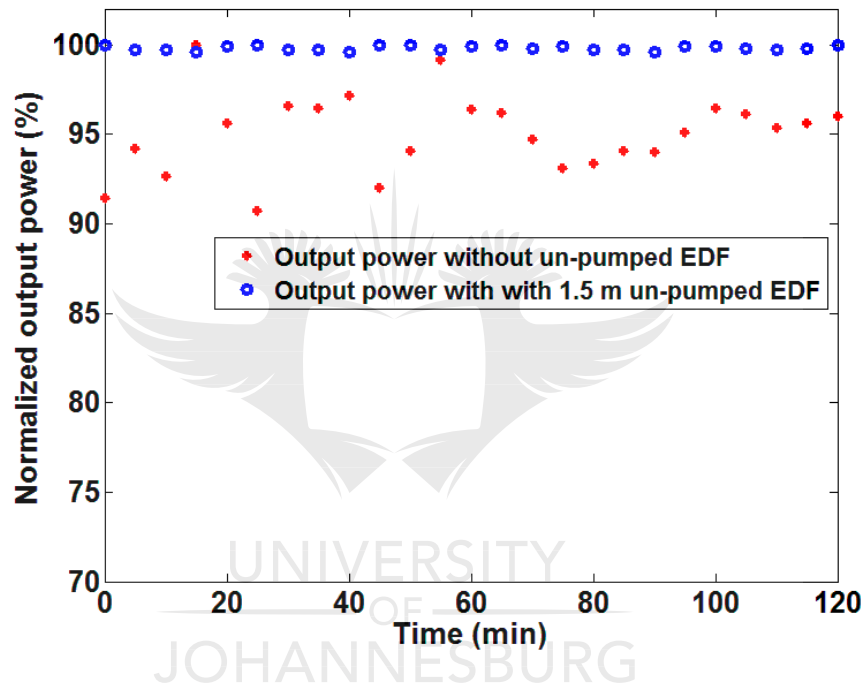


Figure 5.9: Normalized power stability versus time for fiber linear cavity (blue) without additional un-pumped doped fiber (green) with 1.5 m additional un-pumped Erbium-doped fiber.

We find that the maximum output power fluctuation is 9.3 % without the saturable absorber un-pumped Erbium-doped fiber and 0.4 % with the un-pumped Erbium-doped fiber. These power fluctuations correspond to 1.3 dB and 0.04 dB, respectively.

To investigate further the spectral characteristics of the fiber laser, the output power is fed into a Mach-Zehnder interferometer with a 25 km long delay line. The frequency shift from the phase modulator was 80 MHz as shown in Figure 5.8. The measured power spectrum is illustrated in Figure 5.10.

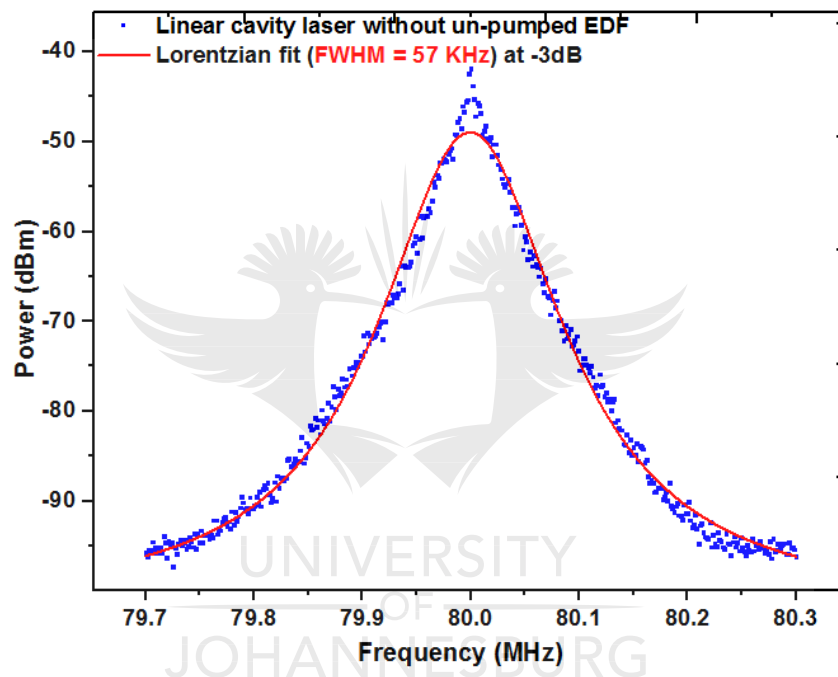


Figure 5.10: Beat spectrum of Erbium-doped fiber linear cavity laser measurements averaged 100 times without un-pumped fiber (blue) experimental collected data (red) Lorentzian fitting for the beat spectrum.

Using a Lorentzian shape the spectral width of 57 kHz at 3 dB below the peak corresponds to a linewidth of 28.5 kHz. In this experiment, only one Erbium-doped fiber was used. Another experiment was performed with an additional un-pumped Erbium-doped fiber used as a saturable absorber. The results are shown in Figure 5.11.

The fitted Lorentzian shape bandwidth is 32 kHz corresponding to 16 kHz fiber laser linewidth. As in the fiber ring laser configuration, we have observed a linewidth narrowing when using an un-pumped Erbium-doped fiber.

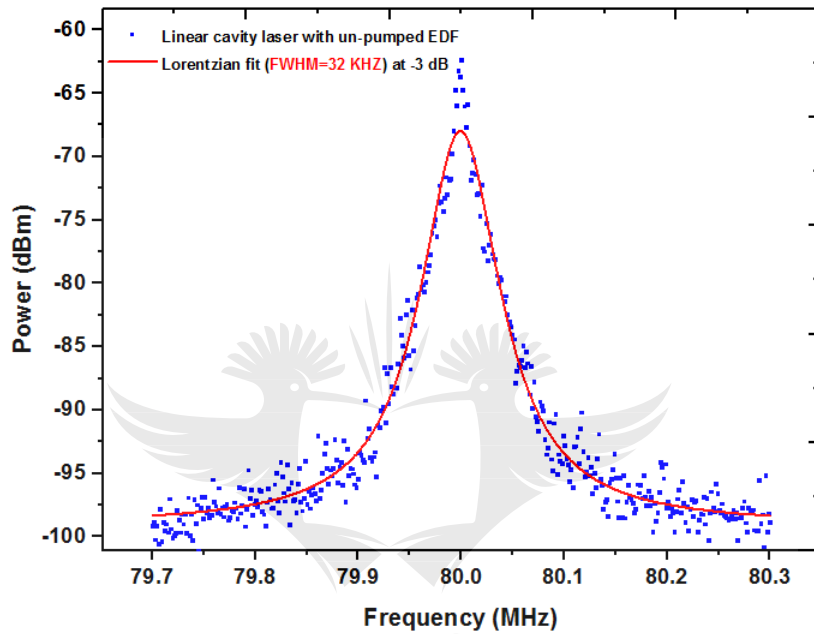


Figure 5.11: Beat spectrum of Erbium-doped fiber linear cavity fiber laser measurements averaged 100 times with un-pumped EDF fiber; (blue) experimental collected data (red) Lorentzian fitting for the beat spectrum.

5.7 Summary

The design and construction of fiber lasers comprising both narrow linewidth ring fiber laser and linear cavity laser has been described in this Chapter. By combining a tunable fiber filter and a fiber Bragg grating together with a saturable absorber, narrow linewidth fiber laser operation was achieved. Ultimately, the output stability of these fiber lasers was demonstrated. We have identified the important source of noise in a fiber laser cavity leading to output power instability and broad linewidth characteristics. Research trend on how to improve the stability of the fiber lasers and narrow the fiber laser linewidth was presented. Parallel to the linewidth and output power stability, we have presented a clear experimental approach to measure the linewidth of a fiber laser. The obtained experimental results have proven that the designed Q-switched fiber lasers are suitable sources for applications such as fiber sensors with a possibility of achieving better frequency shift in Brillouin based distributed fiber sensor due to narrow fiber laser linewidth and stable output power.

Chapter 6

Modelling of a Q-Switched Erbium-doped fiber ring laser



UNIVERSITY
OF
JOHANNESBURG

6.1 Introduction

The main purpose of this project is the designing of Q-switched fiber lasers for potential application in fiber sensor system. In the experimental part we demonstrated a new concept of Q-switching for fiber lasers based on the spectral overlapping of two optical filters namely a fiber Bragg grating and a fiber Fabry-Perot tunable filter. In this Chapter, we develop a numerical method to simulate the pulsed fiber laser based on this Q-switching approach. To the best of our knowledge, no models have been reported for this configuration. An experimentally verified numerical model of an active Q-switched Erbium-doped fiber laser is presented. The study of this fiber laser consists of the analysis of the output pulse characteristics, time duration and peak power. The simulation was done in Matlab. The effects of the pump power, the scanning speed and the length of the Erbium-doped fiber on the output of a Q-switched Erbium-doped fiber laser are highlighted.

6.2 Background

Theoretical modeling is important to investigate the static and dynamic behavior of a fiber laser and to optimize the system parameters. Numerical computing is a powerful tool to confirm experimental results and validate the proposed experiments. To understand the processes in a Q-switched fiber laser and determine the optimum design of the fiber laser cavity, a numerical model is required. Several models of passive and active Q-switched fiber lasers have been reported in the past years.

The numerical models of Q-switched fiber lasers are divided into two groups: point models and “travelling wave models (Gaeta, Digonnet and Shaw, 1987; Digonnet, 2001; Wang and Xu, 2007). The point model is based on the following assumptions: The population inversion density and light intensity are uniform along the axial direction of the laser cavity. The cavity of the Q-switched fiber laser is short and the doped fiber is placed in an optical cavity together with the Q-switch device. The time between low Q-value and high Q-value of the fiber laser cavity is shorter than the pulse build-up time. The spontaneous emission during the release of the output pulse is neglected. Optical pumping is not considered during the emission output pulse. Shang et al. used this approach to optimize a Q-switched Ytterbium-doped double cladding fiber laser (Shang L J *et al.*, 2006). However, this assumption is not suitable for Q-switched fiber lasers with high gain, significant cavity loss, and a long fiber laser cavity. In addition, the point model cannot describe complex Q-switched

characteristics like output pulses with many peaks (Wang and Xu, 2007).

The traveling wave model is preferred for Q-switched fiber lasers (Adachi S. and Y. Koyamada, 2002; Wang Y. and Xu C. Q., 2004; Y. Huo *et al.*, 2005; P. Roy and Pagnoux D., 1996; Renaud C. C. *et al.*, 2001; Y. Wang and Xu C.-Q., 2006; Zhen L., 2013; Kolpakov S. A. *et al.*, 2014). In this model the population inversion and the intensity of radiation inside the laser cavity are treated as functions of the fiber length. Hence, the traveling-wave model allows axial non-uniformity of the gain inside the Q-switched fiber laser cavity. A number of simulations based on the travelling wave model have been conducted. Optimization of actively Q-switched fiber lasers has been reported in the past (L. Xiang *et al.*, 2011; Y. Wang *et al.*, 2003; R. Ciegis *et al.*, 2008; Swiderski J. *et al.*, 2004).

Roy P. and Pagnoux D., (1996) reported an active Q-switched fiber laser using a nanosecond time modulator. They used a travelling wave model and took into account the contribution of amplified spontaneous emission. They modeled the peak power versus fiber length and modulator rise time and optimized the fiber laser accordingly. An active ring cavity Erbium-doped Q-switched fiber laser with an acousto-optic modulator was numerically analyzed with the travelling wave model. With this model it was possible to analyze the multi-peak behavior of the output pulses. The shape of the pulses was simulated using different rise times for the acousto-optic modulator (AOM), namely 35 ns, 105 ns, 350 ns and 10.5 μ s. The total ring cavity length was 70

m and the Erbium-doped fiber was 20 m long. The calculated and measured pulse shapes were in good agreement (Andersen T. V. et al., 2006). In another model the pulse duration and the energy of a neodymium-doped double clad fiber laser was predicted. Although longitudinal and transverse modes were not taken into consideration, the proposed model was sufficiently accurate. Erbium-Ytterbium co-doped clad-pumped fiber lasers were modeled. In these models the wavelength dependence of the laser parameters in the 1550 and 1080 nm bands for Erbium and Ytterbium respectively were highlighted. In another model labeled “simplified,” a single wavelength was assumed for both bands (Cheng X. P., 2007). In both cases, the energy transfer between Erbium and Ytterbium ions was taken into consideration. The “simplified” model agreed with the “full” model within 10%. An experiment was performed using a 4 m clad-pump Erbium-Ytterbium co-doped fiber laser. The results were in good agreement with the theoretical predictions (Adachi S. and Koyamada Y., 2002). In these simulations, an acousto-optic switch with a rise time of a few nanoseconds was assumed together with a linear response for the effective cavity reflectivity.

However, all those simulation and optimization work on actively Q-switched fiber lasers are not suitable for fiber Bragg grating detuning-based Q-switched fiber lasers, in which the FBG’s side-lobes determine the cavity’s transmission and affect the Q-switched pulses according to Cheng et al., 2007. For the first time, Cheng et al. developed a numerical model for FBGs-based Q-switched fiber ring lasers with a

dynamic wavelength response of the FBG. Cheng *et al* (2008) proposed an all-fiber Q-switched Erbium-doped fiber ring laser with a phase-shifted and apodized FBG. However, this configuration presents a drawback in terms of the reliability of the fiber laser because the Q-switching is achieved by applying stress on the fiber Bragg grating. We have proposed and experimentally demonstrated a simple, reliable and cheap solution of an active Q-switched Erbium-doped fiber laser. This fiber laser uses a fiber Bragg grating and a Fabry-Perot tunable filter. Q-switching is obtained by modulating the Fabry-Perot filter with an external voltage, shifting its spectrum. When its spectrum overlaps with that of the grating, the Q factor of the resonator is high and low otherwise. We reported this type of Q-switched fiber laser before (R. M. Manuel, 2016). Nevertheless, the research was only experimental. In this Chapter, a numerical modeling of the Q-switched fiber laser is performed. Obtained simulation results were analyzed and compared with the experimental results.



6.3 Travelling wave model

In Figure 6.1 the fiber laser cavity arrangement used in the study is shown. A pigtailed diode laser was used to pump a 3.5 m Erbium-doped fiber with a concentration of 1200 ppm. Light from the pump was coupled into the gain medium with a WDM coupler. The entire ring cavity was 19 m long. A Corning single mode standard fiber SMF-28 was used in the ring and connected with a WDM coupler to the Erbium-doped fiber, a circulator, a fiber Fabry-Perot tunable filter and output coupler. Port 2 of the circulator was connected to the fiber Bragg grating whose wavelength was 1550 nm and the reflectivity considered here to be 98 %.

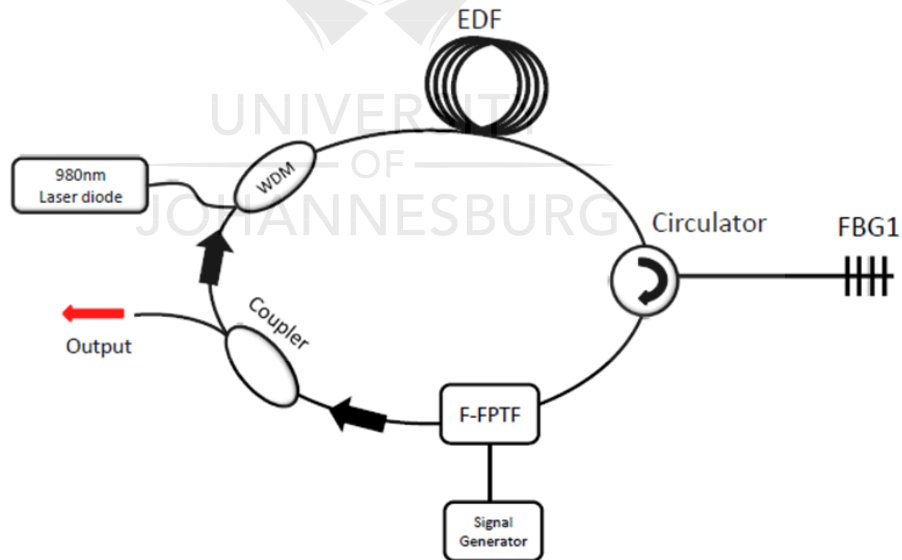


Figure 6.1: Q-switched Erbium-doped fiber laser set-up.

The output coupler ratio was 10/90, with 90 % of light coupled out of the fiber laser. Two isolators have been placed in inside the loop to force unidirectional operation and minimize standing wave patterns inside the cavity. The filter is driven by a sinusoidal signal generator with tunable frequency. The typical frequency in the experiment was 1 kHz. The transmission spectrum of the Fabry-Perot filter varied with the applied voltage. When transmission spectrum of the fiber Fabry-Perot filter matches the fiber Bragg grating reflection spectrum, the Q-factor is high and the huge pulse is released. When the two spectra do not overlap, the Q-factor of the resonator is low and the population inversion is built up further than in a normal laser.

6.4 Active Q-switched fiber laser modeling

To model the fiber laser we use the travelling wave model approach. The travelling wave model for active Q-switched fiber lasers consists of a set of partial differential equations describing the evolution of the pump and signal intensities and rate equations, which are ordinary differential equations, describing the population inversion. These equations are modeled with appropriate time-dependent initial-boundary conditions. The overlap factor between the optical transverse field distribution and doped core of the fiber is calculated assuming the Gaussian

distribution of the LP_{01} mode. Three different approximations can be made to find the profile.

$$N_o = N_1 + N_2 \quad (6.1)$$

$$\begin{aligned} \frac{\partial N_2}{\partial t} = & \frac{\Gamma_p \lambda_p}{hcA} [\sigma_a(\lambda_p) N_1 - \sigma_e(\lambda_p) N_2] P_p \quad (6.2) \\ & + \sum_k \frac{\Gamma_p \lambda_p}{hcA} [\sigma_a(\lambda_k) N_1 - \sigma_e(\lambda_k) N_2] P_k - \frac{N_2}{\tau} \end{aligned}$$

$$\frac{\partial P_p}{\partial z} + \frac{1}{v_p} \frac{\partial P_p}{\partial t} = \Gamma_p [\sigma_e(\lambda_p) N_2 - \sigma_a(\lambda_p) N_1] P_p - \alpha(\lambda_p) P_p \quad (6.3)$$

$$\begin{aligned} \frac{\partial P_k}{\partial z} + \frac{1}{v_k} \frac{\partial P_k}{\partial t} = & \Gamma_k [\sigma_e(\lambda_k) N_2 - \sigma_a(\lambda_k) N_1] P_k - \alpha(\lambda_k) P_k \quad (6.4) \\ & + 2\sigma_e(\lambda_k) N_2 \frac{hc^2}{\lambda_k^3} \Delta\lambda_k \end{aligned}$$

$$k = 1, \dots, K$$

N_0 , N_1 and N_2 are total ion population, ground state ion population and metastable level ion population respectively. Γ_k and Γ_p are overlapping factors for signal wavelength and pump wavelength respectively. P_p and P_k are pump power and signal

power respectively. σ_a and σ_e are wavelength dependent absorption and emission cross-sections respectively. h is the Plank constant, c the speed of light in vacuum and A the radius of the doped fiber core. Overlap factors obtained by assuming a Gaussian profile for the fundamental mode are given by:

$$\Gamma_s = 1 - \exp\left(\frac{-2b^2}{\omega_s^2}\right) \quad (6.5)$$

where b is the Er^{3+} core radius and ω_s^2 the fundamental mode radius given by Desurvire model as follows (Giles C. R. and Desurvire E., 1991).

$$\omega_s = A \left(0.759 + \frac{1.289}{V^{1.5}} + \frac{1.041}{V^6} \right) \quad (6.6)$$

Where A is the core radius and V the normalized frequency given by:

$$V = \frac{2\pi A}{\lambda} NA \quad (6.7)$$

where NA is the numerical aperture and λ the wavelength of interest.

Equations (6.1) to (6.4) have to be solved subject to the initial and boundary conditions. The boundary conditions are derived from the Q-switched fiber laser operation and cavity configuration. The Q-switched fiber laser is pumped while no voltage is applied to the Fabry-Perot filter. The cavity gain is destroyed and population inversion builds up until the steady state condition is reached. The voltage is then

applied to the filter, and the Fabry-Perot filter spectrum starts shifting. When there is an overlap between the filter and grating spectra the gain is re-established and the first pulse is released. After the pulse is released the losses switch back to a high value and population inversion starts to build up again.

The initial boundary conditions for the ring cavity fiber laser are:

$$P_p(0, t) = L_{wdm}P_p \quad (6. 8)$$

$$P_k(0, t) = P_k(L, t)L_{12}L_{23}R_{FBG}T_F(t) R_{OC} \quad (6. 9)$$

The power of the output pulse is given by:

$$P_k(0, t) = P_k(L, t)L_{12}L_{23}R_{FBG}T_F(t) (1 - R_{OC}) \quad (6. 10)$$

where L_{12} and L_{23} are the insertion losses between port 1 and 2 of the circulator and between port 2 and 3 respectively. R_{FBG} is the reflectivity of the fiber Bragg grating. $T_F(t)$ is the transmission coefficient of the Fabry-Perot filter and R_{OC} the coupling ratio of the output coupler.

6.5 Solution algorithm

The resulting set of equations is coupled partial differential equations. An analytical solution of this type of equations is very difficult to find without paying the price of oversimplification leading to inaccurate modeling. Here we use an explicit finite difference scheme. The method allowed us to analyze the effects of spatial powers, population inversion distributions along the length of the cavity and time-dependent switching dynamics. The flowchart of the simulation algorithm is shown in Figure 6.2.

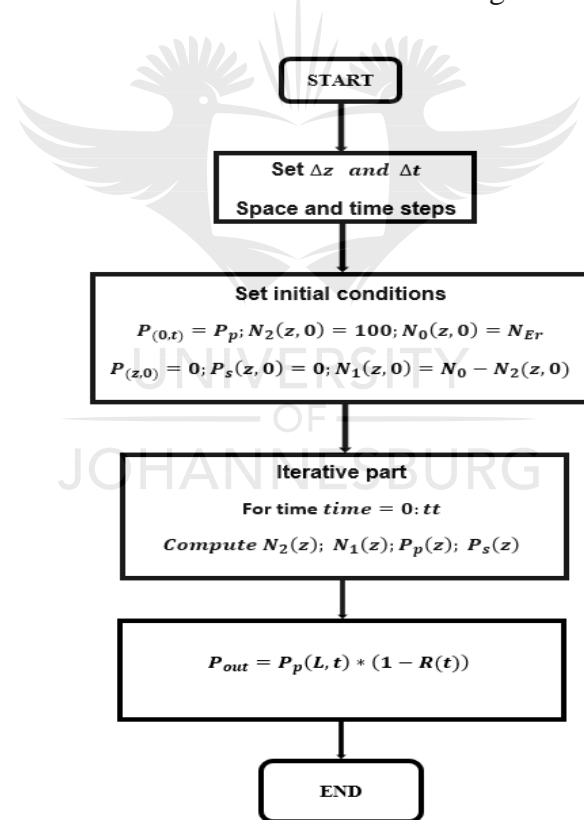


Figure 6.2: Flowchart of the simulation algorithm.

To implement the finite difference method the equations are first discretized at equally spaced points along both the z (space) and t (time) axis. The ring cavity is divided longitudinally into a number of uniform sections Δz in which population inversion and field intensities are assumed to be constant.

Signal intensities from section to section with respect to the discretized equations for the pump and signal fields are calculated. Furthermore, the spatial and temporal step sizes are chosen to satisfy for the stability of the scheme.

$$r = \frac{v\Delta t}{\Delta z} \leq 1, \quad (6.11)$$

Equation 6.11 is known as the Courant-Friedrichs-Levy or CFL condition. In this equation v is the group velocity of the signal wavelength in the Erbium-doped fiber. $v = c/n$ where c is the speed of light in vacuum and n is the refractive index of the fiber.

In this model the Erbium-doped fiber length is divided into 200 sections. For a 3.5 m long fiber, the space step $\Delta z = 0.01750$ m. The corresponding time step Δt was found from the CFL condition to be about 87.5 ps, which is small enough for high-resolution Q-switching simulation and reasonable computational time. With each time step the population of the excited level is found knowing the population of the previous time step. Using the known population inversion distribution, we can find the pump and

signal power distribution for each time step. We repeat this process until we reach the end of the simulation time. The time-dependent transmission of the Fabry- Perot filter is included in the model through time-dependent boundary conditions given by equation 6.5.

The time-dependent transmission was measured for different scanning frequencies and included in the model. The amplified spontaneous emission was not included in the model.

6.6 Simulation results

A systematic analysis of the various physical effects experienced in Q-switched fiber lasers is carried out. The dependence of the output pulse, peak power and time duration on the Erbium-doped fiber length is recognized. The pump power and the scanning speed over the spectrum of the Fabry-Perot tunable filter and the spectrum of the fiber Bragg grating is established. To simulate the Q-switched fiber laser model, parameters in Table 6.1 are used. The simulation results are compared with experimental results to find the pulse features with respect to pump power and repetition rate. Multi-peaks at low frequencies are highlighted.

Table 6.1: Parameters used in the simulation of the actively Q-switched fiber laser.

Symbol	Description	Value
λ_p	Pump wavelength	980nm
λ_k	Lasing wavelength	1550nm
$\sigma_a(\lambda_p)$	Pump absorption cross section	$2.68 \cdot 10^{-25} \text{m}^2$
$\sigma_e(\lambda_p)$	Pump emission cross section	0
$\sigma_a(\lambda_k)$	Signal absorption cross section	$1.206 \cdot 10^{-25} \text{m}^2$
$\sigma_e(\lambda_k)$	Signal emission cross section	$2.11 \cdot 10^{-25} \text{m}^2$
α_p	Absorption coefficient at pump wavelength	0.005
α_k	Absorption coefficient at signal wavelength	0.005
τ	Erbium (13/2) lifetime	10ms
n	Fiber core refractive index	1.45
Γ_k	Signal overlap factor	0.6
Γ_p	Pump overlap factor	0.81
R_{OC}	Output coupling ratio	90%
T	FP filter transmission loss	3dB
R_{FBG}	FBG reflectivity	98%
Δt	Temporal step size	72 ps
r	Courant number	1
Δx	Spatial step size	0.0015

In Figure 6.3 the output Q-switched pulse and the gain evolution of the output pulse are illustrated. The simulation was performed with 90 % of the light coupled out. The Erbium-doped fiber was 3.5 m long and the concentration of Erbium was 1200 ppm.

The fiber was pumped with a 60 mW laser diode emitting at 980 nm. A background loss of 0.05 m^{-1} was assumed. An additional cavity loss was added to account for an additional fiber, the insertion loss in the circulator, WDM, output coupler and Fabry-Perot filter.

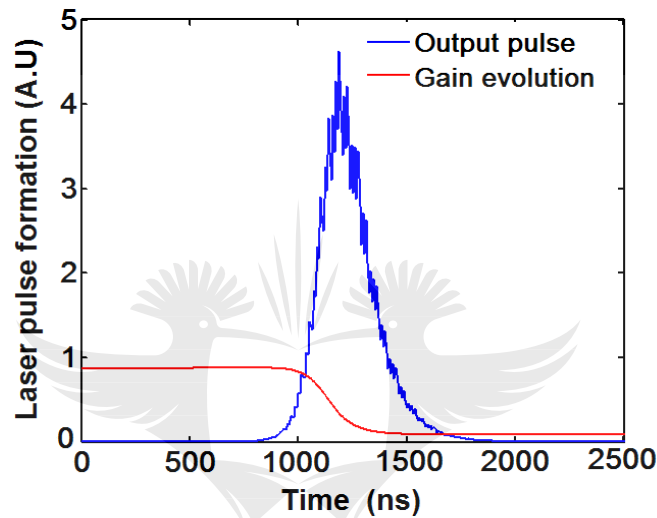


Figure 6.3: Output peak power and gain evolution at 60 mW pump power.

The output peak power dependence on the pump power is illustrated in Figure 6.4. In the simulations the Erbium-doped fiber is assumed to be 3.5 m long. The PZT modulation frequency in the simulation is 1 kHz. The simulations were performed for 40 mW, 60 mW and 80 mW pump power. As the pump power is increased the peak power also increases because of a larger population inversion buildup in the Erbium-doped fiber. At a higher pump power the buildup time of the Q-switched fiber laser is shorter and the width of the pulse narrower. The widths of the simulated Q-switched envelopes are 226 ns, 170 ns and 146 nanoseconds, respectively.

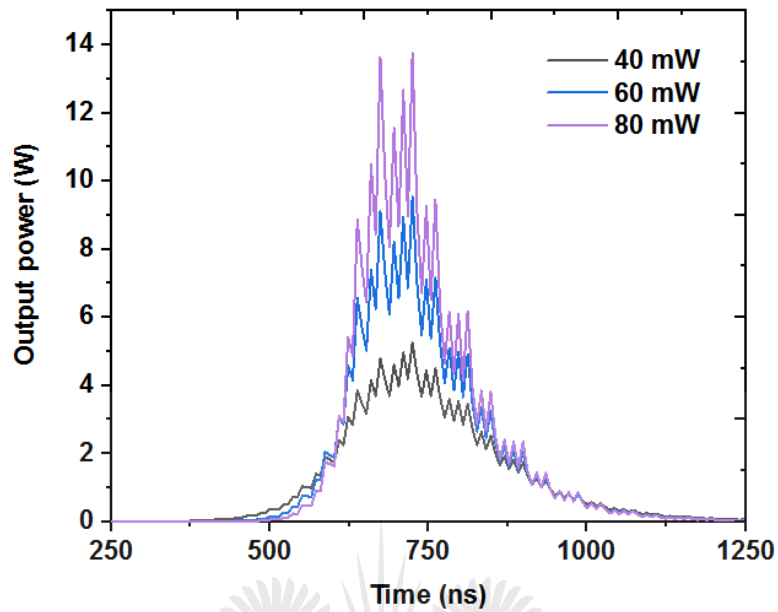


Figure 6.4: Output peak power versus pump power.

The output peak power of the pulses and the pulse duration at repetition rates of 1 kHz, 2 kHz and 3 kHz are shown in Figure 6.5. The simulation of Q-switching was performed far from threshold where the population inversion is greater than required at threshold. The pulse duration decreased as the pump power increased. By contrast, the pulse peak power increased linearly with pump power.

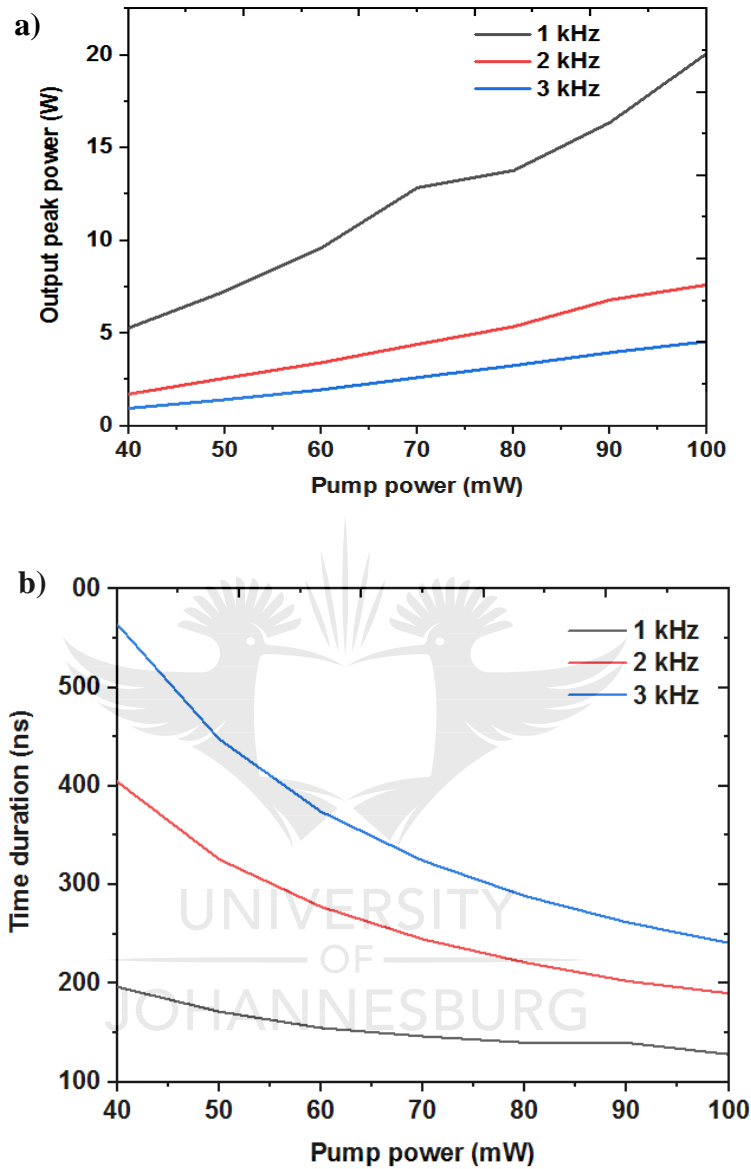


Figure 6.5: a) Output peak power as a function of pump power at different repetition rates and b) pulse time duration versus pump power at different repetition rates.

At higher pump powers the Q-switched laser pulses became narrower approaching the value of the cavity lifetime (Gaeta, 1987; L. Shang, 2008). The peak power of the

pulses increases proportionally with the population inversion produced after threshold is reached. These results agree with the theory of Q-switching and previously reported Q-switched fiber laser experiments (X. P. Cheng *et al.*, 2008; R. M. Manuel, 2016; M. V Andrés *et al.*, 2008; D. W. Huang *et al.*, 2000; C. Cuadrado-Laborde *et al.*, 2007; L. Wu *et al.*, 2016; K. J. Monga, 2017).

Figure 6.6 displays the output peak power and pulse width of the Q-switched fiber lasers versus the repetition rates for 40 mW, 60 mW and 80 mW pump power. In the studies we used a 3.5 m Erbium-doped fiber. We found that the peak power decreases when the frequency increases. The reason is that at high repetition rates the pumping time is short. Therefore, the pump cannot deliver enough power to pump the Erbium-doped fiber. The population inversion generated in one pumping cycle varies at different frequencies.



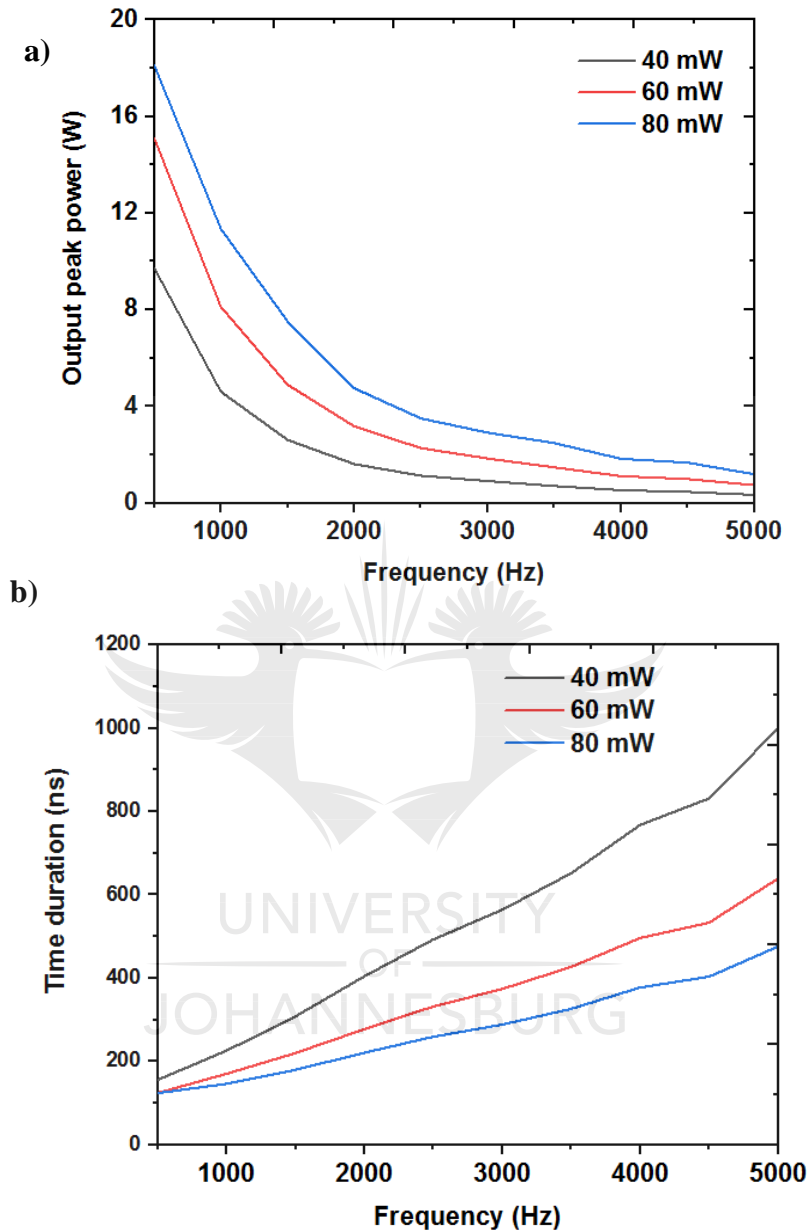


Figure 6.6: a) Output peak power as a function of repetition rate at different pump powers and b) pulse time duration versus repetition rate at different pump powers.

The output pulse peak power as a function of the Erbium-doped fiber length for different repetition rates is illustrated in Figure 6.7. The doped fiber is pumped with

60 mW with 10 % of the fiber laser out power coupled out. The length of the cavity is varied from 0 m to 6 m. The output pulse peak power increases when the cavity length is increased to 1 m at frequencies of 2 kHz and 3 kHz. Here is the maximum output peak power observed. At 1 kHz the maximum power is obtained at 3.5 m cavity length. With a further increase in cavity length the output pulse peak decreases steadily.

These results from the simulation illustrate the dependence of the population inversion distribution along the doped fiber. For any fiber laser cavity, there is an optimal length at which the output power is at the maximum.

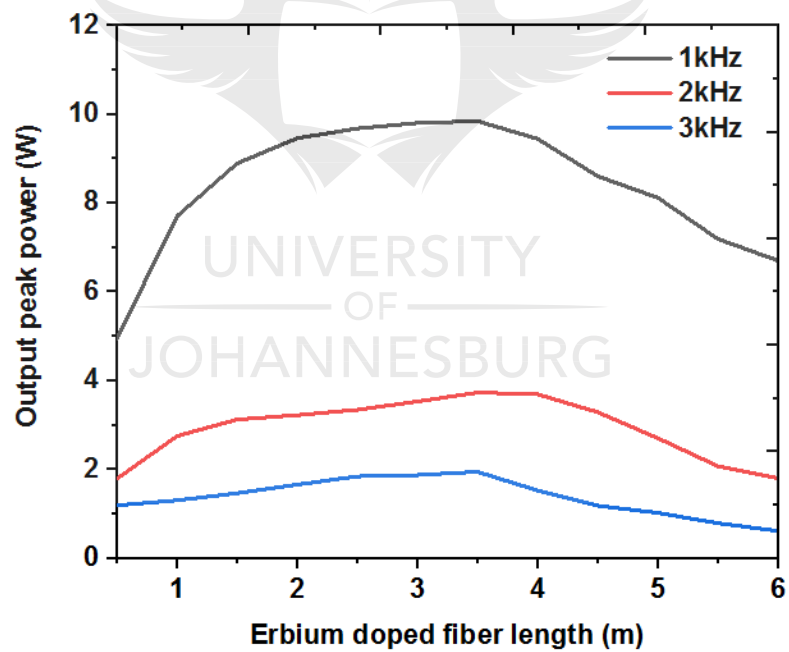


Figure 6.7: Output peak power versus Erbium-doped fiber length.

6.7 Model validation with experimental results

We validated the simulations of the active Q-switched fiber laser with our experimental measurements. In Figure 6.8 the comparison between simulations and experimental results for time duration as a function of scanning frequency is presented. In the simulation, the time duration increased steadily with the scanning frequency while in experimental results first the time duration decreased, reached a minimum around 1.5 kHz, and started then to increase.

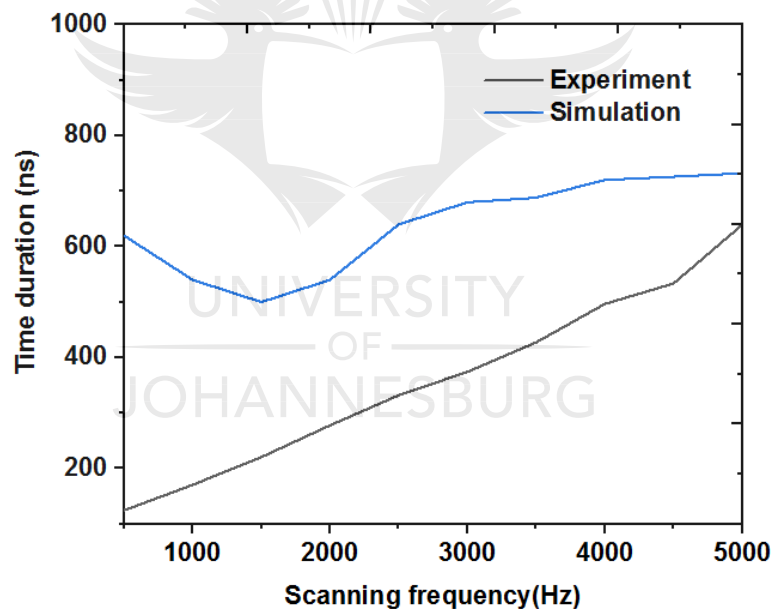


Figure 6.8: Time duration of pulses as a function of the scanning frequency, simulation and experimental results.

This experimental result can be understood as follow: The scanning speed of the transmission spectrum of the tunable fiber Fabry-Perot filter over the fiber grating

spectrum depends on the frequency of the electrical signal. At lower tuning frequencies, the transmission spectrum of the Fabry-Perot filter overlaps with the fiber Bragg grating spectrum slowly. Lasing starts before the filter system achieves maximum transmission. This causes the pulses to have less peak power and longer time duration. Even more than one pulse per scanning cycle might be generated (Manuel et al., 2016). The generation of multi-peaks was also observed at low frequencies in the simulation as shown in Figure 6.9.

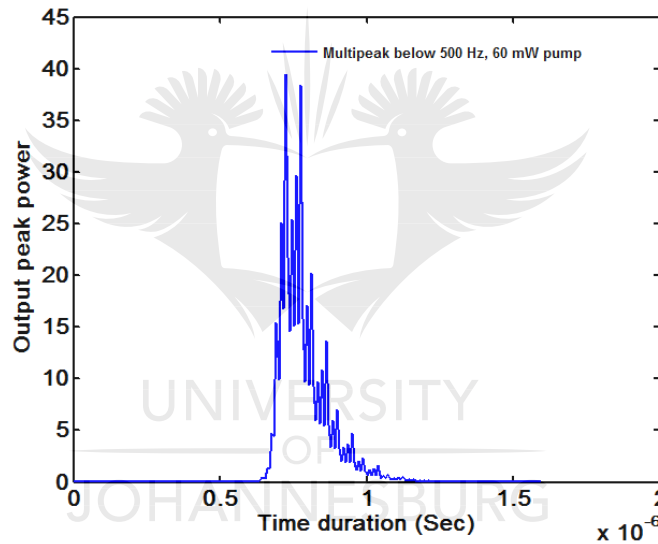


Figure 6.9: Multi-peak generation of Q-switched fiber laser pulses at low scanning frequency of the fiber Fabry-Perot tunable filter.

In order to validate the proposed numerical model, we compare numerical and experimental results under similar cavity parameters and lasing conditions. In Figure 6.10, simulation and experimental results for output peak power as a function of

scanning frequency for a 3.5 m doped fiber pumped at 60 mW are compared. The trend of the two curves is similar for different frequencies.

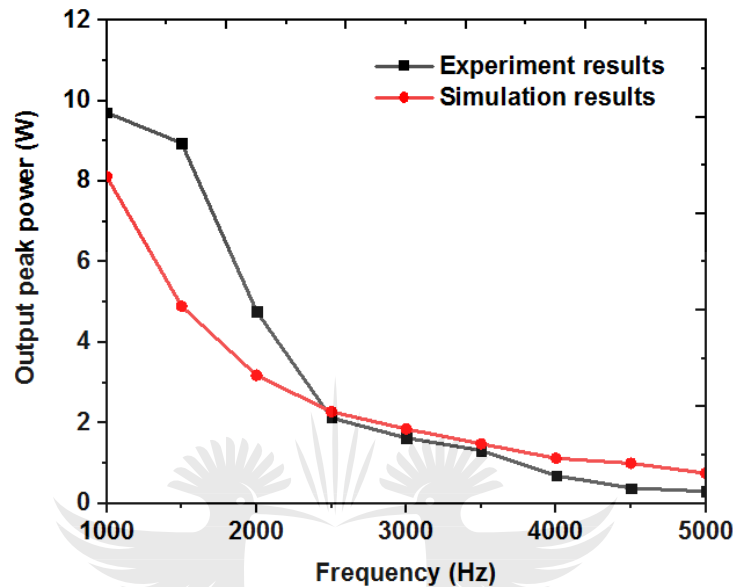


Figure 6.10: Output peak powers as a function of Fabry-Perot filter scanning frequency: simulation results compared to experimental results.

At lower frequencies a discrepancy between the simulation and experiments is observed. The obtained output peak power from the simulation are lower than experimental ones at frequencies below 2500 Hz. At lower repetition rate the scanning frequency of the F-P filter is lower and resonator closes more slowly, but pumping takes longer period. The observed discrepancies are attributed to effects such as amplified spontaneous emission, possible ion-ion interactions and pumping saturation which were not considered in the model.

6.8 Summary

The aim of the simulation of the actively Q-switched Erbium-doped fiber laser was to understand the experimental results. Output pulse energy, pulse time duration and output peak power were investigated as a function of the output coupling ratio, pump power and length of the gain medium. It has been shown that an efficient Q-switched fiber laser is obtained when the pump power is high enough to operate the laser far from the threshold. The coupling ratio that allows the extraction of the maximum output peak power and shortest time duration of the Q-switched fiber laser is obtained by a proper choice of the length of the Erbium-doped fiber laser and the pump power.

We have conducted an investigation of the characteristics of an active Erbium-doped Q-switched fiber laser using a tunable Fabry-Perot filter as switching element. We have developed a theoretical model based on rate equations and propagation equations for the pump and signal intensities in a fiber laser ring cavity. We have performed the simulation based on our model to find optimized laser conditions. Finally, we have validated the model with experimental results. We found that the model is in agreement with the experimental results. By varying the values of parameters like doped fiber length, scanning frequency and pump power, we obtained different features of the fiber laser. Finally, we have observed some discrepancies between the experiment and the simulation. This can be due to some physical effect like amplified

spontaneous emission and possible ion-ion interactions which were not taken into account in the model.



Chapter 7

Conclusions



UNIVERSITY
OF
JOHANNESBURG

7.1 Chapter overview

The objectives of this Chapter are threefold. First is to highlight important points from the thesis in terms of the questions initially addressed for this research, the methodology proposed to perform the experiments, and key research contributions and obtained results. The second objective is to elaborate upon the benefit and shortcoming of the Q-switched fiber laser systems developed in this thesis based on the obtained both experimental and simulation results compared to results already published in the literature. The final objective of this Chapter is to propose future research direction on all-fiber Q-switched fiber lasers and possible optimization for sensing applications.

7.2 Discussions and future work.

There were a number of considerable results in the field of Q-switched fiber laser that were accomplished through the experiments reported in this dissertation. These research outcomes constitute an important milestone in the development of all-fiber-based Q-switching fiber laser systems. All-fiber active Q-switched fiber lasers have been reported in the past decade. New technique to built lossless active Q-switching devices has been reported in the literature. Research direction in the development of new

all-fiber based Q-switching in fiber laser focuses on finding ways to improve the robustness, output peak power, and possible extended repetition rates in these fiber lasers.

The aim of this research project was to experimentally and theoretically demonstrate a new all-fiber Q-switched laser source with suitable characteristics for potential applications. Four main questions were addressed in this project:

1. Can we modulate the quality factor Q of a fiber laser using the dynamic spectral overlap between the transmission spectrum of a fiber Fabry-Perot tunable filter and the reflection spectrum of a fiber Bragg grating?
2. Based on the proposed Q-switching mechanism addressed in question 1, is it possible to demonstrate Q-switched fiber laser in both, ring and linear cavity configuration?
3. Can the characteristics of these fiber lasers, like peak power, pulse width, linewidth, output power stability, extension ratio be suitable for practical applications?
4. Can we demonstrate via numerical modeling that this Q-switching technique agrees well with results in the existing experiments literature?

The purpose of this research project was to design and construct Q-switched Erbium-doped fiber lasers systems. The primary contribution of this research was to propose an alternative concept of Q-switching in fiber laser. Considerable consideration was dedicated to diagnostics of the fiber laser cavity operation in continuous wave

operation, in terms of output power, efficiency, and operating wavelength, output stability and linewidth; and in Q-switched fiber laser in terms of output peak power and time duration of pulses. We have successfully demonstrated Q-switched fiber laser in ring and linear cavity configuration.

A series of experiments were carried out to optimize the fiber laser cavities. In this experimental investigation, two Erbium-doped fibers with different ion concentration were used. The first doped fiber, with an Erbium ion concentration of 2200 ppm was referred to as “high concentration” and the second with an Erbium ion concentration of 960 ppm was referred to as “low concentration”. The contribution of fiber laser cavity parameters to the performance of the fiber laser such as the length of the Erbium-doped fiber, the output coupling ratio, pump power were explored. A coupling ratio of 90 % and a 3.5 m long length were found to be respectively optimal coupling ratio and optimal length of the fiber laser, using low concentration Erbium-doped fiber. The Erbium-doped fiber was pumped with 60 mW and 100 mW for ring cavity and linear cavity, respectively. The operation wavelength was fixed at 1550 nm. In Q-switched fiber laser operation, a successful modulation of the quality factor on a fiber laser was demonstrated using two the spectral overlap between the transmission spectrum of a fiber Fabry-Perot filter and the reflection spectrum of a fiber Bragg grating. When the transmission spectrum of the tunable filter does not overlap with the reflection spectrum of a fiber Bragg grating, the laser cavity has a maximum loss, the cavity is open. In this condition, the pumped energy is absorbed in the fiber laser gain

medium. In turn, the fiber laser cavity has a minimum loss when the spectrum of the two filters overlap, resulting in the release the stored energy in the form of the giant pulse. The output laser pulse characteristics, peak power of 9.7 W and time duration 500 ns, were obtained at 1 kHz of repetition rate, for ring cavity Q-switched fiber laser; and 5.6 W peak power with a 450 ns pulse time duration were achieved for linear cavity Q-switched fiber laser at the same repetition rate. The repetition rate of the pulses can be continuously varied from a single shot to a few kHz. The Q-switched fiber laser pulse behavior was obtained. We have demonstrated that the proposed Q-switching process operates in linear cavity configuration when a proper cavity arrangement and optimization is done. The linear configuration exhibits relatively lower peak power as compared to the ring cavity configuration. This discrepancy is justified by the fact that, because of the bidirectional light propagation, in linear cavity fiber configuration more amplified spontaneous emission are experienced, resulting in a reduction of the population inversion contributing to the output peak power.

We have characterized the output power stability and linewidth of Erbium-doped fiber lasers, in both ring and linear cavities. When these fiber lasers were Q-switched, resulting in laser pulses with different longitudinal modes, characterizing the fiber laser as multimode. A Q-switched laser with a single frequency must contain only one longitudinal mode. Because of the complexity involved in linewidth measurement the linewidth for pulsed fiber lasers, the linewidth were measured with fiber laser operating in a continuous regime. This would indicate how narrow the linewidth would

be in a pulsed system caused by spontaneous emission determine the spectral width of the emission line of the fiber lasers.

The power instability is the difference between the maximum and minimum of the power fluctuations, measured in dB. The values were taken over a period of 120 minutes in 5 minutes time intervals. The measurements show that the output power stability is a function of the output coupling ratio. The maximum output power is obtained when 90 % of the light is coupled out, which correspond to a stable output power. We have obtained fluctuations of 0.08 dB and 1.3 dB in fiber ring lasers and linear cavity lasers, respectively.

It was observed that the stability is improved optimizing the doped fiber laser cavity length. Additionally, we have introduced a 1.5 m un-pumped Erbium-doped fiber as a saturable absorber to prevent spatial hole burning in both ring and linear cavity configurations. The output power is a stable in Erbium-doped fiber ring laser, compared to linear cavity. The maximum fluctuation was 0.04 dB is obtained in a linear Erbium-doped fiber laser.

Narrow linewidth fiber lasers were accomplished by incorporating an un-pumped Erbium-doped fiber in the laser. The linewidth of 10 kHz and 16 kHz were obtained in ring and linear cavity lasers, respectively at 3 dB below the peak of the Lorentzian data fitting curve. Ideally, the linewidth interpretation above refers to context where only fiber lasers linewidth is caused by a white frequency noise spectrum

corresponding to the contribution of spontaneous emission noise within the laser cavity. However, it is known that fiber lasers are susceptible to other type of noise sources such as pump noise, vibrations, and acoustic noise. In these conditions, linewidth spectrum contains a considerable contribution from Gaussian-type noise sources. This implies that the full width at half maximum of Lorentzian represents a poor data fitting approach. Therefore the Lorentzian linewidth is estimated by measuring the spectral width of the self-heterodyne lineshape 20 dB below the peak where the contribution from the Gaussian is less pronounced as shown in table 5.1. (Spiegelberg, C., 2003; Horak, P. and Loh, W.H., 2006; Fu, P et al., 2018; Wang, W. et al., 2018).

The fluctuation in the timing of the pulses in the Q-switched fiber laser pulse train is commonly known as timing jitter. To maintain stable train of pulses in Q-switched fiber laser was placed in a controlled temperature environment to avoid any spectral shift from both fiber Bragg grating and Fabry-Perot filter. Additionally, the coiling on the fiber laser cavity was kept as neat as possible pulses to avoid instability due to cavity losses. Under optimized fiber laser cavity, the standard deviation of the Q-switched fiber laser output peak power between laser pulses was less than 1 %, which demonstrates a stable train pulses from our Q-switched fiber lasers. This instability of pulses was understood to be caused by spontaneous emission, from which the lasing modes start from (Jacob B et al., 2002).

Because of its unique nature, the Q-switching techniques proposed in this thesis were also theoretically investigated. A well-elaborated numerical model was derived to explain the Q-switching process. Numerically solving partial differential equations describing the change of population inversion and the photon density over space and time along the cavity length was proposed. The primary objective in developing this model was to theoretically confirm that the proposed Q-switching approach based on the overlap between two wavelength-selecting elements is effectively consistent with the dynamic behaviors of active Q-switched fiber lasers available in the literature.

As observed from simulation results, a single output pulse is released in each scanning period, which agrees well with the analytical solutions proposed in the earlier investigations of the traditional laser rate equations (Roy and Pagnoux, 1996; Renaud *et al.*, 2001; Wang and Xu, 2007b; Sujecki *et al.*, 2015). In addition, a comprehensive description of the switching dynamics of actively all-Q-switched fiber lasers with ring cavity under different cavity length, pump power, and switching frequency was demonstrated. The obtained simulation results of the output peak power and pulse duration are qualitatively consistent with the experimental results, under similar cavity conditions.

In conclusion, we have constructed robust, narrow linewidth all-fiber Q-switched Erbium-doped fiber laser cavities that operated at 1550 nm. The short pulse widths and high peak power of fiber lasers make them an excellent source for applications like distributed fiber sensors. The theoretical analyses and experimental demonstrations presented in this thesis provide a complete picture of the dynamical behavior of the

proposed Q-switching process. Therefore, the objectives set in this project are fulfilled. A new milestone in the development of active Q-switching has been reached.

Though the results obtained in this thesis clearly illustrated that the model was suitable to describe at first hand the working principle of the proposed Q-switching techniques, and the experimental results demonstrating novel technique for archiving Q-switching in fiber laser, there still a room for new research direction. The Q-switched fiber laser model could be extended by studying the influence of the spectral linewidth of the wavelength-selective element on the stability and linewidth of the fiber laser. The contribution of phenomena such as amplified spontaneous emission, concentration quenching and up-conversion could be included the model. This shall open a new window for the following experiments to be suggested.

Substituting the fiber Bragg grating with a distributed feedback fiber Bragg grating could be proposed to anticipate a narrower linewidth Q-switched fiber laser. The simplicity of the demonstrated Q-switching technique is the key for complex configurations such as multi-wavelength for fiber lasers for sensing applications. New emission wavelength emission could be explored. Finally, effective approach to narrow the pulse duration and increase the repetition still to be investigated.

Bibliography

Adachi, S. and Koyamada, Y. (2002) 'Analysis and design of Q-switched Erbium-doped fiber lasers and their application to OTDR', *Journal of Lightwave Technology*, 20(8), pp. 1506–1511. doi: 10.1109/JLT.2002.800293.

Agrawal, G. (2013) *Nonlinear fiber optics*, *Nonlinear Fiber Optics*. doi: 10.1016/B978-0-12-397023-7.00010-3.

Ahmad, H. et al. (2013) 'Tunable graphene-based Q-switched Erbium-doped fiber laser using fiber Bragg grating', *Journal of Modern Optics*, 60(3), pp. 202–212. doi: 10.1080/09500340.2013.766767.

Ali, A. H., Wahid, S. N. A. and Mohammed, H. A. (2012) 'Analysis of Laser Linewidth Measurements Based on Fabry-Perot Interferometer System', (6), pp. 6–9.

Alvarez-Chavez, J. A. et al. (2000) 'High-energy, high-power Ytterbium-doped Q-switched fiber laser', *Optics Letters*, 25(1), p. 37. doi: 10.1364/OL.25.000037.

Andersen, T. V. et al. (2006) 'All-fiber actively Q-switched Yb-doped laser', *Optics Communications*, 260(1), pp. 251–256. doi: 10.1016/j.optcom.2005.10.036.

Andrés, M. V. et al. (2005) 'All-fiber lasers: Active Q-switching techniques', in *Proceedings of 2005 7th International Conference on Transparent Optical Networks*,

ICTON 2005, pp. 331–336. doi: 10.1109/ICTON.2005.1505817.

Andrés, M. V. et al. (2007) ‘Actively Q-switched all-fiber lasers’, *Laser Physics Letters*, 5(95), pp. 93–99. doi: 10.1002/lapl.200710104.

Arkwright, J. W. and Skinner, I. M. (1996) ‘An investigation of Q-switched induced quenching of the resonant nonlinearity in neodymium doped fibers’, *Journal of Lightwave Technology*, 14(1), pp. 110–120. doi: 10.1109/50.476144.

Ball, G. A., Hull-Allen, C. G. and Livas, J. (1994) ‘Frequency noise of a Bragg grating fiber laser’, *Electronics Letters*, 30(15), pp. 1229–30. doi: 10.1049/el:19940842.

Ball, G. A. and Morey, W. W. (1994) ‘Compression-tuned single-frequency Bragg grating fiber laser’, *Optics Letters*, 19(23), p. 1979. doi: 10.1364/OL.19.001979.

Ball, G. A., Morey, W. W. and Glenn, W. H. (1991) ‘Standing-Wave Monomode Erbium Fiber Laser’, *IEEE Photonics Technology Letters*, 3(7), pp. 613–615. doi: 10.1109/68.87930.

Bao, X. and Chen, L. (2012) ‘Recent progress in distributed fiber optic sensors’, *Sensors (Basel)*, 12(7), pp. 8601–8639. doi: 10.3390/s120708601.

Barnard, G. et al. (1994) ‘Analytical Model for Rare-Earth-Doped Fiber Amplifiers and Lasers’, *IEEE Journal of Quantum Electronics*, 30(8), pp. 1817–1830. doi: 10.1109/3.301646.

Becker, P. C., Olsson, N. A. and Simpson, J. R. (1999) 'Erbium-Doped Fiber Amplifiers', *Erbium-Doped Fiber Amplifiers*, pp. 401–427. doi: 10.1016/B978-012084590-3/50012-0.

Becker, Olsson and Simpson (2003) *Erbium-doped fiber Amplifiers* , Book. doi: 10.1364/OPN.2.1.000006.

Bellemare, A. (2003) 'Continuous-wave silica-based Erbium-doped fiber lasers', *Progress in Quantum Electronics*, pp. 211–266. doi: 10.1016/S0079-6727(02)00025-3.

Bellemare, a et al. (2001) 'A broadly tunable Erbium-doped fiber ring laser: experimentation and modeling', *IEEE Journal of Selected Topics in Quantum Electronics*, 7(1), pp. 22–29. doi: 10.1109/2944.924005.

Canagasabay, A. et al. (2011) 'A comparison of delayed self-heterodyne interference measurement of laser linewidth using mach-zehnder and Michelson interferometers', *Sensors*, 11(10), pp. 9233–9241. doi: 10.3390/s111009233.

Canning, J. (2006) 'Fiber lasers and related technologies', *Optics and Lasers in Engineering*, 44(7), pp. 647–676. doi: 10.1016/j.optlaseng.2005.02.008.

Chandonnet, A. and Larose, G. (1993) 'High-Power Q-switched Erbium Fiber Laser Using an All-Fiber Intensity Modulator', *Optical Engineering*, 32(9), pp. 2031–2035. doi: Doi 10.1117/12.143949.

Chen, N. K., Feng, Z. Z. and Liaw, S. K. (2010) 'All-fiber pulsewidth tunable actively Q-switched Erbium fiber laser using abrupt-tapered Mach-Zehnder block filter', *Laser Physics Letters*, 7(5), pp. 363–366. doi: 10.1002/lapl.201010003.

Chen, W. et al. (no date) 'laser Q -switched and mode-locked Er 3 + -doped fiber laser using a single-multi-single fiber filter and piezoelectric', pp. 3–6. doi: 10.1070/QE2014v044n04ABEH015086.

Chen, X. et al. (2005) 'Single-longitudinal-mode fiber ring laser employing an equivalent phase-shifted fiber Bragg grating', *IEEE Photonics Technology Letters*, 17(7), pp. 1390–1392. doi: 10.1109/LPT.2005.848408.

Chen, X. (2006) *Ultra-Narrow Laser Linewidth Measurement*, PhD Dissertation, Virginia Polytechnic Institute and State University.

Cheng, X. P. et al. (2007) 'Influence of sidelobes on fiber-Bragg-grating-based Q-switched fiber laser', *IEEE Photonics Technology Letters*, 19(20), pp. 1646–1648. doi: 10.1109/LPT.2007.904920.

Cheng, X. P., Tse, C. H., et al. (2008) 'All-fiber Q-switched Erbium-doped fiber ring laser using phase-shifted fiber Bragg grating', *Journal of Lightwave Technology*, 26(8), pp. 945–951. doi: 10.1109/JLT.2008.917370.

Cheng, X. P., Shum, P., et al. (2008) 'Single-longitudinal-mode Erbium-doped fiber ring laser based on high finesse fiber Bragg grating Fabry-Pérot Etalon', *IEEE*

Photonics Technology Letters, 20(12), pp. 976–978. doi: 10.1109/LPT.2008.922974.

Cheng, X. P. et al. (2009) ‘Numerical analysis and characterization of fiber Bragg grating-based Q-switched Ytterbium-doped double-clad fiber lasers’, Optics and Lasers in Engineering, 47(1), pp. 148–155. doi: 10.1016/j.optlaseng.2008.07.001.

Cheng, Y. et al. (1995a) ‘Stable single-frequency traveling-wave fiber loop laser with integral saturable-absorber-based tracking narrow-band filter’, Optics letters, 20(8), pp. 875–877. doi: 10.1364/OL.20.000875.

Cheng, Y. et al. (1995b) ‘Stable single-frequency traveling-wave fiber loop laser with integral saturable-absorber-based tracking narrow-band filter’, 20(8), pp. 875–877.

Čiegis, R., Dement’ev, A. and Laukaityte, I. (2008) ‘A numerical algorithm for simulation of the Q-switched fiber laser using the travelling wave model’, Lithuanian Mathematical Journal, 48(3), pp. 270–281. doi: 10.1007/s10986-008-9011-y.

Cowle, G. ., Payne, D. . and Reid, D. (1991) ‘Single-frequency travelling-wave Erbium-doped fiber loop laser’, Electronics Letters, 27(3), pp. 229–230. doi: 10.1049/el:19910148.

Cuadrado-Laborde, C. et al. (2007) ‘Q-switched all-fiber laser using a fiber-optic resonant acousto-optic modulator’, Optics Communications, 274(2), pp. 407–411. doi: 10.1016/j.optcom.2007.02.032.

Cuadrado-Laborde, C. et al. (2010) ‘Actively Q-switched and modelocked all-fiber

lasers', *Laser Physics Letters*, 7(12), pp. 870–875. doi: 10.1002/lapl.201010075.

Dai, Z. (2010) 'Stable High Power Narrow Linewidth Single Frequency Fiber Laser Using a FBG F-P Etalon and a Fiber Saturable Absorber', pp. 4–7.

Dawson, J. W., Park, N. and Vahala, K. J. (1992) 'An Improved Delayed Self-Heterodyne Interferometer for Linewidth Measurements', *IEEE Photonics Technology Letters*, 4(9), pp. 1063–1066. doi: 10.1109/68.157150.

Degnan, J. J. (1989) 'Theory of the Optimally Coupled Q-switched Laser', *IEEE Journal of Quantum Electronics*, 25(2), pp. 214–220. doi: 10.1109/3.16265.

Delgado-Pinar, M. et al. (2005) 'Q-switched all-fiber laser based on acousto-optic modulation of a fiber Bragg grating', in *Conference on Lasers and Electro-Optics Europe - Technical Digest*. doi: 10.1109/CLEOE.2005.1568295.

Delgado-Pinar, M. et al. (2006) 'Q-switching of an all-fiber laser by acousto-optic modulation of a fiber Bragg grating', *Optics Express*, 14(3), p. 1106. doi: 10.1364/OE.14.001106.

Desurvire, E. (1995) 'Erbium-Doped Fiber Amplifiers: Principles and Applications', *Physics Today*, 48(2), p. 56. doi: 10.1063/1.2807915.

Desurvire, E., Simpson, J. R. and Becker, P. C. (1987) 'High-gain Erbium-doped traveling-wave fiber amplifier', *Optics Letters*, 12(11), p. 888. doi: 10.1364/OL.12.000888.

Diaz, S. et al. (2009) 'Comparison of the Stability of Ring Resonator Structures for Multiwavelength Fiber Lasers Using Raman or Er-Doped Fiber Amplification', 45(12), pp. 1551–1557.

Digonnet, M. J. F. (2001) Rare-earth-doped fiber lasers and amplifiers, Book.

Di, A. and Andre, M. V (2007) 'Q-switched all-fiber laser using a fiber-optic resonant acousto-optic modulator', 274, pp. 407–411. doi: 10.1016/j.optcom.2007.02.032.

Dong, B. et al. (2011) 'Short linear-cavity Q-switched fiber laser with a compact short carbon nanotube based saturable absorber', Optical Fiber Technology, 17(2), pp. 105–107. doi: 10.1016/j.yofte.2010.12.001.

Duan, Z., Zhang, L. and Chen, J. (2007) 'Analytical characterization of an end pumped rare-earth-doped double-clad fiber laser', Optical Fiber Technology, 13(2), pp. 143–148. doi: 10.1016/j.yofte.2006.11.001.

Duchowicz, R. et al. (2003) 'Q-switching of an Erbium-doped fiber laser modulated by a Bragg grating fixed to a piezoelectric', in Journal of Optics A: Pure and Applied Optics. doi: 10.1088/1464-4258/5/5/368.

Feng, T., Yan, F., Liu, S., Peng, W., et al. (2014) 'A switchable and wavelength-spacing tunable single-frequency and single-polarization dual-wavelength Erbium-doped fiber laser based on a compound-cavity structure', Laser Physics, 24(8). doi: 10.1088/1054-660X/24/8/085101.

Feng, T., Yan, F., Liu, S., Bai, Y., et al. (2014) ‘Switchable and tunable dual-wavelength single-longitudinal-mode Erbium-doped fiber laser with special subring-cavity and superimposed fiber Bragg gratings’, *Laser Physics Letters*, 11(12). doi: 10.1088/1612-2011/11/12/125106.

Feng, T. and Yan, F. P. (2012) ‘Stable and High OSNR Compound Linear-Cavity Single-Longitudinal-Mode Erbium-Doped Silica Fiber Laser Based on an Asymmetric Four-Cavity Structure’. doi: 10.1088/0256-307X/29/10/104205.

Feng, X. et al. (2011) ‘Switchable multiwavelength Erbium-doped fiber laser employing wavelength-dependent loss’, *Optical Fiber Technology*, 17(2), pp. 138–140. doi: 10.1016/j.yofte.2011.01.006.

Feng, Z.-Z. F. Z.-Z. et al. (2010) ‘All-fiber Q-switched pulsewidth tunable Erbium fiber laser using abrupt-tapered Mach-Zehnder filter’, *Optoelectronics and Communications Conference (OECC)*, 2010 15th.

Filippov, V. N., Starodumov, a N. and Kir’yanov, a V (2001) ‘All-fiber passively Q-switched low-threshold Erbium laser.’, *Optics Letters*, 26(6), pp. 343–5. doi: 10.1364/OL.26.000343.

Fu, P. et al. (2018) ‘Switchable dual-wavelength SLM narrow linewidth fiber laser based on nonlinear amplifying loop mirror’, *Optics and Laser Technology*, 98, pp. 56–60. doi: 10.1016/j.optlastec.2017.07.041.

Gaeta, C. J., Digonnet, M. J. F. and Shaw, H. J. (1987) 'Pulse Characteristics of Q-switched Fiber Lasers', *Journal of Lightwave Technology*, 5(12), pp. 1645–1651. doi: 10.1109/JLT.1987.1075462.

Giles, C. R. et al. (1991) 'Characterization of Erbium-Doped Fibers and Application to Modeling 980-nm and 1480-nm Pumped Amplifiers', *IEEE Photonics Technology Letters*, 3(4), pp. 363–365. doi: 10.1109/68.82113.

Giles, C. R. and Desurvire, E. (1991) 'Modeling Erbium-doped fiber amplifiers', *Journal of Lightwave Technology*, 9(2), pp. 271–283. doi: 10.1109/50.65886.

Gloag, a. J. et al. (1996) 'Single-frequency travelling-wave Erbium-doped fiber laser incorporating a fiber Bragg grating', *Optics Communications*, 123(4–6), pp. 553–557. doi: 10.1016/0030-4018(95)00595-1.

Goldberg, P., Milonni, P. W. and Sundaram, B. (1991) 'Theory of the fundamental laser linewidth', *Physical Review A*, 44(3), pp. 1969–1985. doi: 10.1103/PhysRevA.44.1969.

González-García, A. et al. (2013) 'High efficiency, actively Q-switched Er/Yb fiber laser', *Optics and Laser Technology*, pp. 182–186. doi: 10.1016/j.optlastec.2012.10.021.

González-García, A. et al. (2015) 'Compact wavelength-tunable actively Q-switched fiber laser in CW and pulsed operation based on a fiber Bragg grating', *Laser Physics*,

25(4), pp. 1–5. doi: 10.1088/1054-660X/25/4/045104.

Guenther, R. D. (1990) *Modern Optics*, Mod. Opt. doi: 10.1080/09500349114551331.

Han, M. and Wang, A. (2005) ‘Analysis of a loss-compensated recirculating delayed self-heterodyne interferometer for laser linewidth measurement’, *Applied Physics B: Lasers and Optics*, 81(1), pp. 53–58. doi: 10.1007/s00340-005-1871-9.

Hanna, D. . (2003) *Rare-earth-doped fiber lasers and amplifiers*, 2nd edition, *Optics and Lasers in Engineering*. doi: 10.1016/S0143-8166(02)00070-2.

Havstad, S. A. et al. (2000) ‘Delayed self-heterodyne interferometer measurements of narrow linewidth fiber lasers’, in *Conference on Lasers and Electro-Optics (CLEO 2000)*. Technical Digest. Postconference Edition. TOPS Vol.39 (IEEE Cat. No.00CH37088), pp. 310–311. doi: 10.1109/CLEO.2000.907051.

He, W. and Zhu, L. (2015) ‘Stable and switchable single-longitudinal-mode dual-wavelength Erbium-doped fiber laser based on a fiber ring filter’, *Optik - International Journal for Light and Electron Optics*, 126(22), pp. 3390–3394. doi: 10.1016/j.ijleo.2015.07.133.

He, W., Zhu, L. and Luo, F. (2016) ‘Tuneable and stable multi-wavelength thulium-doped ring-cavity fiber laser based on Sagnac loop and Mach – Zehnder filter utilizing thin-core fiber’. IOP Publishing. doi: 10.1088/1054-660X/26/12/125102.

He, X. et al. (2009) ‘A tunable and switchable single-longitudinal-mode dual-

wavelength fiber laser with a simple linear cavity', *Optics Express*, 17(24), p. 21773.
doi: 10.1364/OE.17.021773.

He, X. et al. (2013) 'laser using self-developed heavily Tm³⁺-doped germanate glass fiber', 21(18), pp. 875–877. doi: 10.1364/OE.21.020800.

Hill, K. O. and Meltz, G. (1997) 'Fiber Bragg grating technology fundamentals and overview', *Journal of Lightwave Technology*, 15(8), pp. 1263–1276. doi: 10.1109/50.618320.

Horak, P. and Loh, W. H. (2006) 'On the delayed self-heterodyne interferometric technique for determining the linewidth of fiber lasers', *Optics Express*, 14(9), p. 3923.
doi: 10.1364/OE.14.003923.

Horowitz, M. et al. (1994) 'Narrow-linewidth, singlemode Erbium-doped fiber laser with intracavity wave mixing in saturable absorber - *Electronics Letters*', 30(8).

Horowitz, M. et al. (1994) 'Narrow-linewidth, singlemode Erbium-doped fiber laser with intracavity wave mixing in saturable absorber', *Electronics Letters*, 30(8), p. 648.
doi: 10.1049/el:19940448.

Huang, D. W., Liu, W. F. and Yang, C. C. (2000) 'Q-switched all-fiber laser with an acoustically modulated fiber attenuator', *IEEE Photonics Technology Letters*, 12(9), pp. 1153–1155. doi: 10.1109/68.874219.

Huang, S. et al. (2016a) 'Laser Linewidth Measurement Based on Amplitude

Difference Comparison of Coherent Envelope', IEEE Photonics Technology Letters, 28(7), pp. 759–762. doi: 10.1109/LPT.2015.2513098.

Huang, S. et al. (2016b) 'Laser Linewidth Measurement Based on Amplitude Difference Comparison of Coherent Envelope', 28(7), pp. 759–762.

Huo, Y. et al. (2004) 'Kinetic modeling of Q-switched high-power Ytterbium-doped fiber lasers.', Applied optics, 43(6), pp. 1404–1411. doi: 10.1364/AO.43.001404.

Hussein Ali, D. A. (2012) 'Analysis of Self-Homodyne and Delayed Self-Heterodyne Detections for Tunable Laser Source Linewidth Measurements', IOSR Journal of Engineering, 2(10), pp. 01–06. doi: 10.9790/3021-021040106.

Iang, M. A. N. J. et al. (2016) 'All-fiber , narrow linewidth and linearly polarized fiber laser in a single-mode- multimode-single-mode cavity', 55(22), pp. 6121–6124.

Iwatsuki, K., Okamura, H. and Saruwatari, M. (1990) 'Wavelength-tunable single-frequency and single-polarisation er-doped fiber ring-laser with 1.4 kHz linewidth', Electronics Letters, 26(24), p. 2033. doi: 10.1049/el:19901312.

Kaneda, Y. et al. (2004) '200-mW, narrow-linewidth 1064.2-nm Yb-doped fiber laser', Conference on Lasers and Electro-Optics, 2004. (CLEO)., 2, pp. 2–3.

Kaneda, Y. et al. (2004) 'Single-frequency , all-fiber Q-switched laser at 1550-nm', pp. 2–4.

Kao, K. C. and Hockham, G. A. (1966) 'Dielectric-fiber surface waveguides for optical frequencies', Proceedings of the Institution of Electrical Engineers, 113(7), pp. 1151–1158. doi: 10.1049/piee.1966.0189.

Karasek, M. and Bellemare, A. (2000) 'Numerical analysis of multifrequency Erbium-doped fiber ring laser employing periodic filter and frequency shifter', Optoelectronics, IEE Proceedings -, 147(2), pp. 115–119. doi: 10.1049/ip-opt:20000286.

Kashyap, R. et al. (1990) 'All-fiber narrowband reflection gratings at 1500 nm', Electronics Letters, 26(11), pp. 730–732. doi: 10.1049/el:19900476.

Kashyap, R., Taylor, J. R. and Guy, M. J. (1995) 'Single-frequency Erbium fiber ring laser with intracavity phase-shifted fiber Bragg grating narrowband filter', Electronics Letters, 31(22), pp. 1924–5. doi: 10.1049/el:19951297.

Kee, H., Lees, G. and Newson, T. (1998) 'Narrow linewidth CW and Q-switched Erbium-doped fiber loop laser', Electronics Letters, 34(13), pp. 1318–1319. doi: 10.1049/el:19980913.

Kee, H., Lees, G. and Newson, T. (2000) 'Distributed optical fiber sensing at 1.65 μ m using a Q-switched fiber laser', in Proceedings of SPIE - The International Society for Optical Engineering, pp. 280–287.

Kieu, K. and Mansuripur, M. (2006) 'Active Q switching of a fiber laser with a

microsphere resonator.’, *Optics letters*, 31(24), pp. 3568–70. doi: 10.1364/OL.31.003568.

Koechner, W. (2014) *Solid-State Laser Engineering - 6th Edition*, Igarss 2014. doi: 10.1007/s13398-014-0173-7.2.

Koester, C. J. and Snitzer, E. (1964) ‘Amplification in a Fiber Laser’, *Applied Optics*, 3(10), p. 1182. doi: 10.1364/AO.3.001182.

Kolpakov, S. A. et al. (2011) ‘Distributed model for actively Q-switched Erbium-doped fiber lasers’, *IEEE Journal of Quantum Electronics*, 47(7), pp. 928–934. doi: 10.1109/JQE.2011.2143695.

Kolpakov, S. A. et al. (2014) ‘Optimization of Erbium-doped actively Q-switched fiber laser implemented in symmetric configuration’, *IEEE Journal on Selected Topics in Quantum Electronics*, 20(5). doi: 10.1109/JSTQE.2014.2301015.

Lees, G. P. et al. (1997) ‘A Q-switched Erbium-doped fiber laser utilising a novel large mode area fiber’, *Electronics Letters*, 33(5), p. 393. doi: 10.1049/el:19970253.

Leigh, M. et al. (2007) ‘Compact, single-frequency all-fiber Q-switched laser at 1 microm.’, *Optics letters*, 32(8), pp. 897–9. doi: 10.1364/OL.32.000897.

Li, C. et al. (2013) ‘A linearly frequency modulated narrow linewidth single-frequency fiber laser’. doi: 10.1088/1612-2011/10/7/075106.

Li, H. P. et al. (2014) 'A compact graphene Q-switched Erbium-doped fiber laser using optical circulator and tunable fiber Bragg grating', *Chinese Physics B*, 23(2). doi: 10.1088/1674-1056/23/2/024209.

Li, Q. et al. (2012) 'Narrow linewidth, linear cavity, Erbium-doped fiber laser with saturable absorber', in *Proceedings - 2012 International Conference on Computer Science and Information Processing, CSIP 2012*, pp. 275–277. doi: 10.1109/CSIP.2012.6308847.

Lidgard, A. et al. (1991) 'Fluorescence lifetime studies of MeV Erbium implanted silica glass', *Electronics Letters*, 27(11), pp. 993–995. doi: 10.1049/el:19910619.

Lidgard, A., Simpson, J. R. and Becker, P. C. (1990) 'Output saturation characteristics of Erbium-doped fiber amplifiers pumped at 975 nm', *Applied Physics Letters*, 56(26), pp. 2607–2609. doi: 10.1063/1.102852.

Liu, J. et al. (2001) 'Modeling pulse shape of Q-switched lasers', *IEEE Journal of Quantum Electronics*, 37(7), pp. 888–896. doi: 10.1109/3.929588.

Liu, J. (2005) *Photonic devices, Optics*. doi: 10.1017/CBO9780511614255.

Liu, W. and Road, R. (no date) 'Actively Q-switched All-Fiber Laser with a Fiber Bragg Grating of Variable Reflectivity', pp. 224–226.

Liu, X. et al. (2005) 'Stable and uniform dual-wavelength Erbium-doped fiber laser based on fiber Bragg gratings and photonic crystal fiber', 13(1), pp. 142–147.

Lu, Y. et al. (2010) ‘Distributed vibration sensor based on coherent detection of phase-OTDR’, *Journal of Lightwave Technology*, 28(22), pp. 3243–3249. doi: 10.1109/JLT.2010.2078798.

Ludvigsen, H., Tossavainen, M. and Kaivola, M. (1998) ‘Laser linewidth measurements using self-homodyne detection with short delay’, *Optics Communications*, 155(1–3), pp. 180–186. doi: 10.1016/S0030-4018(98)00355-1.

Luo, Z. et al. (2010) ‘Graphene-based passively Q-switched dual-wavelength Erbium-doped fiber laser’, *Optics Letters*, 35(21), pp. 3709–3711. doi: 10.1364/OL.35.003709.

Ma, Y. et al. (2011) ‘Coherent beam combination of 108 kW fiber amplifier array using single frequency dithering technique’, *Optics Letters*, 36(6), p. 951. doi: 10.1364/OL.36.000951.

Maiman, T. H. (1960) ‘Optical and microwave-optical experiments in ruby’, *Physical Review Letters*, 4(11), pp. 564–566. doi: 10.1103/PhysRevLett.4.564.

Manuel, R. et al. (2016) ‘Active Q-switching of a fiber laser using a modulated fiber Fabry–Perot filter and a fiber Bragg grating’, in *2016 Laser Phys.* 26 (2016) 025105 (4pp)

Maiman, T. H. (1960b) ‘Stimulated optical radiation in Ruby’, *Nature*, 187(4736), pp. 493–494. doi: 10.1038/187493a0.

McClung, F. J. and Hellwarth, R. W. (1962) 'Giant optical pulsations from ruby', *Journal of Applied Physics*, 33(3), pp. 828–829. doi: 10.1063/1.1777174.

Mears, R. J. et al. (1986) 'Low-threshold tunable CW and Q-switched fiber laser operating at 1.55 μm ', *Electronics Letters*, 22(3), p. 159. doi: 10.1049/el:19860111.

Mears, R. J. et al. (1987) 'Low-noise Erbium-doped fiber amplifier operating at 1.54 μm ', *Electronics Letters*, 23(19), p. 1026. doi: 10.1049/el:19870719.

Mears, R. J. and Baker, S. R. (1992) 'Erbium fiber amplifiers and lasers', *Optical and Quantum Electronics*, pp. 517–538. doi: 10.1007/BF00619752.

Meltz, G., Morey, W. W. and Glenn, W. H. (1989) 'Formation of Bragg gratings in optical fibers by a transverse holographic method', *Optics Letters*, 14(15), p. 823. doi: 10.1364/OL.14.000823.

Meng, Z., Stewart, G. and Whitenett, G. (2006) 'Stable Single-Mode Operation of a Erbium-Fiber Ring Laser Using a Saturable Absorber', *Optics Letters*, 31(5), pp. 2179–2183.

Mercer, L. B. (1991) '1/f Frequency Noise Effects on Self-Heterodyne Linewidth Measurements', *Journal of Lightwave Technology*, 9(4), pp. 485–493. doi: 10.1109/50.76663.

Minguela-Gallardo, J. A. et al. (2017) 'Spectral Dynamics of Actively Q-switched Erbium-Doped Fiber Lasers', *IEEE Photonics Technology Letters*, 29(8), pp. 683–686. doi: 10.1109/LPT.2017.2677743.

Miniscalco, W. J. (1991) 'Erbium-Doped Glasses for Fiber Amplifiers at 1500 nm', *Journal of Lightwave Technology*, 9(2), pp. 234–250. doi: 10.1109/50.65882.

Monga, K. J. J., Meyer, J. and Manuel, R. M. (2017) 'Implementation of active Q-switching based on a modulated fiber Fabry-Perot filter in linear cavity Erbium-doped fiber laser', in 2017 IEEE AFRICON: Science, Technology and Innovation for Africa, AFRICON 2017, pp. 620–624. doi: 10.1109/AFRCON.2017.8095553.

Morkel, P. R., Jedrzejewski, K. P. and Taylor, E. R. (1993) 'Q-switched Neodymium-Doped Phosphate Glass Fiber Lasers', *IEEE Journal of Quantum Electronics*, 29(7), pp. 2178–2188. doi: 10.1109/3.237492.

Myslinski, P. et al. (1992) 'High-Power Q-switched Erbium-doped Fiber Laser', *Ieee Journal of Quantum Electronics*, 28(1), pp. 371–377. doi: Doi 10.1109/3.119537.

Nezu, T., Tanaka, Y. and Kurokawa, T. (2003) 'Delayed self-heterodyne linewidth measurement of fiber Bragg grating laser', in Pacific Rim Conference on Lasers and Electro-Optics, CLEO - Technical Digest, p. 388. doi: 10.1109/CLEOPR.2003.01274840.

Nilsson, J. et al. (2005) 'High power fiber lasers', OFCNFOEC Technical Digest Optical Fiber Communication Conference 2005, 2(July), pp. 1–15. doi: 10.1364/OPN.10.1.000026.

Offerhaus, H. L. et al. (1998) 'High-energy single-transverse-mode Q-switched fiber

laser based on a multimode large-mode-area Erbium-doped fiber', *Optics Letters*, 23(21), pp. 1683–1685. doi: 10.1364/OL.23.001683.

Okoshi, T., Kikuchi, K. and Nakayama, A. (1980) 'Novel method for high resolution measurement of laser output spectrum', *Electronics Letters*, 16(16), p. 630. doi: 10.1049/el:19800437.

Ono, S. and Tanabe, S. (2006) 'Evaluation of quenching effect on gain characteristics in silica-based Erbium-doped fiber using numerical simulation', in *Journal of Alloys and Compounds*, pp. 732–736. doi: 10.1016/j.jallcom.2004.12.083.

Ortaç, B. et al. (2008) 'Passively mode-locked single-polarization microstructure fiber laser.', *Optics express*, 16(3), pp. 2122–2128. doi: 10.1364/OE.16.002122.

Ouslimani, H., Bastard, L. and Broquin, J. (2015) 'Narrow-linewidth Q-switched DBR laser on Ytterbium-doped glass', *Ceramics International*. Elsevier, 41(7), pp. 8650–8654. doi: 10.1016/j.ceramint.2015.03.076. 'Page 1 of 1' (2017), p. 2017.

Pan, L. et al. (2007) 'Passively Q -switched Ytterbium-Doped Double-Clad Fiber Laser With a Cr 4 + : YAG Saturable Absorber', 19(24), pp. 1979–1981.

Pan, L. et al. (2010) 'Experiment and Numerical Modeling of High-Power Fiber Lasers', 46(1), pp. 68–75.

Paschotta, R. et al. (1997) 'Lifetime quenching in Yb-doped fibers', *Optics Communications*, 136(5–6), pp. 375–378. doi: 10.1016/S0030-4018(96)00720-1.

Paschotta, R. et al. (1997) 'Single-frequency Ytterbium-doped fiber laser stabilized by spatial hole burning', 22(1), pp. 40–42.

Paschotta, R. et al. (2006) 'Optical phase noise and carrier-envelope offset noise of mode-locked lasers', Applied Physics B: Lasers and Optics, 82(2 SPEC. ISS.), pp. 265–273. doi: 10.1007/s00340-005-2041-9.

Paschotta, R. (2009) Encyclopedia of Laser Physics and Technology, Laser Physics. Available at: www.rp-photonics.com.

Payne, D. N. and Reekie, L. (1988a) 'Rare-earth-doped fiber lasers and amplifiers', in IEE Conference Publication.

Payne, D. N. and Reekie, L. (1988b) 'Rare-earth-doped fiber lasers and amplifiers', in Fourteenth European Conference on Optical Communication, ECOC 88 (Conf. Publ. No.292), Brighton, pp. 49–53. Available at: <https://eprints.soton.ac.uk/350285/>

Peng, Y. (2013) 'A novel scheme for hundred-hertz linewidth measurements with the self-heterodyne method', Chinese Physics Letters, 30(8). doi: 10.1088/0256-307X/30/8/084208.

Pérez-Millán, P. et al. (2005) 'Q-switched all-fiber laser based on magnetostriction modulation of a Bragg grating', Optics express, 13(13), pp. 5046–51. doi: 10.1364/OPEX.13.005046.

Pérez-Herrera, R. A. *et al.* (2010) 'Experimental optimization in terms of power stability and output power of highly erbium-doped fiber lasers with single and hybrid cavities', *Fiber and Integrated Optics*, 29(2), pp. 106–120. doi: 10.1080/01468031003611124.

Pfeiffer, T., Schmuck, H. and Bulow, H. (1992) 'Output power characteristics of Erbium-doped fiber ring lasers', *IEEE Photonics Technology Letters*, 4(8), pp. 847–849. doi: 10.1109/68.149883.

Philippov, V. N., Kir'yanov, A. V. and Unger, S. (2004) 'Advanced Configuration of Erbium Fiber Passively Q-switched Laser with Co²⁺:ZnSe Crystal as Saturable Absorber', *IEEE Photonics Technology Letters*, 16(1), pp. 57–59. doi: 10.1109/LPT.2003.819397.

Philippov, V. N., Kir'yanov, A. V. and Unger, S. (2004) 'Advanced configuration of Erbium fiber passively Q-switched laser with Co²⁺: ZnSe saturable absorber', *Ieee Photonics Technology Letters*, 16(1), pp. 57–59. doi: Doi 10.1109/Lpt.2003.819397.

Phing, H. S. *et al.* (2007) 'Fiber Bragg grating modeling, simulation and characteristics with different grating lengths', *Journal of Fundamental Sciences*, 3, pp. 167–175. Available at: <http://jfs.ibnusina.utm.my/index.php/jfs/article/viewFile/9/8>.

Piper, A. *et al.* (2004) 'High-power high-brightness, mJ Q-switched Ytterbium-doped fiber laser', *Electronics Letters*, 40(15), pp. 928–929. doi: 10.1049/el:20045661.

Quintela, M. A. et al. (2010) 'Stabilization of dual-wavelength Erbium-doped fiber ring lasers by single-mode operation', *IEEE Photonics Technology Letters*, 22(6), pp. 368–370. doi: 10.1109/LPT.2009.2039867.

Renaud, C. C. et al. (2001) 'Characteristics of Q-switched cladding-pumped Ytterbium-doped fiber lasers with different high-energy fiber designs', *IEEE Journal of Quantum Electronics*, 37(2), pp. 199–206. doi: 10.1109/3.903069.

Roy, P. and Pagnoux, D. (1996) 'Analysis and optimization of a Q-switched Erbium-doped fiber laser working with a short rise time modulator', *Optical Fiber Technology*, 2(3), pp. 235–240. doi: 10.1006/ofte.1996.0029.

Russo, N. A. et al. (2002) 'High-efficiency Q-switched Erbium fiber laser using a Bragg grating-based modulator', *Optics Communications*, 210(3–6), pp. 361–366. doi: 10.1016/S0030-4018(02)01815-1.

Rutten, T. P., Veitch, P. J. and Munch, J. (2008) 'Efficient pulse stretching of Q-switched lasers', *IEEE Journal of Quantum Electronics*, 44(10), pp. 911–915. doi: 10.1109/JQE.2008.925140.

Saffari, P. et al. (2010) 'Single Polarisation Output of Erbium-Doped Fiber Ring Laser Utilising a Small Tilted Fiber Grating Structure', *Advanced Photonics & Renewable Energy*, 1, p. JThA41. doi: 10.1364/BGPP.2010.JThA41.

Saleh, B. E. A., Teich, M. C. and Masters, B. R. (2008) 'Fundamentals of Photonics,

Second Edition', Journal of Biomedical Optics, 13(4), p. 49901. doi: 10.1117/1.2976006.

Saleh, Z. S. et al. (2014) 'Q-switched Erbium-doped fiber laser using graphene-based saturable absorber obtained by mechanical exfoliation', Ukrainian Journal of Physical Optics, 15(1), pp. 24–29. doi: 10.3116/16091833/15/1/24/2014.

Sanchez-Martin, J. A. et al. (2008) 'Experimental verification of a theoretical model for Erbium-doped fiber ring lasers', Journal of Modern Optics, 55(17), pp. 2865–2874. doi: 10.1080/09500340802263083.

Sanchez, F. et al. (1995) 'Output-coupling optimization of Nd-doped fiber lasers', 34(33), pp. 7674–7679.

Schawlow, A. L. and Townes, C. H. (1958) 'Infrared and optical masers', Physical Review, 112(6), pp. 1940–1949. doi: 10.1103/PhysRev.112.1940.

Schmidt, O. et al. (2007) 'Millijoule pulse energy Q-switched short-length fiber laser', Opt. Lett., 32(11), pp. 1551–1553. doi: 10.1364/OL.32.001551.

Selvakennedy, S. et al. (1999) 'Design optimization of Erbium-doped fiber ring laser through numerical simulation', Optics Communications, 170(4), pp. 247–253. doi: 10.1016/S0030-4018(99)00462-9.

Selvakennedy, S. et al. (2000) 'Behavioral Investigations of an Erbium-Doped Fiber Ring Laser through Numerical Simulations', Optical Fiber Technology, 6(2), pp. 155–

163. doi: 10.1006/ofte.1999.0321.

Selvakennedy, S. et al. (2000) 'Erbium-doped fiber ring laser cavity in transient and steady states studied by a numerical approach', 17(6), pp. 914–918.

Shang, L. et al. (2007) 'Novel methods to improve pulse energy of Q-switched fiber laser', Modern Physics Letters B, 21(8), pp. 489–495. doi: 10.1142/S0217984907013031.

Shang, L. J. et al. (2006) 'Effective methods to improve pulse energy of Q-switched fiber laser', Journal of Optoelectronics and Advanced Materials, 8(3), pp. 1254–1257.

Shang, L. J. et al. (2006) 'Effective methods to narrow pulse width of Q-switched fiber laser', in Journal of Optoelectronics and Advanced Materials, pp. 851–854.

Sharma, U., Kim, C. and Kang, J. U. (2004) 'Highly Stable Tunable Dual-Wavelength Q-Switched Fiber Laser for DIAL Applications', 16(5), pp. 1277–1279.

Sharma, U., Kim, C. S. and Kang, J. U. (2004) 'Highly stable tunable dual-wavelength Q-switched fiber laser for DIAL applications', IEEE Photonics Technology Letters, 16(5), pp. 1277–1279. doi: 10.1109/LPT.2004.825991.

Sheu, F. W. and Kang, J. J. (2007) 'All-fiber actively Q-switched fiber laser tuned by a pair of temperature controlled fiber Bragg gratings', Optics Communications, 278(1), pp. 132–137. doi: 10.1016/j.optcom.2007.05.049.

Shi, W. et al. (2014) 'Fiber lasers and their applications', *Applied Optics*, 53(28), pp. 6554–6568. doi: 10.1364/AO.53.006554.

Shiner, W., Snitzer, E. and Woodcock, R. (1966) 'Self Q-switched Nd³⁺+glass laser', *Physics Letters*, 21(4), pp. 412–413. doi: 10.1016/0031-9163(66)90509-9.

Sholokhov, E. M. et al. (2010) 'Grating All-fiber pulsewidth tunable actively Q-switched Erbium fiber laser using abrupt-tapered Mach-Zehnder block filter'. doi: 10.1002/lapl.201010003.

Siegman, A. E. (1986) *Lasers, Lasers*.

Silfvast, W. T. (2011) 'Lasers', *Cochrane database of systematic reviews (Online)*, 11, p. CD007152. doi: 10.1002/14651858.CD007152.pub2.

Snitzer, E. (1961) 'Optical maser action of Nd³⁺ in a barium crown glass', *Physical Review Letters*, 7(12), pp. 444–446. doi: 10.1103/PhysRevLett.7.444.

Sousa, J. M. and Okhotnikov, O. G. (1999) 'Multimode Er-doped fiber for single-transverse-mode amplification', *Applied Physics Letters*, 74(11), pp. 1528–1530. doi: 10.1063/1.123605.

Spiegelberg, C. et al. (2003) 'Compact 100 mW fiber laser with 2 kHz linewidth', in *Conference on Optical Fiber Communication, Technical Digest Series*, p. PD45.1-PD45.3. doi: 10.1109/OFC.2003.316027.

Spiegelberg, C. et al. (2004) 'High power narrow linewidth fiber lasers', (520), pp. 2–4.

Spiegelberg, C., Geng, J., Hu, Y., Kaneda, Y., Jiang, S. and Peyghambarian, N. (2004) 'Low-Noise Narrow-Linewidth Fiber Laser at 1550 nm (June 2003)', in *Journal of Lightwave Technology*, pp. 57–62. doi: 10.1109/JLT.2003.822208.

Stone, D. H. (1992) 'Effects of Axial Nonuniformity in Modeling Q-switched Lasers', *IEEE Journal of Quantum Electronics*, 28(10), pp. 1970–1973. doi: 10.1109/3.159504.

Sun, Y., Szkopek, T. and Smith, P. W. E. (2003) 'Demonstration of narrowband high-reflectivity Bragg gratings in a novel multimode fiber', *Optics Communications*, 223(1–3), pp. 91–95. doi: 10.1016/S0030-4018(03)01636-5.

Svelto, O. (2010) *Principles of lasers*, Principles of Lasers. doi: 10.1007/978-1-4419-1302-9.

Swiderski, J. et al. (2004) 'Numerical model of a Q-switched double-clad fiber laser', *Optics Express*, 12(15), p. 3554. doi: 10.1364/OPEX.12.003554.

Takushima, Y., Yamashita, S. and Kikuchi, K. (1998) 'Polarization-Stable and Single-Frequency', 16(4), pp. 661–669.

Tsang, K. S. et al. (2015) 'Single-frequency single-polarization fiber ring laser at 1053 nm', pp. 1–2.

Urquhart, P. (1988) 'Review of rare earth doped fiber lasers and amplifiers', Optoelectronics, IEE Proceedings J, 135(6), pp. 385–407. doi: 10.1049/ip-j:19880071.

Verdeyen, J. (1995) Laser electronics, Laser electronics/2nd edition/, by JT Verdeyen, Available at: <http://adsabs.harvard.edu/abs/1989lael.book.....V>.

Voo, N. Y. et al. (2005) 'Anomalous linewidth behavior in short-cavity single-frequency fiber lasers', IEEE Photonics Technology Letters, 17(3), pp. 546–548. doi: 10.1109/LPT.2004.841004.

Wang, Y., Å, Y. W. and Xu, C. (2016) 'Actively Q-switched fiber lasers : Switching dynamics and nonlinear processes Actively Q-switched fiber lasers : Switching dynamics and nonlinear processes', (January). doi: 10.1016/j.pquantelec.2007.06.001.

Wang, Y., Martinez-Rios, A. and Po, H. (2003b) 'Pulse evolution of a Q-switched Ytterbium-doped double-clad fiber laser', Optical Engineering, 42(9), p. 2521. doi: 10.1117/1.1592168.

Wang, Y. and Xu, C.-Q. (2004) 'Understanding multipeak phenomena in actively Q-switched fiber lasers.', Optics letters, 29(10), pp. 1060–1062. doi: 10.1364/OL.29.001060.

Wang, Y. and Xu, C.-Q. (2006) 'Modeling and optimization of Q-switched double-clad fiber lasers', Applied Optics, 45(9), p. 2058. doi: 10.1364/AO.45.002058.

Wang, Y. and Xu, C.-Q. (2007) 'Actively Q-switched fiber lasers: Switching dynamics

and nonlinear processes', *Progress in Quantum Electronics*, 31(3–5), pp. 131–216. doi: 10.1016/j.pquantelec.2007.06.001.

Wang, Y. and Xu, C. Q. (2004) 'Switching-induced perturbation and influence on actively Q-switched fiber lasers', *IEEE Journal of Quantum Electronics*, 40(11), pp. 1583–1596. doi: 10.1109/JQE.2004.835212.

Ward, C. A. (1892) 'Atomic theory', *Notes and Queries*, p. 494. doi: 10.1093/nq/s8-I.25.494.

Williams, R. J. et al. (2010a) 'All-optical, actively Q-switched fiber laser.', *Optics express*, 18(8), pp. 7714–7723. doi: 10.1364/OE.18.007714.

Williams, R. J. et al. (2010b) 'All-optical , actively Q-switched fiber laser', 18(8), pp. 2804–2806.

Williams, R. J. et al. (2010) 'Optically switched Erbium fiber laser using a tunable fiber-Bragg grating', *fiber lasers VII: technology, systems, and applicationS*, p. 75800P. doi: 10.1117/12.839450.

Wu, B. et al. (2008) 'High efficient and narrow linewidth fiber laser based on fiber grating Fabry-Perot cavity', 1, pp. 215–218. doi: 10.1007/s12200-008-0012-6.

Wu, L. et al. (2016) 'Q-switched Erbium-doped fiber ring laser with piezoelectric transducer-based PS-CFBG', *Laser Physics Letters*, 13(9). doi: 10.1088/1612-2011/13/9/095101.

Wu, M. et al. (2016) 'Wavelength switchable graphene Q-switched fiber laser with cascaded fiber Bragg gratings'. Elsevier, 368, pp. 81–85. doi: 10.1016/j.optcom.2016.01.069.

X.P, D. et al. (2000) 'Multiwavelength Erbium-doped fiber laser based on a high-birefringence fiber loop mirror', Electronics Letters, 36(19), pp. 1609–1610. doi: 10.1049/el.

Xiang, L. et al. (2011) 'Research on the characteristics of the Q-switched Ytterbium-doped fiber lasers', in Journal of Physics: Conference Series. doi: 10.1088/1742-6596/276/1/012135.

Yamashita, S. and Hotate, K. (1996) 'Narrow linewidth, O-switched Erbium-doped fiber laser - Electronics Letters', 32(14), pp. 1299–1300.

Yang, X. X. et al. (2008) 'High-power single-longitudinal-mode fiber laser with a ring Fabry-Pérot resonator and a saturable absorber', IEEE Photonics Technology Letters, 20(11), pp. 879–881. doi: 10.1109/LPT.2008.922332.

Yariv, A. and Yariv, A. (1997) 'Optical Electronics in Modern Communications, 5th ed', New York: Oxford University Press, pp. 404–407.

Yb, E. et al. (2005) 'Modeling and Experiments of Actively Q -Switched', 41(4), pp. 573–580.

Yin, B. et al. (2015) 'Switchable Dual-Wavelength SLM Fiber Laser Using

Asymmetric PM FBG Fabry–Perot Cavities’, *IEEE Photonics Technology Letters*, 27(12), pp. 1281–1284. doi: 10.1109/LPT.2015.2417869.

Yu, Z. et al. (2010) ‘Actively Q-switched all-fiber laser with an electrically controlled microstructured fiber.’, *Optics express*, 18(11), pp. 11052–11057. doi: 10.1364/OE.18.011052.

Yu Yao et al. (2006) ‘Dual-wavelength Erbium-doped fiber laser with a simple linear cavity and its application in microwave generation’, *IEEE Photonics Technology Letters*, 18(1), pp. 187–189. doi: 10.1109/LPT.2005.861309.

Yüksel, K. et al. (2010) ‘Novel monitoring technique for passive optical networks based on optical frequency domain reflectometry and fiber bragg gratings’, *Journal of Optical Communications and Networking*, 2(7), pp. 463–468. doi: 10.1364/JOCN.2.000463.

Zayhowski, J. J. and Kelley, P. L. (1991) ‘Optimization of Q-switched Lasers’, *IEEE Journal of Quantum Electronics*, 27(9), pp. 2220–2225. doi: 10.1109/3.135181.

Zhang, J. et al. (1996) ‘Stable single-mode compound-ring Erbium-doped fiber laser’, *Journal of Lightwave Technology*, 14(1), pp. 104–109. doi: 10.1109/50.476143.

Zhang, K. and Kang, J. U. (2008) ‘C-band wavelength-swept single-longitudinalmode Erbium-doped fiber ring laser.’, *Optics express*, 16(18), pp. 14173–14179. doi: 10.1364/OE.16.014173.

Zhang, N. et al. (2013) 'Linewidth study of the frequency-modulated laser based on the delayed self-heterodyne scheme', *Optics and Laser Technology*, 45(1), pp. 267–271. doi: 10.1016/j.optlastec.2012.06.036.

Zhen, L. (2013) 'The split pulses from actively Q -switched fiber lasers', *Laser Physics*, 23(12), p. 125105. doi: 10.1088/1054-660X/23/12/125105.

Zheng, J. and Zheng, J. (2006) 'Optical frequency-modulated continuous-wave interferometers',

Zyskind, J. L. et al. (1991) 'Singlemode diode-pumped tunable Erbium-doped fiber laser with linewidth less than 5.5 kHz', *Electronics Letters*, 27(23), p. 2148. doi: 10.1049/el:19911330.

Zyskind, J. L. et al. (1992) 'Short single frequency Erbium-doped fiber laser', *Electronics Letters*, 28(15), p. 1385. doi: 10.1049/el:19920881.